*Royal Norwegian Council*
*for Scientific and Industrial Research*
*(NTNF)*

NORSAR

NORSAR Scientific Report No. 2-87/88

# Semiannual Technical Summary

## 1 October 1987 – 31 March 1988

L.B. Loughran (ed.)

Kjeller, June 1988

**APPROVED FOR PUBLIC RELEASE, DISTRIBUTION UNLIMITED**

UNCLASSIFIED
SECURITY CLASSIFICATION OF THIS PAGE

# REPORT DOCUMENTATION PAGE

*Form Approved*
*OMB No. 0704-0188*

1a. REPORT SECURITY CLASSIFICATION
UNCLASSIFIED

1b. RESTRICTIVE MARKINGS
NOT APPLICABLE

2a. SECURITY CLASSIFICATION AUTHORITY
NOT APPLICABLE

2b. DECLASSIFICATION / DOWNGRADING SCHEDULE
NOT APPLICABLE

3. DISTRIBUTION / AVAILABILITY OF REPORT
APPROVED FOR PUBLIC RELEASE
DISTRIBUTION UNLIMITED

4. PERFORMING ORGANIZATION REPORT NUMBER(S)
Scientific Report 2-87/88

5. MONITORING ORGANIZATION REPORT NUMBER(S)
Scientific Report 2-87/88

6a. NAME OF PERFORMING ORGANIZATION
NTNF/NORSAR

6b. OFFICE SYMBOL *(If applicable)*

7a. NAME OF MONITORING ORGANIZATION
HQ/AFTAC/TTS

6c. ADDRESS *(City, State, and ZIP Code)*
POST BOX 51
N-2007 KJELLER, NORWAY

7b. ADDRESS *(City, State, and ZIP Code)*
PATRICK AFB, FL 32925-6001

8a. NAME OF FUNDING / SPONSORING ORGANIZATION
DEFENCE ADVANCED RESEARCH PROJECTS AGENCY

8b. OFFICE SYMBOL *(If applicable)*
NMRO

9. PROCUREMENT INSTRUMENT IDENTIFICATION NUMBER
CONTRACT NO. F08606-86-C-0004

8c. ADDRESS *(City, State, and ZIP Code)*
1400 WILSON BLVD.
ARLINGTON, VA 22209-2308

10. SOURCE OF FUNDING NUMBERS

| PROGRAM ELEMENT NO. | PROJECT NO. | TASK NO. | WORK UNIT ACCESSION NO. |
|---|---|---|---|
| R&D | NORSAR PHASE 3 | SOW TASK 5.0 | SEQUENCE NO. 003A2 |

11. TITLE *(Include Security Classification)*
SEMIANNUAL TECHNICAL SUMMARY 1 OCT 87 - 31 MAR 88 (UNCLASSIFIED)

12. PERSONAL AUTHOR(S)
L.B. LOUGHRAN (ED.)

13a. TYPE OF REPORT
SCIENTIFIC SUMMARY

13b. TIME COVERED
FROM 1 Oct 87 TO 31 Mar 88

14. DATE OF REPORT *(Year, Month, Day)*
Jun 1988

15. PAGE COUNT
127

16. SUPPLEMENTARY NOTATION
NOT APPLICABLE

17. COSATI CODES

| FIELD | GROUP | SUB-GROUP |
|---|---|---|
| 8 | 11 | |
| | | |

18. SUBJECT TERMS *(Continue on reverse if necessary and identify by block number)*
NORSAR, NORWEGIAN SEISMIC ARRAY

19. ABSTRACT *(Continue on reverse if necessary and identify by block number)*

This Semiannual Technical Summary describes the operation, maintenance and research activities at the Norwegian Seismic Array (NORSAR) for the period 1 Oct 87 - 31 Mar 88.

20. DISTRIBUTION / AVAILABILITY OF ABSTRACT
☐ UNCLASSIFIED/UNLIMITED ☐ SAME AS RPT. ☐ DTIC USERS

21. ABSTRACT SECURITY CLASSIFICATION
UNCLASSIFIED

22a. NAME OF RESPONSIBLE INDIVIDUAL
MAJOR JAMES A. ROBB

22b. TELEPHONE *(Include Area Code)*
(305) 494-7665

22c. OFFICE SYMBOL
AFTAC/TTS

**DD Form 1473, JUN 86** *Previous editions are obsolete.* SECURITY CLASSIFICATION OF THIS PAGE

UNCLASSIFIED

Abstract (cont.)

The NORSAR Dectection Processing System has been operated throughout the reporting period with an average uptime of 96.9 per cent. A total of 1651 seismic events has been reported in the NORSAR monthly seismic bulletin. The performance of the continuous alarm system and the automatic bulletin transfer by telex to AFTAC has been satisfactory. Processing of requests for full NORSAR/NORESS data on magnetic tapes has progressed according to established schedules.

The satellite link for transmitting NORESS data in real time to the U.S. has had an average uptime of 97.7 per cent, with a power break during 16-19 October 1987 being the main contributor to the downtime. On-line NORESS detection processing and data recording at the NORSAR Data Center (NDPC) has been conducted throughout the period, with an average uptime of 95.4 per cent.

The ARCESS array started operation in mid-October 1987, and data have since been recorded and processed off-line at NDPC. As this system has been in an initial phase, there have been several interruptions in data recording, and the monthly average uptimes have ranged from 67.3 to 93.0 per cent.

Field maintenance activity has included regular preventive maintenance at all array sites and occasional corrective actions when required. In particular, much work has been conducted at the ARCESS array site. Among problems encountered, we note in particular that NORSAR subarray 02B had a prolonged outage due to cable and power problems, and that the ARCESS horizontal broad-band instruments have been malfunctioning since they were installed.

A substantial effort has been made to improve the local area network connecting the NDPC computers (IBM, Sun, Vax) and to interface this network to other national and international systems. This work has been important in preparing for future automatic data exchange using telecommunication links, both with the United States and the Nordic countries.

A study has been conducted to determine the achievable P-phase SNR gains at various frequencies for the NORESS array geometry. It has been found that by carefully choosing the proper array subgeometry at different frequencies, gains exceeding 10 dB can be consistently achieved over almost the entire frequency band 0.5 - 10 Hz. The optimum subgeometries are as follows:

0.5 - 1.0 Hz : A0, D-ring (10 elements)
1.0 - 2.3 Hz : A0, C, D-rings (17 elements)
2.3 - 5.0 Hz : A0, B, C, D-rings (22 elements)
5.0 - 10.0 Hz : A0, A, B, C, D-rings (25 elements, i.e., full array)

An assessment has also been made of the processing gains that could be achieved using arrays smaller than NORESS. Thus, for an intermediate array (comprising A0, A,B,C-rings, i.e., 16 elements, 1.4 km diameter) gains exceeding 8 db could be consistently achieved from 1.5 - 10 Hz. For a small array (A0, A,B-rings, i.e., 9 elements, 0.65 km diameter), gains exceeding 6 dB could be achieved from 3 - 10 Hz.

The azimuthal and temporal distribution of low-velocity detections (< 3.0 km/s), which occasionally causes several hundred triggers of the NORESS detector during a single day, have been studied in detail. It has been established that these detections are strongly correlated with increased water flow in the nearby large river Glomma, with arrival azimuth being very consistent over time. Although the exact generation mechanism remains unknown, it is clear that these detections have no tectonic origin, and can therefore be masked from further processing using the phase velocity as a masking criterion.

As part of a project to evaluate the relative precision of 3-component versus vertical component array solutions for event location, the scatter of Pn solutions from 3-component data at different sites within the NORESS array has been studied. A digitized representation of the NORESS topography has been developed and used in conjunction with a recently developed method to synthesize multiple scattering by surface topography. The results suggest that surface topographic relief significantly perturbs the surface particle motion and hence 3-component slowness solutions. The perturbation varies from site to site within the NORESS array, and it also depends on details of the input signal spectrum. On the other hand, the array slowness solution based on vertical component phase delays is relatively stable since the additional phase perturbations are negligible.

The coupling mode technique for modelling surface wave propagation in 2-D structures presented in the previous Semiannual Technical Summary has been applied to a model of the North Sea Graben. The purpose has been to examine how a large-scale and very strong lateral variation of the crustal structure affects the propagation of the short-period surface wavetrains. It appears that the observed extinction of the Lg phase across the North Sea Graben cannot be attributed to coupled mode effects. Thus, some other phenomena, such as a strong attenuation or small-scale heterogeneities able to reflect energy, must be associated with the sedimentary thickening and the Moho uprising to explain the extinction of the Lg phase. On the other hand, results from this study concerning Rayleigh-Love couplings have been found to agree well with observations of anomalously high tranversal motions of Lg wavetrains for explosive sources.

Data from the ARCESS array in conjunction with recordings from the Northern Norway seismic network have been used to assess the seismicity in the surrounding areas. A relatively high seismic activity has been observed along the escarpments and associated fault zones, and in particular the western Barents Sea appears to be exposed to a greater scale of seismicity than earlier known. On the other hand, the southern and eastern parts of the Barents Sea appear to be seismically quiet, with no observed earthquakes during the last year in spite of a detection threshold as low as magnitude 1.5 for that region. A longer time period of observation will be needed to further assess these seismicity data.

Initial analysis of ARCESS recordings has indicated that the propagation of very high frequency signals (> 30 Hz) out to 500 km is similar to, although not quite as efficient as, previously observed for the NORESS array. Nevertheless, significant energy contents beyond 30 Hz is seen for P phases of low magnitude events ($M_L = 2.5$) within this distance range. The propagation of the low-frequency Rg phase is far more efficient at ARCESS than at NORESS, and clear Rg has been observed at distances beyond 400 km, whereas such phases are never seen at NORESS beyond 70-90 km. A detectability study, based on 271 reference events in the Leningrad-Estonia region (mostly mining explosions) has given an estimated 90 per cent P-wave detection threshold for ARCESS of $M_L = 2.5$. The Helsinki seismic bulletin has been used as a reference, and the distance range of the events was 800-1200 km. This compares favorably to the NORESS threshold of $M_L = 2.7$ estimated for a similar epicentral distance range. An assessment of the joint ARCESS-NORESS regional event location capability has shown that for distant events (> 500 km from both arrays) the joint location accuracy is of the order of 30 km, whereas single-array location estimates at such ranges typically are uncertain by more than 100 km.

Recordings of Lg waves from 39 Semipalatinsk explosions have been analyzed for the Gräfenberg array, and compared to similar analyses earlier conducted for NORSAR data. It has been found that Lg magnitude estimates are very consistent for the two arrays, with the standard deviation of the difference being less than 0.05 magnitude units for well-recorded events. Furthermore, the Gräfenberg data analysis has confirmed the previously observed Lg-P anomaly between the northwestern and southeastern parts of the Shagan River test site.

| | | |
|---|---|---|
| AFTAC Project Authorization | : | T/6141/B/PMP |
| ARPA Order No. | : | 4138 |
| Program Code No. | : | 0F10 |
| Name of Contractor | : | Royal Norwegian Council for Scientific and Industrial Research |
| Effective Date of Contract | : | 1 October 1985 |
| Contract Expiration Date | : | 30 September 1988 |
| Project Manager | : | Frode Ringdal (06) 81 71 21 |
| Title of Work | : | The Norwegian Seismic Array (NORSAR) Phase 3 |
| Amount of Contract | : | $ 3,702,816 |
| Contract Period Covered by Report | : | 1 Oct 1987 - 31 Mar 1988 |

This research was supported by the Advanced Research Projects Agency of the Department of Defense and was monitored by AFTAC, Patrick AFB, FL 32925, under contract no. F08606-86-C-0004.

NORSAR Contribution No. 394

# TABLE OF CONTENTS

# I. SUMMARY

This Semiannual Technical Summary describes the operation, maintenance and research activities at the Norwegian Seismic Array (NORSAR), Norwegian Regional Seismic Array (NORESS) and the Arctic Regional Seismic Array (ARCESS) for the period 1 October 1987 - 31 March 1988.

The NORSAR Detection Processing System has been operated throughout the reporting period with an average uptime of 96.9 per cent. A total of 1651 seismic events have been reported in the NORSAR monthly seismic bulletin. The performance of the continuous alarm system and the automatic bulletin transfer by telex to AFTAC has been satisfactory. Processing of requests for full NORSAR/NORESS data on magnetic tapes has progressed according to established schedules.

The satellite link for transmitting NORESS data in real time to the U.S. has had an average uptime of 97.7 per cent, with a power break during 16-19 October 1987 being the main contributor to the downtime. On-line NORESS detection processing and data recording at the NORSAR Data Center (NDPC) has been conducted throughout the period, with an average uptime of 95.4 per cent.

The ARCESS array started operation in mid-October 1987, and data have since been recorded and processed off-line at NDPC. As this system has been in an initial phase, there have been several interruptions in data recording, and the monthly average uptimes have ranged from 67.3 to 93.0 per cent.

Field maintenance activity has included regular preventive maintenance at all array sites and occasional corrective actions when required. In particular, much work has been conducted at the ARCESS array site. Among problems encountered, we note in particular that NORSAR subarray 02B had a prolonged outage due to cable and power problems, and that the ARCESS horizontal broad-band instruments have been malfunctioning since they were installed.

A substantial effort has been made to improve the local area network connecting the NDPC computers (IBM, Sun, Vax) and to interface this network to other national and international systems. This work has been important in preparing for future automatic data exchange using telecommunication links, both with the United States and the Nordic countries.

The research activity is summarized in Section VII. Section VII.1 describes a means of exploiting small-aperture NORESS type arrays for enhanced P-wave detectability. In Section VII.2 sources of short-term fluctuations in the seismic noise level at NORESS are presented. Surface topographic effects on arrays and three-component stations are described in Section VII.3. Section VII.4 takes up the coupling of short period surface wavetrains across the North Sea Graben. In Section VII.5 the seismicity of northern Norway and adjacent areas as inferred from ARCESS and SEISNOR data is outlined. Section VII.6 presents new results from processing of data recorded at the ARCESS regional array. An analysis of Gräfenberg Lg recordings of Semipalatinsk explosions is presented in Section VII.7.

# II. NORSAR OPERATION

## II.1 Detection Processor (DP) Operation

There have been 134 breaks in the otherwise continuous operation of the NORSAR online system within the current 6-month reporting interval. The uptime percentage for the period is 96.9 as compared to 98.9 for the previous period.

Fig. II.1.1 and the accompanying Table II.1.1 both show the daily DP downtime for the days between 1 October 1987 and 31 March 1988. The monthly recording times and percentages are given in Table II.1.2.

The breaks can be grouped as follows:

| | | |
|---|---|---|
| a) | Hardware failure | 18 |
| b) | Stops related to program work or error | 16 |
| c) | Hardware maintenance stops | 3 |
| d) | Power jumps and breaks | 8 |
| e) | TOD error correction | 22 |
| f) | Communication lines | 67 |

The total downtime for the period was 134 hours and 59 minutes. The mean-time-between-failures (MTBF) was 1.3 days, as compared to 2.5 for the previous period.

J. Torstveit

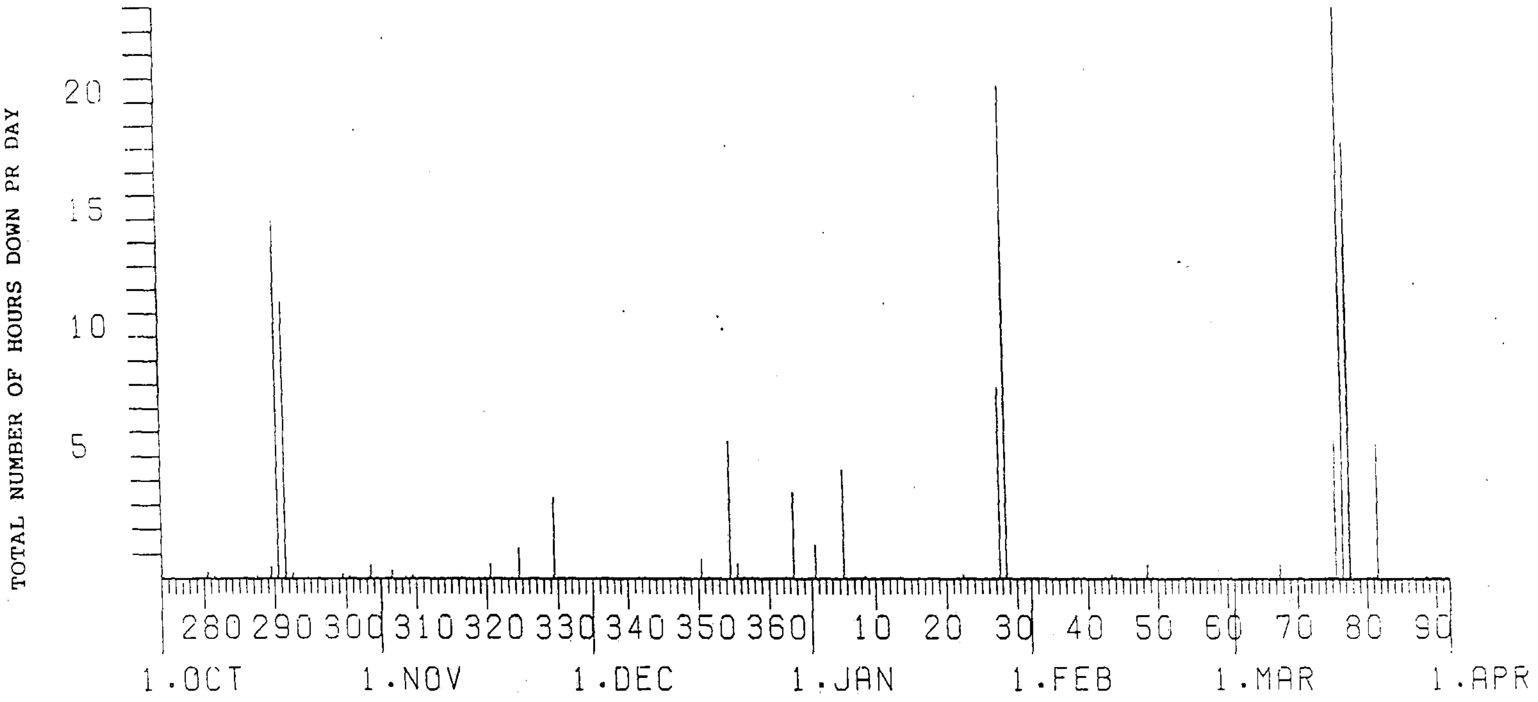

Fig. II.1.1 Detection Processor downtime in the period 1 October 1987 - 31 March 1988.

```
LIST OF BREAKS IN DP PROCESSING THE LAST    HALF-YEAR
DAY    START       STOP     COMMENTS...........

280     9   15      9    30 SERVICE MODCOMP
281    21   50     21    55 LINE FAILURE
287     8   16      8    20 LINE FAILURE
287    14   20     14    22 LINE FAILURE
288     7    7      7     8 LINE FAILURE
288     7   13      7    14 LINE FAILURE
289     9   20      9    32 PROG TEST
289     9   48      9    50 LINE FAILURE
289    15   44     15    57 POWER FAILURE
290     8   50     24     0 POWER FAILURE
291     0    0     11    25 POWER FAILURE
291    20   21     20    22 LINE FAILURE
291    20   44     20    45 LINE FAILURE
291    20   48     20    49 LINE FAILURE
292     7   28      7    29 LINE FAILURE
292    16   59     17    15 POWER FAILURE
293    14   39     14    40 LINE FAILURE
296    11   51     11    52 LINE FAILURE
299     7    9      7    19 TOD FAILURE
299     7   47      7    49 TOD ADJUSTMENT
300     7    7      7     8 TOD RETARED 65MS
300    12   36     12    40 LINE FAILURE
303     7    8      7     9 LINE FAILURE
303     7   36      7    37 LINE FAILURE
303     7   43      7    49 LINE FAILURE
303     7   54      7    56 LINE FAILURE
303    11    0     11    19 POWER FAILURE
303    11   24     11    26 LINE FAILURE
304     9   55      9    56 LINE FAILURE
304    10    0     10     1 LINE FAILURE
306     7   14      7    15 LINE FAILURE
306     7   19      7    20 LINE FAILURE
306     8    1      8    17 POWER FAILURE
308     7    0      7     1 TOD RETARED 13MS
309    12   24     12    31 LINE FAILURE

DAY    START       STOP     COMMENTS...........

309    13    1     13     2 LINE FAILURE
313     7   38      7    39 LINE FAILURE
313     8   44      8    45 LINE FAILURE
313     8   49      8    50 LINE FAILURE
315     7   52      7    53 TOD RETARED 5MS
316    12   59     13     0 LINE FAILURE
320    11   40     12    15 SOFTWARE TEST
322     7    1      7     3 TOD RETARED 11MS
323     7   58      7    59 LINE FAILURE
324    12    9     12    10 CE MAINTENANCE DISK
324    12   27     13    39 CE MAINTENANCE DISK
327     7    1      7     2 LINE FAILURE
327    13   47     13    48 LINE FAILURE
328    12   57     12    59 LINE FAILURE
329     3   44      7     2 POWER BREAK
330     7    0      7     2 LINE FAILURE
333    10   15     10    16 LINE FAILURE
334     7   28      7    29 LINE FAILURE
335     8   10      8    11 LINE FAILURE
335    10   12     10    13 LINE FAILURE
336     7   29      7    30 LINE FAILURE
336    10    1     10     2 LINE FAILURE
338     7    2      7     3 TOD RETARED 10MS
341     8   43      8    44 LINE FAILURE
343     7    1      7     2 TOD RETARED 10MS
347     8   40      8    41 LINE FAILURE
350     9   32      9    46 MODCOMP FAILURE
350    10    3     10    23 MODCOMP SERVICE
350    15   40     15    53 MODCOMP SERVICE
351     7    1      7     2 TOD RETARED 7MS
354    13   54     14     1 SYSTEM SOFT. WORK
354    16    4     20    40 SYSTEM SOFT. WORK
354    22   26     23    23 SYSTEM SOFT. WORK
355     4   52      5    19 SYSTEM SOFT. WORK
355     5   27      5    34 SYSTEM SOFT. WORK
```

<u>Table II.1.1</u> Daily DP downtime in the period 1 October 1987 - 31 March 1988.

LIST OF BREAKS IN DP PROCESSING THE LAST HALF-YEAR

| DAY | START | | STOP | | COMMENTS........... |
|---|---|---|---|---|---|
| 355 | 9 | 53 | 9 | 54 | MODCOMP RESET |
| 356 | 7 | 9 | 7 | 10 | TOD RETARED 11MS |
| 358 | 12 | 22 | 12 | 23 | LINE FAILURE |
| 362 | 8 | 52 | 8 | 53 | LINE FAILURE |
| 363 | 11 | 13 | 12 | 55 | SYSTEM SOFT. WORK |
| 363 | 14 | 16 | 15 | 35 | SYSTEM SOFT. WORK |
| 363 | 15 | 40 | 16 | 9 | SYSTEM SOFT. WORK |
| 1 | 8 | 40 | 9 | 50 | SYSTEM SOFT. WORK |
| 1 | 10 | 43 | 10 | 44 | SYSTEM SOFT. WORK |
| 1 | 10 | 55 | 10 | 57 | SYSTEM SOFT. WORK |
| 1 | 11 | 8 | 11 | 10 | SYSTEM SOFT. WORK |
| 1 | 11 | 45 | 11 | 49 | SYSTEM SOFT. WORK |
| 1 | 11 | 59 | 12 | 1 | SYSTEM SOFT. WORK |
| 4 | 7 | 1 | 7 | 2 | TOD RETARED 22MS |
| 5 | 3 | 8 | 7 | 36 | CPU FAILURE |
| 8 | 7 | 5 | 7 | 9 | TOD RETARED 10MS |
| 9 | 9 | 57 | 9 | 58 | LINE FAILURE |
| 12 | 8 | 48 | 8 | 49 | LINE FAILURE |
| 13 | 7 | 1 | 7 | 2 | LINE FAILURE |
| 21 | 7 | 21 | 7 | 22 | LINE FAILURE |
| 22 | 6 | 28 | 6 | 29 | LINE FAILURE |
| 22 | 6 | 37 | 6 | 42 | LINE FAILURE |
| 22 | 10 | 6 | 10 | 7 | LINE FAILURE |
| 25 | 7 | 0 | 7 | 2 | TOD RETARED 10MS |
| 27 | 8 | 33 | 8 | 34 | LINE FAILURE |
| 27 | 16 | 7 | 24 | 0 | MACHINE FAILURE |
| 28 | 0 | 0 | 20 | 39 | MACHINE FAILURE |
| 32 | 7 | 1 | 7 | 2 | TOD RETARED 12MS |
| 35 | 6 | 44 | 6 | 45 | LINE FAILURE |
| 35 | 13 | 19 | 13 | 20 | LINE FAILURE |
| 39 | 7 | 1 | 7 | 2 | TOD RETARED 10MS |
| 40 | 10 | 3 | 10 | 4 | LINE FAILURE |
| 42 | 7 | 11 | 7 | 12 | TOD RETARED 5MS |
| 43 | 10 | 0 | 10 | 8 | SERVICE MODCOMP |
| 46 | 14 | 26 | 14 | 27 | LINE FAILURE |
| 48 | 11 | 34 | 12 | 8 | POWER BREAK |
| 50 | 9 | 45 | 9 | 47 | LINE FAILURE |
| 53 | 7 | 1 | 7 | 2 | TOD RETARED 10MS |
| 54 | 7 | 1 | 7 | 2 | LINE FAILURE |
| 54 | 10 | 5 | 10 | 6 | LINE FAILURE |
| 55 | 13 | 24 | 13 | 26 | LINE FAILURE |
| 56 | 7 | 53 | 7 | 55 | TOD RETARED 13MS |
| 60 | 7 | 1 | 7 | 2 | TOD RETARED 4MS |
| 63 | 7 | 0 | 7 | 1 | TOD RETARED 10MS |
| 67 | 7 | 0 | 7 | 1 | LINE FAILURE |
| 67 | 7 | 18 | 7 | 50 | POWER FAILURE |
| 67 | 7 | 1 | 7 | 2 | TOD RETARED 20MS |
| 67 | 8 | 21 | 8 | 22 | LINE FAILURE |
| 75 | 12 | 36 | 12 | 37 | MODCOMP FAILURE |
| 75 | 13 | 5 | 13 | 6 | MODCOMP FAILURE |
| 75 | 13 | 7 | 13 | 8 | MODCOMP FAILURE |
| 75 | 13 | 39 | 13 | 40 | MODCOMP FAILURE |
| 75 | 14 | 1 | 14 | 7 | MODCOMP FAILURE |
| 75 | 16 | 25 | 17 | 5 | MODCOMP FAILURE |
| 75 | 17 | 18 | 17 | 36 | MODCOMP FAILURE |
| 75 | 19 | 27 | 24 | 0 | MODCOMP FAILURE |
| 76 | 0 | 0 | 24 | 0 | MODCOMP FAILURE |
| 77 | 0 | 0 | 17 | 30 | MODCOMP FAILURE |
| 77 | 17 | 38 | 18 | 9 | MODCOMP FAILURE |
| 77 | 19 | 10 | 19 | 18 | MODCOMP FAILURE |
| 81 | 6 | 56 | 7 | 0 | CPU FAILURE |
| 81 | 8 | 6 | 13 | 34 | CPU FAILURE |
| 86 | 10 | 24 | 10 | 25 | LINE FAILURE |
| 88 | 6 | 16 | 6 | 18 | TOD RETARED 15MS |
| 88 | 6 | 28 | 6 | 29 | LINE FAILURE |
| 88 | 9 | 46 | 9 | 47 | LINE FAILURE |
| 88 | 12 | 13 | 12 | 14 | LINE FAILURE |
| 89 | 12 | 57 | 12 | 58 | LINE FAILURE |
| 90 | 8 | 3 | 8 | 4 | LINE FAILURE |

Table II.1.1 (cont.)

| Month | DP Uptime hours | DP Uptime % | No. of DP Breaks | No. of Days with Breaks | DP MTBF* (days) |
|---|---|---|---|---|---|
| OCT 87 | 715.30 | 96.1 | 29 | 14 | 1.0 |
| NOV | 714.18 | 99.2 | 23 | 16 | 1.2 |
| DEC | 733.27 | 98.6 | 24 | 14 | 1.2 |
| JAN 88 | 709.35 | 95.3 | 19 | 13 | 1.5 |
| FEB | 695.02 | 99.9 | 16 | 14 | 1.7 |
| MAR | 689.90 | 92.7 | 23 | 16 | 1.2 |

* Mean-time-between-failures = total uptime/no. of up intervals.

Table II.1.2 Online system performance, 1 October 1987 - 31 March 1988.

## II.2 Array communications

Table VII.2.1 reflects the performance of the systems in the reporting period. As in the last reporting period, 04C and 06C have been frequently affected, and in addition the performance of the 02B communications line gradually decreased, until it finally broke down at the end of November 1987.

Although subarray 02B was still down at the end of the reporting period due to lack of power (the CTV has not been accessible due to extremely deep snow in the area and danger of snowslides), the communication lines were declared operational medio March by NTA/Hamar, after 12 km of cables (on poles) had been replaced.

The 02B telemetry station, which has its own power system (solar cells) will as soon as conditions permit be inspected and put back into operation.

Otherwise the performance of the remaining communications systems has been extremely good.

### October

A storm hit the southern part of Norway 16-17 October and damaged 01A, 02B and 06C power lines. By the end of the month, 02B was still out of operation, but 01A and 06C resumed operation 21 and 20 October, respectively. Besides, 04C data were affected by a bad communications cable, causing data spikes. After NTA/Hamar repaired the cable 7 October, the performance improved significantly.

### November

On 13 November 02B was back in operation after a storm had damaged the power line 16-17 October. The same subarray including 02B (telemetry) was affected 25 November by a progressively worse communication cable. In addition, 04C and 06C were affected frequently. Regarding 04C, it was assumed that the reason was varying line and cable quality. It was decided not to ask for NTA engagement before the NMC staff had checked modem, Slem and related equipment first. NTA/Lillehammer measured the 06C line quality (point to point) 11 November and declared it satisfactory. The CTV modem was replaced 12 November, but also afterwards irregularities were observed.

December

NTA/Hamar decided not to repair 02B, including 02B (telemetry) communications line until a decision has been made whether to change part of the line (on poles), or replace the junction boxes along the line. 04C had periods of short outages (week 49), as did 06C.
In order to get 06C back to normal operation, the Modcomp communications processor at NDPC had to be restarted.

January

NTA/Hamar decided to replace part of the communications cable, approximately 12 km, with installation beginning in March. At 04C loss of power occurred due to a broken power line caused by heavy snow. Another problem which was believed to be caused by the CTV equipment (SLEM/Modem or both) had to be investigated very quickly. At 06C a relatively high error rate had been observed week 3 (max. 2.4%). A timing problem had occurred which was compensated for by restarting the communication machine (Modcomp).

February

NTA/Hamar continued their work on subarray 02B regarding replacement of approx. 12 km of communications cable, and expected to complete the work ultimo March. The NMC staff was scheduled to visit 04C in connection with attempts to replace the modem and/or Slem in order to improve the performance of the communications system. However, access to the subarray was hampered by the snow conditions in the area. At 06C resynchronization was also necessary in February.

March

NTA/Hamar finished replacement of 12 km communications cable (on poles) as planned in connection with 02B and 02B (telemetry). Another problem arose, which will delay the final after cable replacement. The power line to 02B is broken, but people from the power plant will not be able to enter the area for a while due to danger of snowslides. 04C was visited 3 and 7 March, and the Slem power supply was replaced with improved performance resulting.

As stated in previous reports, there have been timing problems at 06C. On 15 March the Slem and modem were replaced with successful results.

O.A. Hansen

| Sub-array | OCT 87 (5) (28.9-1.11) | NOV 87 (4) (2-29.11) | DEC 87 (5) (30.11-3.1.88) | JAN 88 (4) (4-31.1.88) | FEB 88 (4) (1-28.2) | MAR 88 (5) (29.2-3.4) | Average ½ yr |
|---|---|---|---|---|---|---|---|
| 01A | 8.97 | 0.01 | 0.03 | 0.02 | 0.03 | 0.07 | 1.52 |
| 01B | 0.08 | 0.05 | 0.03 | 0.06 | 0.05 | 0.06 | 0.05 |
| 02B | *41.8 | *28.14 | *100.00 | *100.00 | *100.00 | *100.00 | *78.32 |
| 02C | 0.04 | 0.02 | 2.87 | 0.02 | 0.02 | 0.41 | 0.56 |
| 03C | 0.05 | 0.02 | 1.46 | 0.02 | 0.03 | 0.07 | 0.27 |
| 04C | 5.64 | 3.32 | 4.42 | *26.07 | *35.93 | 0.87 | *12.70 |
| 06C | *26.44 | *31.56 | 1.93 | 0.76 | 7.66 | 2.31 | *11.77 |
| AVER | 11.86 | 9.00 | 15.82 | 18.13 | 20.53 | 14.83 | 15.03 |
| Less | 01A,02B<br>06C99 | 02B,06C | 02B | 02B,04C | 02B,04C<br>06C | 02B | 02B,04C<br>06C |
|  | 1.45 | 0.68 | 1.79 | 0.17 | 0.03 | 0.63 | 0.60 |

* see item II.2 regarding figures preceded by an asterisk.

Table II.2.1 Communications performance. The numbers represent error rates in per cent based on total transmitted frames/week (1 Oct 87 - 31 Mar 88).

## II.3 Event Detection Operation

In Table II.3.1 some monthly statistics of the Detection and Event Processor Operation are given. The table lists the total number of detections (DPX) triggered by the on-line detector, the total number of detections processed by the automatic event processor (EPX) and the total number of events accepted after analyst review (Teleseismic phases, core phases and total):

| | Total DPX | Total EPX | Accepted events P-phases | Accepted events Core Phases | Sum | Daily |
|---|---|---|---|---|---|---|
| OCT 87 | 13136 | 1601 | 215 | 47 | 262 | 8.5 |
| NOV 87 | 11777 | 1220 | 235 | 54 | 289 | 9.6 |
| DEC 87 | 13692 | 1344 | 183 | 55 | 238 | 7.7 |
| JAN 88 | 13316 | 1239 | 209 | 79 | 288 | 9.3 |
| FEB 88 | 11338 | 1090 | 215 | 44 | 259 | 8.9 |
| MAR 88 | 10942 | 1044 | 262 | 53 | 315 | 10.2 |
| | | | 1319 | 332 | 1651 | 9.0 |

Table II.3.1 Detection and Event Processor statistics, October 1987 - March 1988.

B. Paulsen
B.Kr. Hokland

# III. OPERATION OF NORESS AND ARCESS

## III.1 Satellite transmission of NORESS data to the U.S.

The satellite transmission of data to the U.S. from the NORESS field installation has generally been very stable, except for occasional interruptions due to power breaks. These outage periods are listed in Table III.1.1.

| | | | | |
|---|---|---|---|---|
| 16 Oct 1818 | to | 19 Oct 1422 | due to power break |
| 22 Oct 1415 | to | 1421 | due to power break |
| 24 Oct 1348 | to | 1415 | due to power break |
| 1 Nov 0701 | to | 1100 | due to power break |
| 13 Nov 0104 | to | 1038 | due to power break |
| 13 Nov 1235 | to | 1338 | due to power break |
| 13 Nov 1447 | to | 1514 | due to power break |
| 19 Nov 1141 | to | 1434 | due to power break |
| 22 Nov 0732 | to | 1747 | due to power break |
| 27 Nov 2322 | to | 2328 | due to power break |
| 2 Dec 2302 | to | 3 Dec 0103 | due to power break |
| 10 Jan 1026 | to | 1059 | due to power break |
| 13 Jan 2247 | to | 2256 | due to power break |
| 15 Mar 1250 | to | 1251 | due to Intelsat request |

Table III.1.1 Outage period for the NORESS satellite transmission system October 1987 - March 1988.

The total uptime for the NORESS Earth Station for satellite transmission of data to the U.S. was thus 97.7%. The major contributor to the downtime is the period 16-19 October. The problems during this interval were due to power breaks caused by a severe storm, and it took the local electricity company several days to repair damage to the power lines.

## III.2 Recording of NORESS data at NDPC, Kjeller

The recording of NORESS data at NDPC was affected by the mentioned power outages in the field as well as occasional short outages at NDPC. As documented below, the average recording time was 91% during Oct-Dec 1987, when the system was affected by several power outages. During Jan-Mar 1988, the recording performance was excellent, averaging 99.8%.

The interruptions in recording NORESS data at Kjeller are listed in detail in Table III.2.1, with the nature of the problem indicated.

| Date | Time | Duration | Cause |
|---|---|---|---|
| 5 Oct | 1813-0643 (6 Oct) | 12 h 30 m | Tranmission line failure |
| 5 Oct | 0652-0654 | 2 m | -"- |
| 12 Oct | 0904-0926 | 22 m | -"- |
| 13 Oct | 1203-1226 | 23 m | Service Hub |
| 16 Oct | 1543-1606 | 23 m | Power failure at NDPC |
| 16 Oct | 1617-1627 | 10 m | Power failure at Hub |
| 16 Oct | 2026-1528 (19 Oct) | 67 h 02 m | Power failure at Hub |
| 19 Oct | 1700-1714 | 14 m | Power failure at NDPC |
| 21 Oct | 1415-1425 | 10 m | Transmission line failure |
| 21 Oct | 1430-1433 | 3 m | -"- |
| 21 Oct | 2132-0741 (22 Oct) | 10 h 9 m | Hardware error at NDPC |
| 22 Oct | 1415-1421 | 6 m | Power failure at Hub |
| 24 Oct | 1348-1444 | 56 m | -"- |
| 1 Nov | 0701-1516 | 8 h 14 m | Power failure at Hub |
| 2 Nov | 0801-0822 | 21 m | Power failure at NDPC |
| 2 Nov | 1624-0642 (3 Nov) | 14 h 18 m | Alarm system failure |
| 13 Nov | 0104-0206 | 1 h 1 m | Power failure at Hub |
| 13 Nov | 0546-1039 | 4 h 53 m | -"- |
| 13 Nov | 1224-1230 | 6 m | -"- |
| 13 Nov | 1447-1501 | 14 m | -"- |
| 19 Nov | 1141-1253 | 1 h 12 m | -"- |
| 22 Nov | 0733-1810 | 10 h 43 m | -"- |
| 23 Nov | 1305-1315 | 10 m | Tranmission line failure |
| 25 Nov | 0344-0526 | 1 h 42 m | Power failure at NDPC |
| 25 Nov | 1223-1327 | 1 h 4 m | Maintenance at Hub |
| 25 Nov | 1425-1455 | 30 m | -"- |

| | | | |
|---|---|---|---|
| 2 Dec | 1353-1404 | 11 m | Transmission line failure |
| 4 Dec | 1251-0737 (7 Dec) | 66 h 46 m | Power break modem at NDPC |
| 22 Dec | 0803-0814 | 11 m | Maintenance at NDPC |
| 1 Jan | 0818-1006 | 1 h 48 m | Software error |
| 26 Jan | 1528-1635 | 1 h 7 m | Transmission line failure |
| 17 Feb | 1134-1155 | 21 m | Power failure at NDPC |
| 24 Feb | 1506-1517 | 11 m | Tranmission line failure |
| 7 Mar | 0718-0755 | 37 m | -"- |
| 7 Mar | 0803-0804 | 1 m | -"- |

<u>Table III.2.1</u> Interruptions in NORESS recordings at NDPC, October 1987 - March 1988.

Monthly uptimes for the NORESS on-line data recording task, taking into account all factors (field installations, transmission line, data center operation) affecting this task were as follows:

| | |
|---|---|
| October | 87.6% |
| November | 93.9% |
| December | 91.0% |
| January | 99.6% |
| February | 99.9% |
| March | 99.9% |

Fig. III.2.1 shows the uptime for the data recording task, or equivalently, the availability of NORESS data in our tape archive, on a day-by-day basis, for the reporting period.

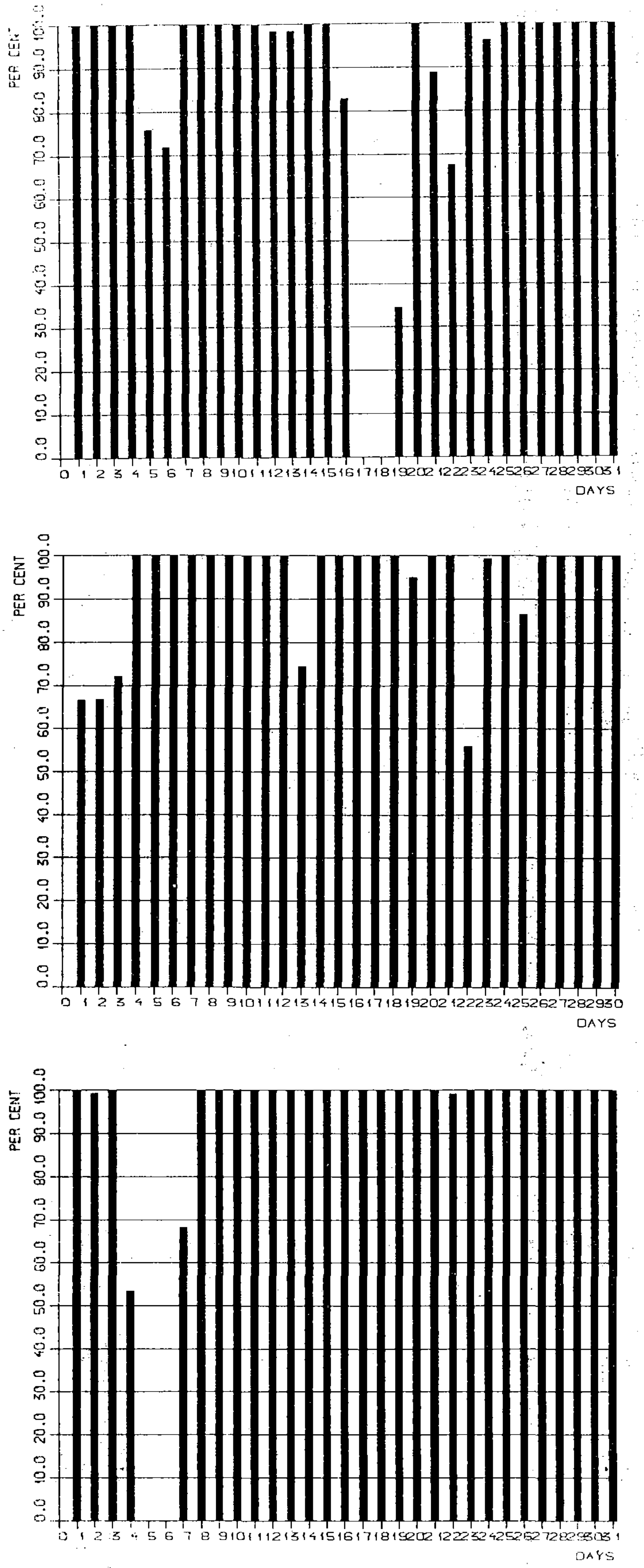

**Fig. III.2.1** NORESS data recording uptime for October (top), November (middle) and December 1987 (bottom).

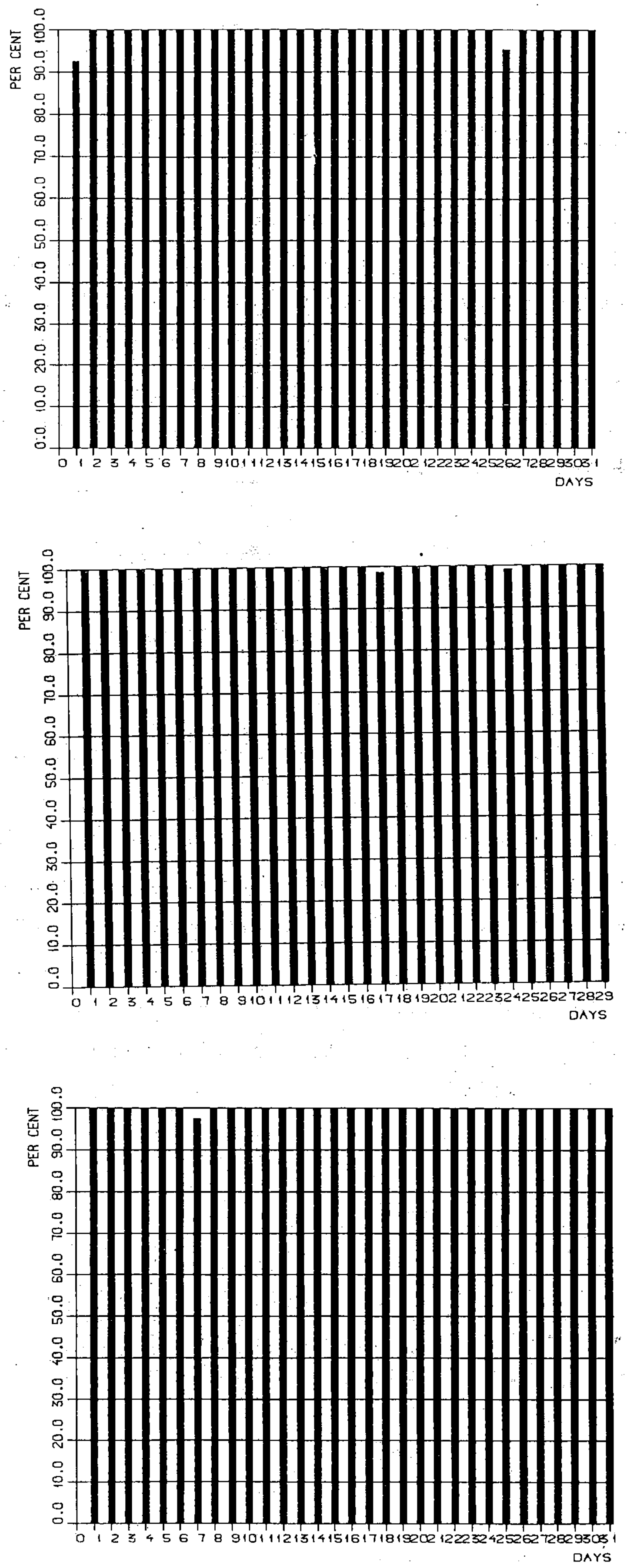

Fig. III.2.1 (cont.) NORESS data recording uptime for January (top), February (middle) and March 1988 (bottom).

## III.3 Recording of ARCESS data at Kjeller

The new ARCESS regional array in Karasjok, county of Finnmark, northern Norway, was installed during the fall of 1987. From mid-October, data from ARCESS have been transmitted continuously to the NDPC at Kjeller, using a Norwegian domestic satellite link. The monthly uptimes for the ARCESS on-line data recording task, taking into account all factors (field installations, transmission line, data center operation) affecting this task were as follows:

October : 48.9% (transmission started on 16 Oct)
November : 80.0%
December : 87.2%
January : 67.3%
February : 93.0%
March : 89.2%

It must be noted that these relatively low recording percentages are due to the system being in an initial phase, and the performance is expected to improve significantly as more experience is gained.

Fig. III.3.1 shows the uptime for the recording task, or equivalently, the availability of ARCESS data in our tape archive, on a day-by-day basis, for the reporting period.

## III.4 Data processing and bulletin transfer

The real time processing of NORESS data, using the RONAPP processing package, has continued during the reporting period. 24,305 detections were declared by the automatic processor during October 1987 - March 1988.

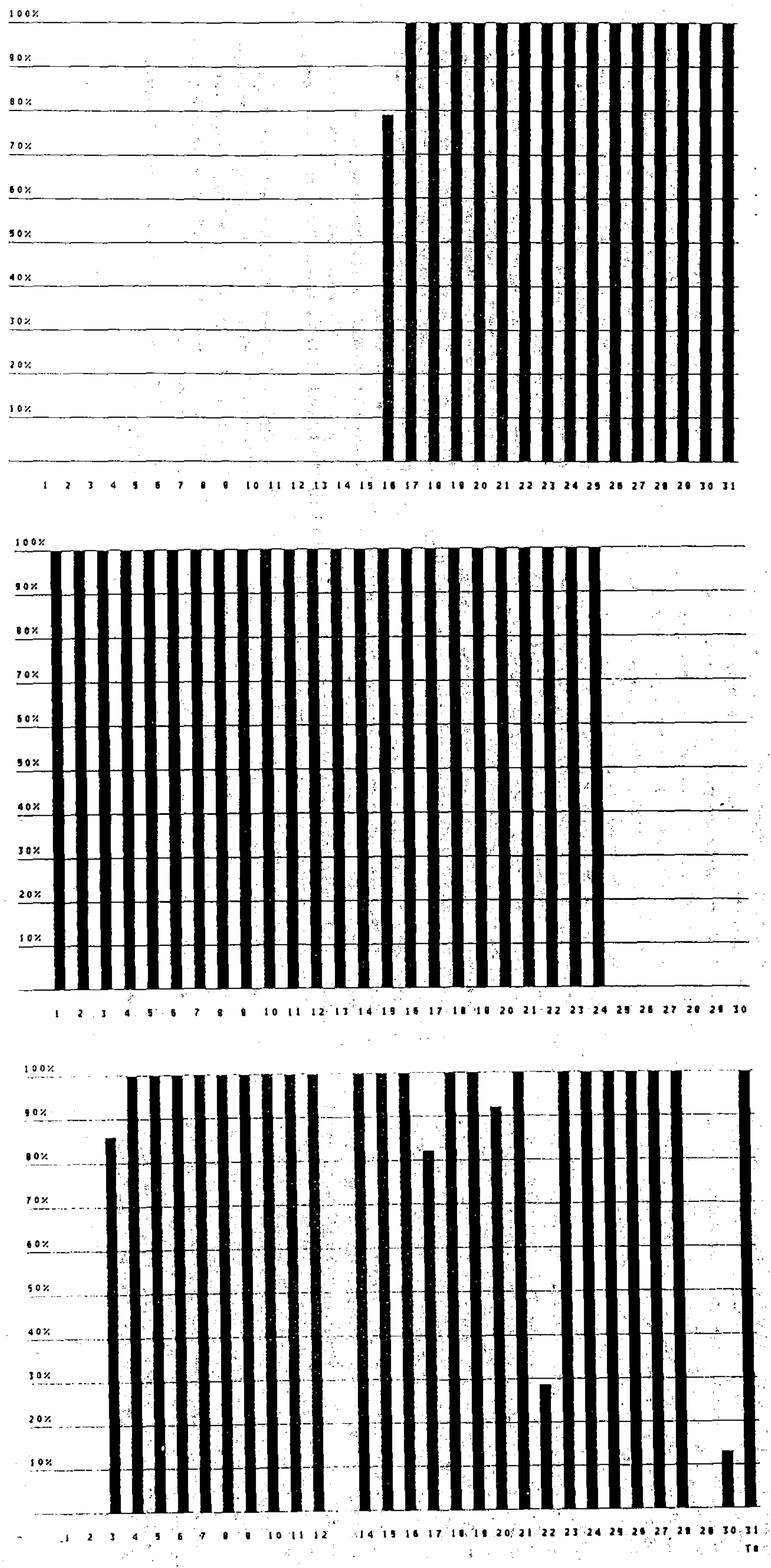

Fig. III.3.1 ARCESS data recording uptime for October (top), November (middle), and December 1987 (bottom).

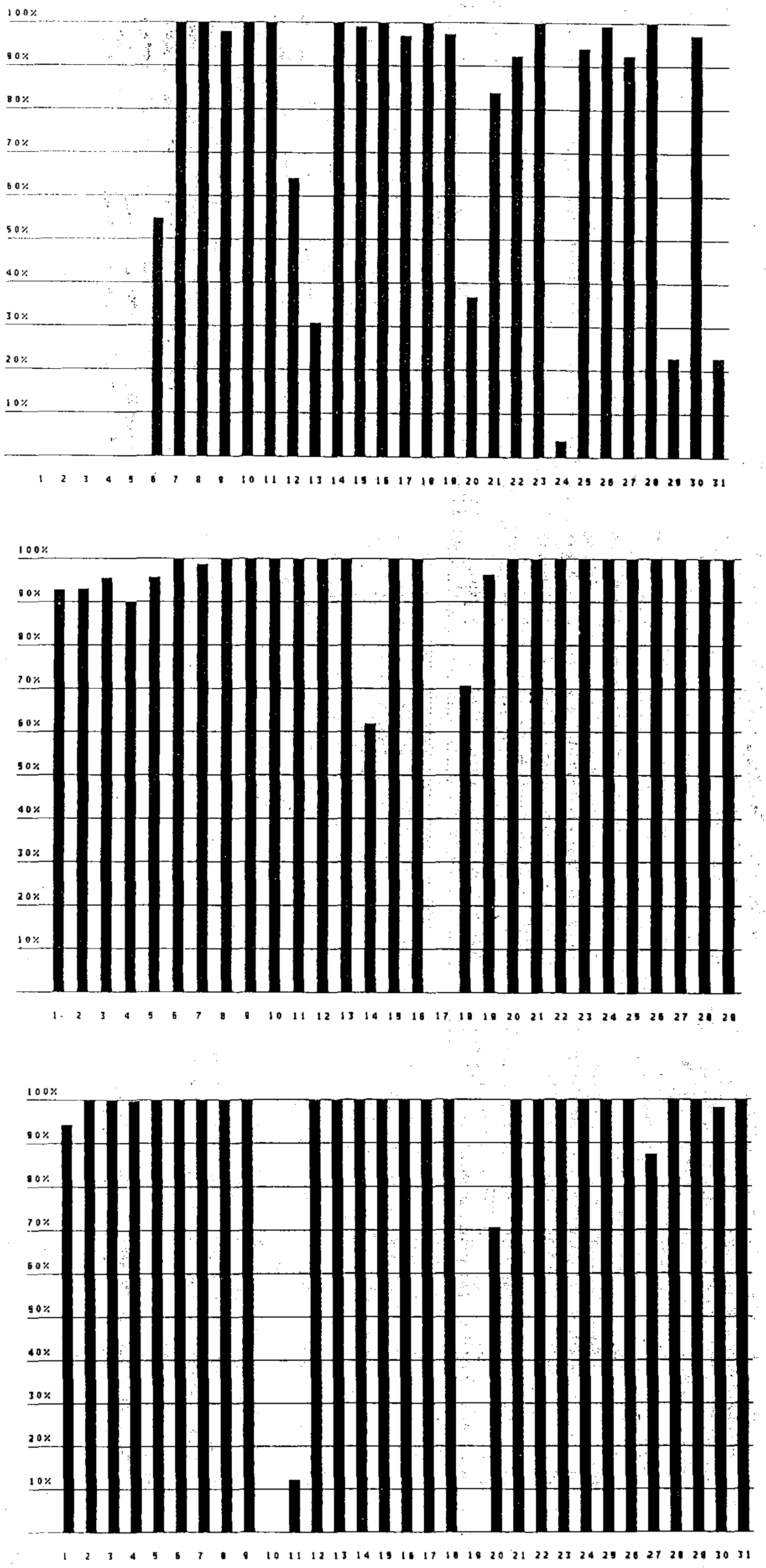

Fig. III.3.1 (cont.) ARCESS data recording uptime for January (top), February (middle) and March 1988 (bottom).

The bulletin with processing results for NORESS has been transmitted daily to the Center for Seismic Studies in Rosslyn, Virginia, via the ARPANET.

The processing of ARCESS data has during this initial period been done in an off-line mode, and listings of detections on ARCESS for the reporting period are available. The complete real time processing of ARCESS data awaits the installation at Kjeller of a new Sun-based data processing system, expected to be completed during the summer of 1988.

J. Torstveit
O.A. Hansen
S. Mykkeltveit

## IV. IMPROVEMENTS AND MODIFICATIONS

During the reporting period, the main efforts regarding system modifications and improvements have been devoted to the ARCESS array, in order to establish reliable operation, data transmission, recording and on-line processing of this system. These tasks have comprised:

- Establishment of a domestic 64 Kbps dedicated satellite link from the field site to Kjeller
- Interfacing the satellite link to the ARCESS Hub station and to the NDPC Sun computer system, in cooperation with Sandia and Science Horizons personnel
- Establishing reliable data recording and system monitoring at NDPC using the Sun computers
- Implementing an off-line detection processing system for ARCESS, using the IBM 4381 to process data from magnetic tape input
- Making several modifications and improvements in the field system, as described in Section V, in order to ensure data integrity.

At the end of the reporting period, the ARCESS data acquisition system at NDPC was still based on a temporary solution, using a Sun-2 computer on loan from Science Horizons. Plans for upgrading the computer equipment and including on-line detection processing in a larger Sun-based system have been developed and will be implemented when the scheduled delivery of additional computer hardware is completed (Summer 1988).

Another significant effort has been to improve the local area network connecting the NDPC computers (IBM, Sun, Vax) and interfacing this internal network to other national and international systems. The main purpose is twofold: first to enable easy communication between the NORSAR, NORESS and ARCESS recording systems at NDPC, and, second, to prepare for future seismic data exchange by telecommunication means, both to other Nordic countries and to the United States.

Fig. IV.1 shows the main computer systems at NDPC and how they are connected together through Ethernet and PRONET. NORSAR is also connected to other institutions in the area as indicated. NORSAR is the responsible institution for ARPANET in Norway, and a 64 Kbps satellite link is used for transmitting data from Norway to USA. The other 64 Kbps satellite link shown on the figure will be up and running in October this year. This link will be used to connect the Ethernet at the Center for Seismic Studies with an Ethernet at NORSAR in connection with the planned Intelligent Array System. A third satellite connection not shown on the figure is used for transmitting data from ARCESS to NORSAR.

The NORSAR local area network is based on the TCP/IP protocol which is supported by most computer manufacturers. This protocol gives us the possibility for electronic mail, file transfer and remote login. The file transfer utility is used daily to transfer results from NORESS and ARCESS to CSS. The TCP/IP protocols allow our IBM mainframe to transfer data directly to the VAX/UNIX computers at CSS.

R. Paulsen
F. Ringdal
S. Mykkeltveit
P.W. Larsen
J. Fyen

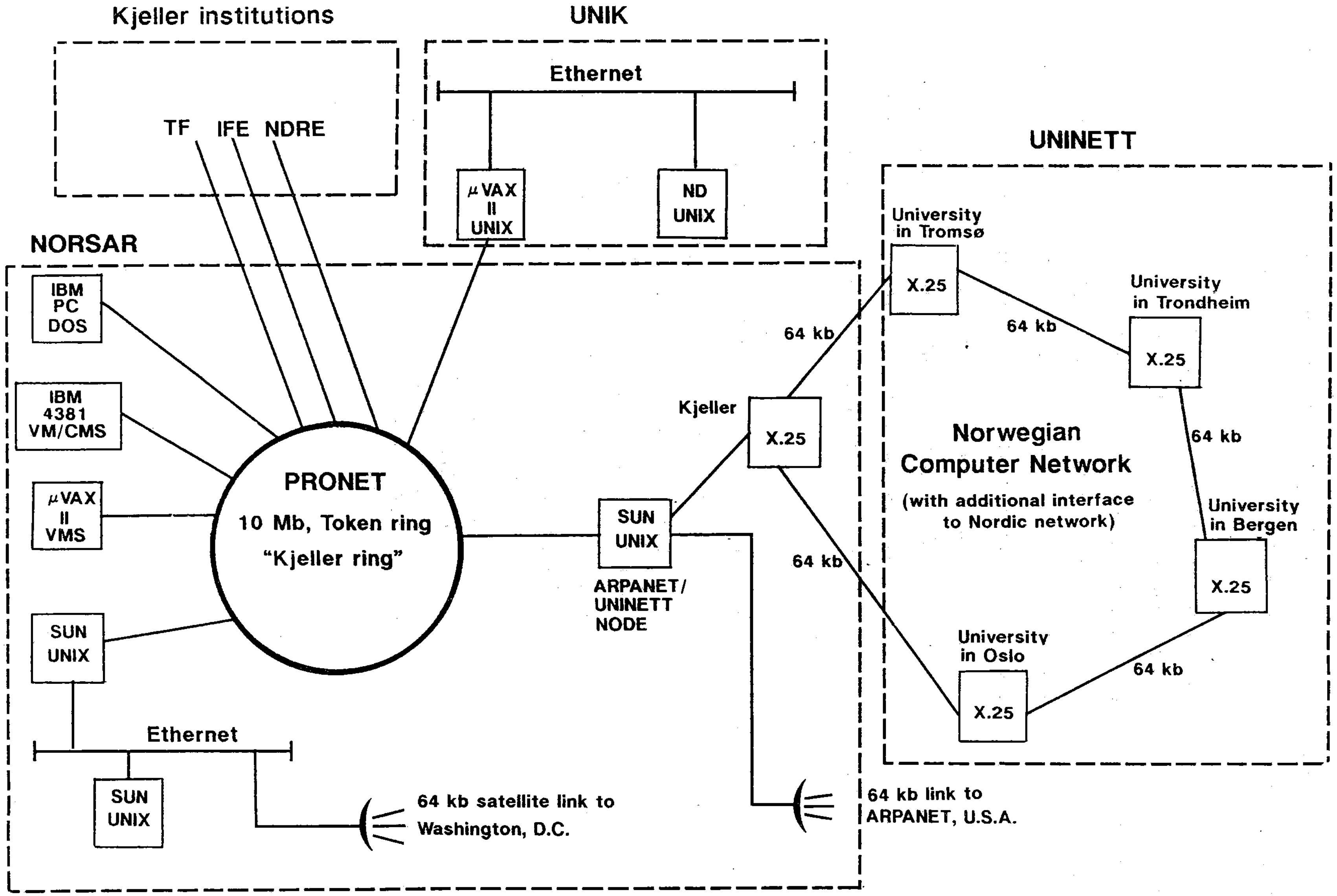

Fig. IV.1 Schematic view of the NORSAR local area network and its external interfaces.

# V. MAINTENANCE ACTIVITIES

## V.1 Activities in the field and at the Maintenance Center

This section summarizes maintenance activities undertaken in the field and at the NORSAR Maintenance Center (NMC) at Hamar.

For the NORSAR and NORESS arrays, these activities have been mostly limited to routine maintenance functions. In the case of the new ARCESS array, several system modifications have been necessary in the initial operative phase. The following general comments apply, with additional details given in Table V.1.

The subarray electronics have been monitored regularly from the NDPC, as have the communications systems. Repairs of various components, adjustments of gains and LP mass positions and system restarts after power failures have been undertaken as listed in Table V.1.

NORESS
On Oct 2, the TWTA gain of the NORESS satellite ground station for transmission of data to the U.S. was increased by 5 dB.

On a few occasions, it has been necessary to restart the high-frequency system manually following power outages.

ARCESS
During a vist 14-17 October, the polarities of the clock pulses from the Communications Interface Module (CIM) were reversed. During the same visit, it was found necessary to mount the Hub 69 card outside the Hub rack, because this card picked up the noisy clock pulses from the CIM, which in turn created a severe loss of data. Some of the channels having many errors were adjusted, and reduced error rates were

obtained. For site A0 the data transmission to the Hub building was changed to a spare fiber.

During a visit 27-30 October, it was found that the CIM processor for array data was malfunctioning. A new card was constructed at the site from a couple of spare cards.

Problems related to difficulties in receiving timing signals via radio made it necessary to move the receiving antenna during a visit 10-11 December. On the same visit, a unit (which had been borrowed) for satellite reception of such timing signals was tested and found to work satisfactorily. Such a unit will be acquired for the ARCESS site and installed during the summer of 1988. For site C6, a change was made to the spare fibers.

The UPS has failed on a couple of occasions, and repair services by the vendor have been necessary.

A power supply that failed on 1 January was replaced.

| Subarray Area | Task | Date |
|---|---|---|
| 01A | Slem reset after power failure | 21 Oct |
| 01B | Preventive maintenance carried out, beside adjustment of SP/LP equipment | 21 Oct |
| 02B (tel) | Channel 3 dead, seismometer cable replaced | 20 Oct |
| 02C | Preventive maintenance incl. adj. of SP/LP equipment | 13 Oct |
| 06C | Slem reset after power failure | 20 Oct |
| 06C | Preventive maintenance incl. adj. of SP/LP equipment | 14, 22 Oct |
| NORESS | Restart of HF-system after power outage | 26 Oct |
| ARCESS | Visits in connection with system outages and readjustments (weeks 42 and 44) | Oct |
| NDPC | Daily check of SP/LP data. Weekly calibration SP/LP seismometers. | Oct |
| 01A | Adjusted Mass Position (MP) Vert., NS and EW, Free Period (FP) Vert. seismometers | 9 Nov |
| 02B | LP instruments checked. Adjusted MP NS, EW and FP EW. All channels were checked regarding SP gain and offset. | 4 Nov |
| 02B (tel) | Amplifier channel 28 reinstalled after repair | 6 Nov |
| 04C | Survey together with the highway authorities in connection with localizing cable trenches along the road in Julussdalen | 3 Nov |
| 04C | Julussdalen. Due to changes in road structure, seismic and comm. cables were cut and extended by approx. 40 meters | |
| 06C | The modem was replaced | 9 Nov |
| 06C | Modem installed 9 Nov failed and was replaced | 12 Nov |

| Subarray Area | Task | Date |
|---|---|---|
| NORESS | Site D6 was out of operation while the cable between Hub and vault was temporarily repaired | 12 Nov |
| FINESA | NMC staff carried out extension of the array in Finland | 17,18,19 Nov |
| NORESS | HF equipment hooked up to the uninterruptible Power Supply (UPS) | |
| NDPC | Daily check of SP/LP data. Weekly calibration of SP/LP seismometers carried out | Nov |
| ARCESS | In connection with loss of carrier to the clock, antenna position was changed, the receiver was adjusted. Beside a fiber optic cable on site C6 was replaced | 3,4 Nov |
| NMC | At the NMC DDS 1105 Data Acquisition System was overhauled and repaired | Dec |
| NDPC | Daily check of SP/LP data. Weekly calibration of SP/LP seismometers carried out | Dec |
| NORESS | In the LPV a transfomrer caused noise on HF channels | 15 Dec |
| | | <u>1988</u> |
| 04C | The subarray was visited in connection with loss of power and line check | 25,27 Jan |
| ARCESS | Lack of 28 Volt DC fed from common power source in the Hub caused system outage | 6 Jan |
| FINESA | DDS 1105 reinstalled and put into operation after expension mentioned under item 1 | 13 Jan |
| NDPC | Daily check of SP/LP data. Weekly calibration of SP/LP seismometers carried out | Jan |
| | Data acquisition and channel analysis pertaining to the SP channels 01A,01B, 02C, 03C and 06C. | Jan |

| Subarray Area | Task | Date |
|---|---|---|
| NDPC | On the same subarrays, plus 04C, data acquisition and analysis have been carried out in order to verify the A/D convertors' ability to reproduce all possible numbers within a given range. | Jan |
| NMC | Instrumentation repair/maintenance. Different activities | Feb |
| NDPC | Daily check of SP/LP data and com. systems. Weekly calibration of SP/LP seismometers. Adjustment/measurements of LP seismometers with respect to MP and FP | Feb |
| 04C | The Slem power supply was replaced, and on the SP channels gain and DC offset were adjusted | 3,7 Mar |
| 06C | A new modem and Slem were installed | 15 Mar |
| NORESS | New Hub 15 card installed at CID 21 due to a high failure rate between remote site and the Hub unit | |
| ARCESS | The system had to be restarted after a failing UPS (Uninterruptible Power Supply) | 12 Mar |
| NDPC | Daily check of SP/LP data and com. system. Weekly calibration of SP/LP seismometers, and adj./measurements with respect to MP and FP carried out. | Mar |

Table V.1 Activities in the field and the NORSAR Maintenance Center, including NDPC activities related to the NORSAR array, 1 October 1987 - 31 March 1988.

## V.2 Array status

**NORSAR**

No changes or modifications have been carried out since the last report.

As of 31 March 1988 the following channels deviated from tolerances:

| | | |
|---|---|---|
| 01A | 01 | 8 Hz filter |
| | 02 | 8 Hz filter |
| | 04 | 30 dB attenuation |
| 01B | 05 | |
| 04C | 01 | |
| | 08 | |
| 06C | 04 | |
| | 05 | Broadband filter installed |
| | 06 | |

**NORESS**

As of 31 March 1988, all channels were within specified tolerances.

**ARCESS**

As of 31 March 1988, all channels were within specified tolerances, except the two horizontal broadband components, which were inoperative.

P.W. Larsen
O.A. Hansen

## VI. DOCUMENTATION DEVELOPED

Fyen, J. (1988): Diurnal and seasonal variations in the macroseismic noise level observed at the NORESS array. Submitted Phys. Earth Planet. Inter.

Kvamme, L. and J. Havskov: Q in southern Norway. Submitted to Bull. Seism. Soc. Am.

Kværna, T.: Sources of short-term fluctuations in the seismic noise level at NORESS. Submitted to Phys. Earth Planet. Inter.

Loughran, L.B. (ed.): Semiannual Technical Summary, 1 Apr - 30 Sep 1987, NORSAR Sci. Rep. 2-86/87.

Mykkeltveit, S., J. Fyen, F. Ringdal and T. Kværna: Spatial characteristics of the NORESS noise field and the implications for array detection processing. Submitted to Phys. Earth Planet. Inter.

Paulsen, R.: State of Health System NORESS/ARCESS. NORSAR Tech. Rep. 1/88.

Ringdal, F., S. Mykkeltveit, J. Fyen and T. Kværna: Spectral analysis of seismic signals and noise recorded at the NORESS High Frequency Element. Submitted to Phys. Earth Planet. Inter.

# VII. SUMMARY OF TECHNICAL REPORTS / PAPERS PUBLISHED

## VII.1 On exploitation of small-aperture NORESS type arrays for enhanced P-wave detectability

### Introduction

Under potential future nuclear test bans, small-aperture NORESS type arrays can provide significant contribution to the performance of the monitoring system. By their ability to detect, locate and characterize weak seismic signals, the probability of a successful treaty evasion can be considerably reduced.

In this paper, we concentrate on the detection aspect of small-aperture (regional) arrays, and focus on detection of primary phases preceded by pure noise. By beamforming, we can exploit the incoherent structure of seismic noise and the coherent structure of P-arrivals to enhance the signal-to-noise ratio (SNR). On the other hand, detection of secondary phases from events at regional distances (up to 2000 km) will not be addressed in this paper, since they in most cases are not embedded in pure noise, but in the relatively coherent coda of the preceding signal arrivals. SNR enhancement by beamforming will not be efficient for these phases unless the single station noise level is higher than the coda level. Under such conditions, the noise can be efficiently suppressed until the level of the underlying coda is reached.

To realistically assess the potential of the NORESS array for event detection, it is necessary to compute the actual beamforming gains for a variety of representative seismic signals. From such calculations, the objective is to infer the best set of beams for the detection of regional and teleseismic P-waves. The results from this study can then be applied to other arrays of the NORESS type.

## NORESS design considerations -- a brief review

The design of the NORESS array involved balancing of several partly conflicting demands on array performance. For details, see Followill and Harris (1983), and Mykkeltveit (1985).

Under the condition of equal signal and noise amplitudes at each sensor, we can express the beamforming gain G by the normalized zero-lag cross-correlations via the formula:

$$G^2 = \sum_{i,j=1}^{N} C_{ij} \Big/ \sum_{i,j=1}^{N} \rho_{ij}$$

where $C_{ij}$ is the signal correlation between sensors i and j, and $\rho_{ij}$ is the corresponding noise correlation. Numerical models for these correlations as a function of intersensor separation were constructed for several filter bands based on data from a provisional installation at NORSAR subarray 06C, see Mykkeltveit et al (1983). Some important findings from these investigations were that the noise correlation curves consistently had negative minima at certain interstation separations before tending to zero at larger separation distances, while the signal correlations degraded continuously as the distances increased, see Fig. VII.1.1. These results indicated a possibility for noise suppression in excess of $\sqrt{N}$ which is the theoretically expected value if all noise cross-correlations were 0. If the signal decorrelation was sufficiently small, SNR gains also in excess of $\sqrt{N}$ could be obtained.

In addition to the constraint that the array should have an equal capability to process signals from all directions (symmetry), it was required that the SNR enhancement (gain) by beamforming should be close to optimum for a wide range of frequencies (1-10 Hz). It was then realized that the array should consist of instruments where a large span of intersensor separations were represented, and that sub-configurations of the array must be used to detect different phases in different frequency bands. This study deals with how one should exploit the sub-configurations to achieve the best SNR gain for P-phases in different frequency bands, and to quantify the gain values.

The array's ability to estimate the apparent velocity and azimuth of seismic signals, to resist spatial aliasing, to properly sample the wavefield and to have an option for a good three-component subarray were also considered important factors in the design work. From the criteria outlined above, it was decided to build an array with a geometry based on four concentric rings spaced at log-periodic intervals in radius R, according to the relation:

$$R = R_{min} \cdot \alpha^n, \quad n = 0,1,2,3, \quad R_{min} = 150 \text{ m}, \quad \alpha = 2.15$$

The final configuration of the NORESS array, shown in Fig. VII.1.2, has 3 elements in the innermost ring called the A-ring (radius 150 m), 5 elements in the B-ring (radius 320 m), 7 in the C-ring (radius 690 m), 9 in the D-ring (radius 1490 m), plus one in the center, called A0. A0, C2, C4 and C7 are all equipped with three-component instrumentation.

**Data analysis procedure**

Applying a short-term to long-term average (STA/LTA) algorithm to a set of filtered beams has proved to be a robust and reliable way of detecting seismic signals. In this study we want to link the calculation of SNR gain, noise suppression and signal loss by beamforming to the current operational detection algorithm, and hence avoid indirect measurement methods. The analysis procedure has been as follows:

1. Twelve partly overlapping filter bands that in our general experience have appeared most appropriate for regional and teleseismic P-wave detection were defined, see Table VII.1.1.

Three years of routine processing of regional array data from NORESS have shown that P-waves can have dominant frequencies varying from below 1.0 Hz to well above 10 Hz. This observation together with results from a previous study by Kværna and Mykkeltveit (1986), formed the basis for the selection of the filter bands.

2. From the 25 short-period vertical component instruments of the NORESS array, ten sub-geometries that appeared reasonable in the detection process were used to form beams in the respective twelve filter bands. These sub-geometries were symmetric, so all elements of each array ring had either weight 1 or weight 0, see Table VII.1.2.

3. For each of the twelve frequency bands, five high SNR regional and/or teleseismic P-wave signals were selected, see Table VII.1.3. The events were all found by searching through the bulletins generated from real-time processing of NORESS data. Events with peak signal frequencies close to the lower cutoff of the bands were chosen. This was done in order to ensure that the signal was analyzed in the band for which the SNR for that signal attains its maximum value. The approach chosen satisfied this requirement, since the noise amplitudes almost always decrease monotonically with increasing frequencies in the range of interest for this study.

   In the search for representative events for each filter band, it turned out, as expected, that teleseismic events fully dominated the frequency range up to 2 Hz. In the range between 2 and 5 Hz, both teleseismic and regional events were present, whereas teleseismic events were almost absent for frequencies above 5 Hz.

4. The beamforming steering delays for all events were calculated using the wide-band slowness estimation method (Kværna and

Doornbos, 1986). The apparent velocity and azimuth of each P-phase was estimated by processing all 25 channels in the frequency band representative for that event, see 3) above.

5. All events were then subjected to STA/LTA detection processing using a new program system developed at NORSAR (Fyen, 1987). The SNR, STA and LTA detection values for all beams as well as for all single channels were stored to compute the SNR gain, noise suppression and signal loss. The SNR (STA/LTA) gain was defined as the SNR of the beam divided by the average SNR of the single channels applied in the beamforming. The corresponding noise suppression was defined as the average LTA of the single channels applied in the beamforming divided by the LTA of the beam, while the signal loss was defined as the similar ratio of STA values. When expressing the values in decibels, the following relation holds:

$$\text{SNR gain} = \text{Noise suppression} - \text{Signal loss}$$

Table VII.1.4 shows the output from processing one of the sixty events in the data base.

**Detailed presentation of results for two geometries**

When plotting the noise suppression values for all events as a function of the lower cutoff of the filter band applied in the analysis, we get for the full array configuration (A0Z, A-ring, B-ring, C-ring and D-ring) the representation shown in Fig. VII.1.3a. As seen from the spread of the five values of each filter band, some averaging must be done to produce meaningful results. Some of the filters show differences up to 5 dB. After calculating the mean of the values within each of the twelve passbands and introducing some slight smoothing, the curve in Fig. VII.1.3a was obtained. Rather than progressing with the discrete measurement points, we will mostly present and apply the smoothed curves in the following presentation and discussion.

In the full array configuration, a large span of intersensor separations are represented. As seen from Fig. VII.1.3a, the $\sqrt{N}$ noise suppression level was not reached for frequencies below 3.5 Hz. This is due to the fact that at such frequencies, the noise is correlated between some of the sensors, and even though some of the sensor pairs produce negative correlations, the total noise suppression does not reach the $\sqrt{N}$ level (13.98 dB for 25 sensors).

The noise suppression for the sub-geometry A0Z, C-ring and D-ring is given in Fig. VII.1.3b. In contrast to the results using the full array, we here achieved values in excess of $\sqrt{N}$ (now 12.3 dB for 17 sensors) in the frequency band 1 to 4 Hz. For this sub-geometry, only relatively large intersensor separations (700 m or more) are represented, which in the band 1 to 4 Hz have negative noise cross-correlations. Negative cross-correlations imply destructive interference when forming a beam. Above 4 Hz the noise suppression curve approaches the $\sqrt{N}$ level, which is consistent with an assumption of uncorrelated noise.

Figs. VII.1.3c and VII.1.3d give the signal loss for the two configurations discussed above. The signal losses are less than 1 dB for frequencies up to about 3 Hz, at which point the signal decorrelation starts to increase for both configurations.

Finally, the SNR gain curves are given in Figs. VII.1.3e and VII.1.3f. The full array does not reach the $\sqrt{N}$ level for any frequency. When the noise suppression finally reaches this level at about 3.5 Hz, the signal loss is exceeding 1.5 dB. For the sub-geometry A0Z, C-ring and D-ring the signal loss is negligible between 1 and 3 Hz. In this frequency band, the noise suppression is exceeding $\sqrt{N}$, and the SNR-gain is therefore also exceeding this value.

## Composite gain curves

In determining which sub-geometry should be utilized to achieve optimal beamforming gain in the different frequency bands, it is necessary to directly compare the absolute gain values. The question of beamforming gain relative to $\sqrt{N}$ serves more as an indicator of the noise field characteristics, and is therefore more relevant in the array design phase. Now, it turns out that in order to cover the entire 0-10 Hz band, only four different sub-geometries (out of the ten considered) are needed, and each of which provides the highest absolute SNR gain within a certain frequency interval. This result is presented in Fig. VII.1.4 in the form of a composite gain curve, along with the corresponding composite curves for the noise suppression and signal loss. The following comments apply regarding the four frequency intervals given in Fig. VII.1.4.

0.5-1.0 Hz: To guard against the relatively high noise spectral level in the lower part of this band, the NORESS system response is designed with a strong rolloff. Therefore the dominant recorded noise amplitudes seldom have frequencies below 0.8 Hz, so a filter band, e.g., from 0.8 to 1.6 Hz would probably produce similar results. Nevertheless, for frequency bands with lower cutoffs below 1.0 Hz, the AOZ, D-ring configuration is capable of producing array gains between 9 and 12 dB. The signal loss is negligible in this frequency band.

1.0-2.3 Hz: For detection of the teleseismic signals that are abundant in this frequency range, beamforming applying the AOZ, C-ring and D-ring geometry provides SNR enhancement of about 13 dB. Under favorable noise conditions, almost 15 dB has been measured. The signal loss is less than 1 dB, and the noise suppression is well above the $\sqrt{N}$ level of 12.3 dB (17 sensors).

2.3-5.0 Hz: Intersensor separations introduced by adding the B-ring enhance the noise suppression for frequencies above 2.3 Hz, so the SNR gain is still kept at about 13 dB out to about 3.5 Hz. Between 3.5 and 4.0 Hz, the signal loss increases sharply to more than 2 dB, and the best SNR gain curve produced by the A0Z, B-ring, C-ring and D-ring subgeometry drops to about 11 dB at 5 Hz.

5.0-10.0 Hz: The full array noise suppression stays at the $\sqrt{N}$ level (13.98 dB) in almost the entire band. Even though the signal decorrelation starts to be significant for frequencies above 6 Hz, the full array provides the best SNR gain all the way out to 10 Hz. The gain values stay at about 11 dB from 5 to 7 Hz, and then drop to 8.5 dB at 10 Hz.

### Comparison of different array geometries

The main emphasis of this study has been on determining optimum subgeometries in various frequency bands and corresponding SNR gains for a full NORESS-type array. However, the study has in addition provided a basis for comparing the projected performance of regional arrays of different sizes. Thus, we have compared optimum SNR gains for the following three arrays:

i) A full regional array (NORESS type)
Diameter: 2980 m
Number of instruments: 25
Geometry: A0Z, A-ring, B-ring, C-ring, D-ring

ii) An intermediate regional array
Diameter: 1390 m
Number of instruments: 16
Geometry: A0Z, A-ring, B-ring, C-ring

iii) A small regional array

Diameter: 650 m
Number of instruments: 9
Geometry: A0Z, A-ring, B-ring

SNR gains by the full array have already been discussed. For the intermediate and small arrays, processing to determine optimum SNR gains was done as for the full array, but taking into account only those instruments included in the respective array configurations.

First we consider the intermediate array, i.e., all subgeometries with the D-ring excluded. The results given in Fig. VII.1.5a are consistent with the findings when processing the full array, see Fig. VII.1.4. Out to 2.3 Hz, the A0Z and C-ring is the best sub-geometry, then the B-ring instruments start to contribute positively and gain values between 10 and 12 dB are achieved to about 5 Hz. In the frequency band 5 to 10 Hz, all available rings (A0Z, A-ring, B-ring and C-ring) should be included.

In analyzing the performance of the small array, we excluded both the C-ring and the D-ring in the selection of sub-geometries. From Fig. VII.1.5b, it turns out that 6.5 to 8 dB SNR gain is produced between 3.5 and 10 Hz. The best sub-geometry below 5 Hz comprises A0Z and the B-ring, whereas the A-ring starts to contribute positively above 5 Hz. Again, this frequency dependency of the optimum sub-geometry is consistent with the overall trend noticed for the full and intermediate arrays.

## Conclusions

This study has demonstrated that the NORESS array geometry provides P-phase signal-to-noise ratio (SNR) gains (relative to the average single sensor) of 10 dB or more over almost the entire frequency range 0.5-

10 Hz, the only exception being slightly lower gains at the low and high end of this band.

In the frequency range 1-4 Hz, which is by far the most important both for regional and teleseismic P-phase detection, these gains are consistently as high as 12-14 dB, i.e., 0.6-0.7 $m_b$ units. Such an excellent performance over a wide range of frequencies is to our knowledge unmatched by any previous array design.

As described in this paper, and illustrated in Fig. VII.1.4, these SNR gains are obtained through beamforming on selected subarrays, where the choice of subarray is governed exclusively by the frequency range considered.

As expected, some of the rings produce intersensor separations that should be avoided for certain frequency rantges. Below 1.0 Hz, all instruments except A0Z and the D-ring produce positive noise correlations and were therefore excluded. At 1 Hz, the C-ring starts to contribute to an increased SNR gain, at about 2.3 Hz, the B-ring and finally at 5 Hz, the A-ring.

The main reason why the subsets of the array, at lower frequencies, outperform the full array lies in the spatial noise correlation properties. As is well known, the beam SNR may actually deteriorate if too many highly correlated sensors are included in the beamforming process. The procedure outlined in this paper, where a number of different bandpass filters are applied in parallel, and the beams are based on the best sub-geometry for each frequency band, ensures excellent SNR gain and signal detection performance at all frequencies.

A comparison of the projected overall performance of the full NORSESS array and two smaller arrays (denoted the intermediate and small array, respectively) has been carried out. The results, as summarized in Fig. VII.1.6, are as follows:

The intermediate array provides SNR gains relative to the average single sensor that exceed 8 dB in the 1.5-10 Hz frequency range. Thus, such an array would be very capable for regional P-phase detection, although somewhat inferior to the full NORESS-type array. The degradation in performance would be quite significant at frequencies below 3 Hz.

The small array configuration has SNR gains exceeding 6 dB in the range 3-10 Hz, but the performance is considerably lower than the two larger configurations, except at the very high frequency end, where the difference is modest.

Under the assumption that the beam is steered towards the azimuth and apparent velocity of the incoming P-phase, we know from the results presented in this paper which sub-geometry provides the best beamforming gain in each of the 12 filter bands. We also know which sub-geometries are best when discarding the D-ring or both the C-ring and D-ring from the selection.

This latter point is important, not only for the possible design of smaller arrays, but also in view of practical considerations when deploying a beam set to be processed in real time. The essential point here is that a smaller array geometry provides broader beam lobes, and thus requires fewer beams to be deployed for complete coverage. If the computer load is a limiting factor, the fewer beams might be an important tradeoff factor against the lower achievable SNR gains.

To arrive at a recommended beam deployment for the respective filter bands, the optimum values have to be seen in conjunction with other factors like mis-steering of the beams, false alarm rate and computer load. In future work, the dependencies between these factors and their implications on a final beam deployment will be studied in detail.

T. Kværna

## References

Followill, F. and D.B. Harris (1983): Comments on Small Aperture Array Designs. Informal Report, Lawrence Livermore National Laboratory.

Fyen, J. (1987): Improvements and Modifications. Semiannual Technical Summary, 1 October 1986 - 31 March 1987, NORSAR Sci. Rep. No. 2-86/87, Kjeller, Norway.

Kværna, T. and D.J. Doornbos (1986): An integrated approach to slowness analysis with arrays and three-component stations. Semiannual Technical Summary, 1 October 1985 - 31 March 1986, NORSAR Sci. Rep. No. 2-85/86, Kjeller, Norway.

Kværna, T. and S. Mykkeltveit (1986): Optimum beam deployment for NORESS P-wave detection. Semiannual Technical Summary, 1 April - 30 September 1986, NORSAR Sci. Rep. No. 1-86/87, Kjeller, Norway.

Mykkeltveit, S. (1985): A new regional array in Norway: Design work and results from analysis of data from a provisional installation. In: The VELA Program. A twenty-five year review of basic research. Ed. A.U. Kerr. Defense Advanced Research Projects Agency.

Mykkeltveit, S., K. Åstebøl, D.J. Doornbos and E.S. Husebye (1983): Seismic array configuration optimization. Bull. Seism. Soc. Am., 73, 173-186.

| No. | Prototype | Type | Low | High | Order |
|---|---|---|---|---|---|
| BP01 | BU | BP | 0.5 | 1.0 | 3 |
| BP02 | BU | BP | 1.0 | 2.0 | 3 |
| BP03 | BU | BP | 1.5 | 3.0 | 3 |
| BP04 | BU | BP | 2.0 | 4.0 | 3 |
| BP05 | BU | BP | 2.5 | 5.0 | 3 |
| BP06 | BU | BP | 3.0 | 6.0 | 3 |
| BP07 | BU | BP | 3.5 | 7.0 | 3 |
| BP08 | BU | BP | 4.0 | 8.0 | 3 |
| BP09 | BU | BP | 5.0 | 10.0 | 3 |
| BP10 | BU | BP | 6.0 | 12.0 | 3 |
| BP11 | BU | BP | 8.0 | 16.0 | 3 |
| BP12 | BU | HP | 10.0 |  | 3 |

Table VII.1.1 The table shows the twelve filters applied in the experiment; all were recursive Butterworth filters of order 3 with one octave bandwidth.

| AOZ | A-RING | B-RING | C-RING | D-RING |
|---|---|---|---|---|
| 1 | 0 | 0 | 0 | 1 |
| 1 | 0 | 0 | 1 | 1 |
| 1 | 0 | 1 | 1 | 1 |
| 1 | 1 | 1 | 1 | 1 |
| 1 | 0 | 0 | 1 | 0 |
| 1 | 0 | 1 | 1 | 0 |
| 1 | 1 | 1 | 1 | 0 |
| 1 | 0 | 1 | 0 | 0 |
| 1 | 1 | 1 | 0 | 0 |
| 1 | 1 | 0 | 0 | 0 |

Table VII.1.2 Array ring weights for the ten sub-geometries considered in this study.

| ORIGIN DATE | ORIGIN TIME | LAT | LON | MAG | ARRIVAL TIME | APP VEL | AZIM | FILT | NO. |
|---|---|---|---|---|---|---|---|---|---|
| 03/12/87 | 23.10.30.7 | 0.3S | 18.1W | 5.5 | 23.21.11.8 | 16.4 | 205.4 | 1 | 1 |
| 09/07/87 | 11.57.13.8 | 31.1S | 178.1W | 5.8 | 12.16.50.6 | 35.7 | 35.4 | 1 | 2 |
| 07/15/87 | 07.16.13.5 | 17.5N | 97.1W | 5.9 | 07.28.36.9 | 21.5 | 266.6 | 1 | 3 |
| 04/29/87 | 01.45.22.6 | 27.4N | 56.1E | 5.9 | 01.53.37.7 | 16.7 | 122.4 | 1 | 4 |
| 05/12/87 | 01.30.25.0 | 7.1N | 126.7E | 6.2 | 02.00.39.5 | 29.2 | 267.9 | 1 | 5 |
| 07/20/87 | 16.47.48.1 | 33.7N | 57.0E | 5.0 | 16.55.17.7 | 14.1 | 115.0 | 2 | 6 |
| 05/09/87 | 06.32.34.9 | 11.3S | 165.7E | 5.5 | 06.51.36.1 | 39.4 | 35.6 | 2 | 7 |
| 07/15/87 | 16.11.02.8 | 47.0N | 154.1E | 5.2 | 16.22.01.2 | 22.9 | 19.6 | 2 | 8 |
| 07/22/87 | 08.23.04.3 | 15.8N | 93.4W | 5.1 | 08.35.21.5 | 20.1 | 280.1 | 2 | 9 |
| 03/15/87 | 05.11.17.0 | 15.6N | 94.6W | 5.6 | 05.23.45.8 | 21.0 | 294.3 | 2 | 10 |
| 04/30/87 | 05.17.37.0 | 39.8N | 74.6E | 5.7 | 05.25.39.8 | 15.7 | 89.3 | 3 | 11 |
| 07/11/87 | 06.15.51.0 | 82.2N | 17.6W | 5.5 | 06.20.55.0 | 10.5 | 347.8 | 3 | 12 |
| 07/04/87 | 17.16.52.1 | 10.9N | 62.2W | 4.7 | 17.28.14.8 | 19.2 | 255.5 | 3 | 13 |
| 03/12/87 | 01.57.17.2 | 49.9N | 78.8W | 5.5 | 02.04.37.4 | 16.2 | 79.4 | 3 | 14 |
| 08/15/87 | 00.31.49.2 | 52.7N | 152.6E | 4.9 | 00.41.22.4 | 14.1 | 29.2 | 3 | 15 |
| 03/22/87 | 17.45.04.6 | 52.1N | 171.4W | 5.3 | 17.55.57.4 | 12.1 | 7.2 | 4 | 16 |
| 02/27/87 | 23.34.52.0 | 38.5N | 20.3E | 5.3 | 23.39.57.1 | 11.4 | 161.6 | 4 | 17 |
| 02/19/87 | 22.41.25.2 | 40.2N | 21.6E | 4.1 | 22.46.08.8 | 9.9 | 159.4 | 4 | 18 |
| 07/27/87 | 21.20.50.5 | 40.8N | 22.1E | 4.5 | 21.25.32.1 | 10.1 | 159.1 | 4 | 19 |
| 07/16/87 | 16.36.17.7 | 59.5N | 28.0E | 2.8 | 16.37.50.0 | 8.3 | 83.7 | 4 | 20 |
| 07/23/87 | 19.28.01.6 | 46.4N | 153.5E | 5.3 | 19.39.01.8 | 24.4 | 29.7 | 5 | 21 |
| 11/05/87 | 18.31.25.8 | 37.0N | 21.4E | 4.0 | 18.36.42.4 | 10.6 | 146.1 | 5 | 22 |
| 04/12/87 | 09.00.51.8 | 42.7N | 26.6E | 3.8 | 09.05.28.4 | 10.2 | 141.9 | 5 | 23 |
| 03/09/87 | 19.50.21.2 | 39.4N | 20.5E | 3.7 | 19.55.13.3 | 10.0 | 159.0 | 5 | 24 |
| 04/16/87 | 01.10.20.6 | 55.0N | 158.0E | 5.0 | 01.20.05.6 | 14.4 | 27.0 | 5 | 25 |
| 04/12/87 | 12.13.51.0 | 31.8N | 75.8E | 4.2 | 12.22.43.8 | 14.2 | 100.6 | 6 | 26 |
| 07/11/87 | 13.55.54.2 | 36.6N | 26.8E | 4.5 | 14.01.12.0 | 10.6 | 148.4 | 6 | 27 |
| 07/24/87 | 02.42.59.0 | 32.0N | 75.5E | 4.1 | 02.51.49.9 | 14.0 | 98.3 | 6 | 28 |
| 12/13/87 | 06.22.39.0 | 32.8N | 73.9E | 4.2 | 06.31.17.9 | 14.5 | 100.1 | 6 | 29 |
| 09/10/87 | 21.53.14.6 | 43.9N | 147.8E | 5.2 | 22.04.21.4 | 12.8 | 32.9 | 6 | 30 |
| 11/01/87 | 20.39.33.0 | 65.1N | 11.9E | 3.6 | 20.40.37.0 | 8.6 | 358.7 | 7 | 31 |
| 07/20/87 | 00.29.38.2 | 52.2N | 156.3E | 4.4 | 00.39.49.5 | 14.6 | 33.8 | 7 | 32 |
| 12/26/87 | 08.58.31.0 | 45.4N | 152.5E | 4.6 | 09.09.36.5 | 16.2 | 36.6 | 7 | 33 |
| 03/31/87 | 01.18.36.8 | 53.2N | 156.5E | 5.2 | 01.28.46.0 | 14.9 | 38.4 | 7 | 34 |
| 01/19/87 | 04.07.24.2 | 55.6N | 5.6E | 3.6 | 04.08.54.5 | 9.1 | 213.6 | 7 | 35 |

Table VII.1.3 (page 1 of 2) Events applied in the data analysis procedure. The analysis filter number (FILT) corresponds to the filters given in Table VII.1.1. The event locations were given by one of the following agencies: PDE, University of Helsinki, University of Bergen or NORESS automatic bulletin. In the cases where no location is given, the only availabe event information is a P-phase detected on the NORESS array.

| | | | | | | | | | |
|---|---|---|---|---|---|---|---|---|---|
| 09/04/87 | 08.38.18.8 | 61.4N | 3.1E | 3.4 | 08.39.20.8 | 9.4 | 289.6 | 8 | 36 |
| 04/24/87 | | | | | 11.59.42.9 | 9.1 | 130.3 | 8 | 37 |
| 03/01/87 | | | | | 12.49.39.0 | 16.7 | 107.0 | 8 | 38 |
| 07/16/87 | 12.07.54.5 | 60.1N | 29.4E | 2.6 | 12.10.01.6 | 9.0 | 76.6 | 8 | 39 |
| 07/06/87 | 22.48.49.4 | 60.0N | 29.5E | 2.6 | 22.50.58.4 | 11.2 | 83.3 | 8 | 40 |
| 07/03/87 | 10.38.49.6 | 59.5N | 24.0E | 3.0 | 10.40.23.3 | 9.7 | 106.7 | 9 | 41 |
| 07/25/87 | 19.08.32.1 | 60.1N | 4.8E | 2.1 | 19.09.24.4 | 9.4 | 253.3 | 9 | 42 |
| 04/18/87 | 02.51.08.6 | 61.6N | 2.6E | 2.4 | 02.52.12.4 | 9.5 | 292.9 | 9 | 43 |
| 07/22/87 | 21.36.35.4 | 61.0N | 2.6E | 2.6 | 21.37.38.6 | 9.4 | 285.1 | 9 | 44 |
| 04/19/87 | 22.16.20.2 | 57.1N | 7.8E | 3.2 | 22.17.23.0 | 8.0 | 203.3 | 9 | 45 |
| 04/25/87 | | | | | 16.30.56.7 | 8.2 | 196.3 | 10 | 46 |
| 03/01/87 | 06.42.03.0 | 57.1N | 7.1E | 3.5 | 06.43.07.7 | 9.0 | 211.8 | 10 | 47 |
| 08/31/87 | 17.32.59.9 | 59.7N | 10.6E | 1.7 | 17.35.08.3 | 7.1 | 209.0 | 10 | 48 |
| 07/07/87 | 01.44.40.4 | 60.2N | 29.7E | 2.7 | 01.46.50.4 | 12.1 | 82.9 | 10 | 49 |
| 05/25/87 | | | | | 04.14.34.2 | 8.7 | 182.4 | 10 | 50 |
| 05/25/87 | 04.26.04.5 | 57.7N | 11.5E | 2.8 | 04.28.12.0 | 8.7 | 179.5 | 11 | 51 |
| 01/19/88 | 07.00.54.1 | 62.3N | 4.0E | 2.5 | 07.03.01.8 | 9.6 | 288.2 | 11 | 52 |
| 08/01/87 | 19.57.29.3 | 57.5N | 5.8E | 2.2 | 19.59.39.3 | 8.2 | 204.6 | 11 | 53 |
| 01/12/88 | | | | | 09.04.40.1 | 8.9 | 186.7 | 11 | 54 |
| 01/16/88 | | | | | 13.26.34.4 | 8.7 | 181.6 | 11 | 55 |
| 02/04/87 | 12.02.41.0 | 61.7N | 5.0E | 3.5 | 12.03.33.0 | 9.6 | 294.3 | 12 | 56 |
| 05/25/87 | 02.35.26.4 | 61.8N | 5.3E | 3.1 | 02.36.15.9 | 9.8 | 297.0 | 12 | 57 |
| 01/07/88 | 12.51.09.8 | 59.5N | 11.0E | 1.6 | 15.53.16.7 | 7.0 | 199.4 | 12 | 58 |
| 10/31/87 | 10.09.14.1 | 61.1N | 4.5E | 4.2 | 10.10.07.4 | 9.5 | 289.2 | 12 | 59 |
| 12/01/87 | 12.08.00.6 | 59.3N | 10.4E | 1.6 | 12.10.10.0 | 6.8 | 206.0 | 12 | 60 |

Table VII.1.3 (page 2 of 2)

| SNR-gain(dB) | Noise-suppression(dB) | Signal-loss(dB) | LTA | A0 | A | B | C | D |
|---|---|---|---|---|---|---|---|---|
| 9.03 | 10.53 | 1.50 | 31.7 | 1 | 0 | 0 | 0 | 1 |
| 14.67 | 15.69 | 1.02 | 17.3 | 1 | 0 | 0 | 1 | 1 |
| 12.76 | 13.58 | 0.82 | 21.6 | 1 | 0 | 1 | 1 | 1 |
| 10.88 | 11.60 | 0.72 | 26.9 | 1 | 1 | 1 | 1 | 1 |
| 9.04 | 9.38 | 0.34 | 34.8 | 1 | 0 | 0 | 1 | 0 |
| 7.84 | 8.11 | 0.27 | 39.4 | 1 | 0 | 1 | 1 | 0 |
| 6.67 | 6.90 | 0.23 | 45.0 | 1 | 1 | 1 | 1 | 0 |
| 2.85 | 2.95 | 0.10 | 68.8 | 1 | 0 | 1 | 0 | 0 |
| 2.06 | 2.16 | 0.10 | 75.7 | 1 | 1 | 1 | 0 | 0 |
| 0.48 | 0.53 | 0.05 | 92.1 | 1 | 1 | 0 | 0 | 0 |

Table VII.1.4 The table gives the SNR-gain, noise suppression, signal loss, the detection LTA value and the corresponding array ring weights from processing event number 13 (see Table VII.1.3). This is a teleseismic event which has been analyzed in the filter band 1.5-3.0 Hz.

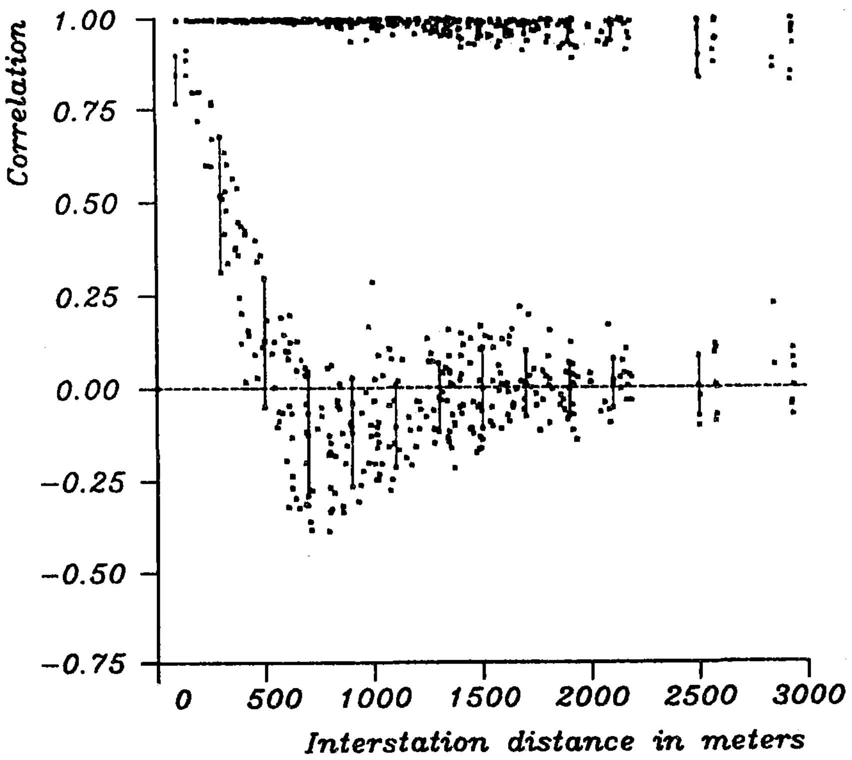

Fig. VII.1.1 Signal (upper part) and noise (lower part) correlations in the 2-4 Hz frequency band. The arrival time of the P-phase is 1985 - 115:01.02.27. After preshifting the traces with steering delays corresponding to the apparent velocity and azimuth of the incoming P-phase, the signal correlations were calculated from a 1 sec time window at the beginning of the P-phase. The noise correlations were calculated from a 60 sec long time window prior to the signal. The error bars reflect a scatter of plus/minus one standard deviation.

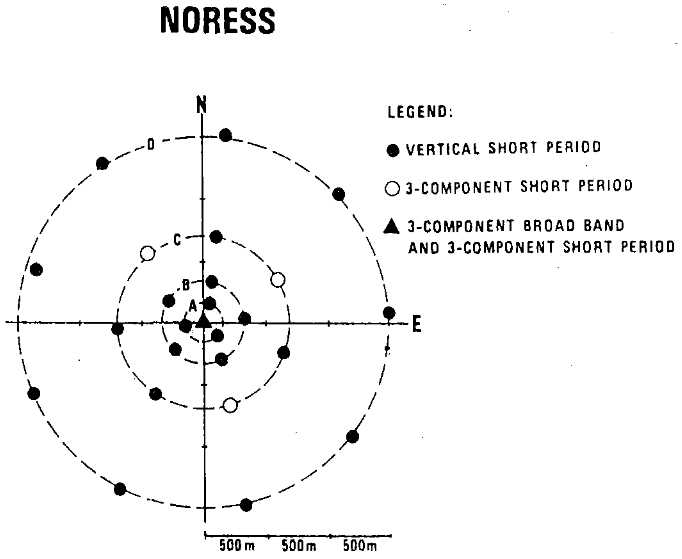

Fig. VII.1.2 The geometry of the NORESS array. The short period instrument at the center of the array is denoted A0. In this study, only the vertical short period instruments were applied.

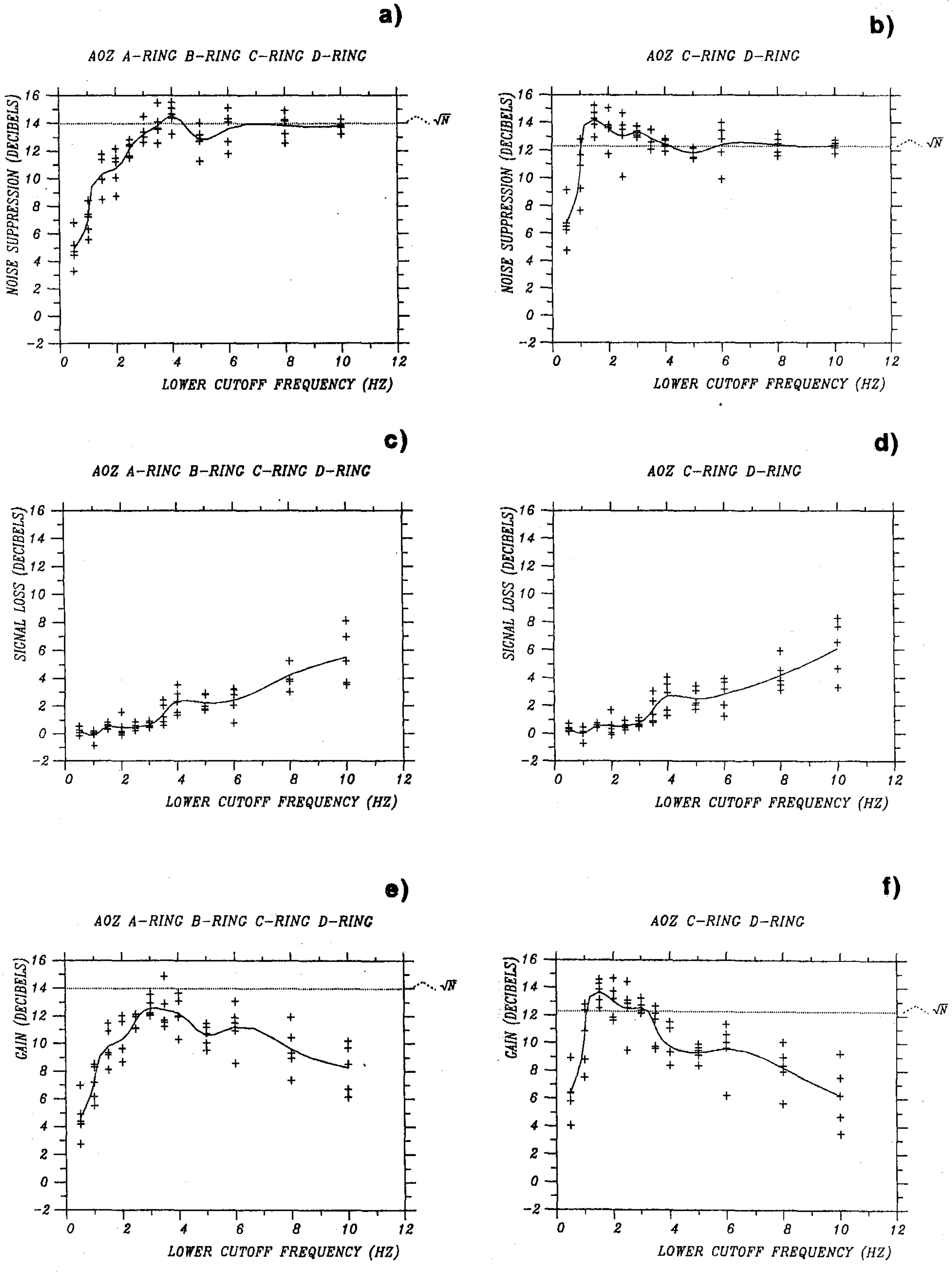

Fig. VII.1.3 Noise suppression, signal loss and SNR gain for the 25-element full array geometry (a,c,e) and for the 17-element AOZ, C-ring and D-ring sub-geometry (b,d,f).

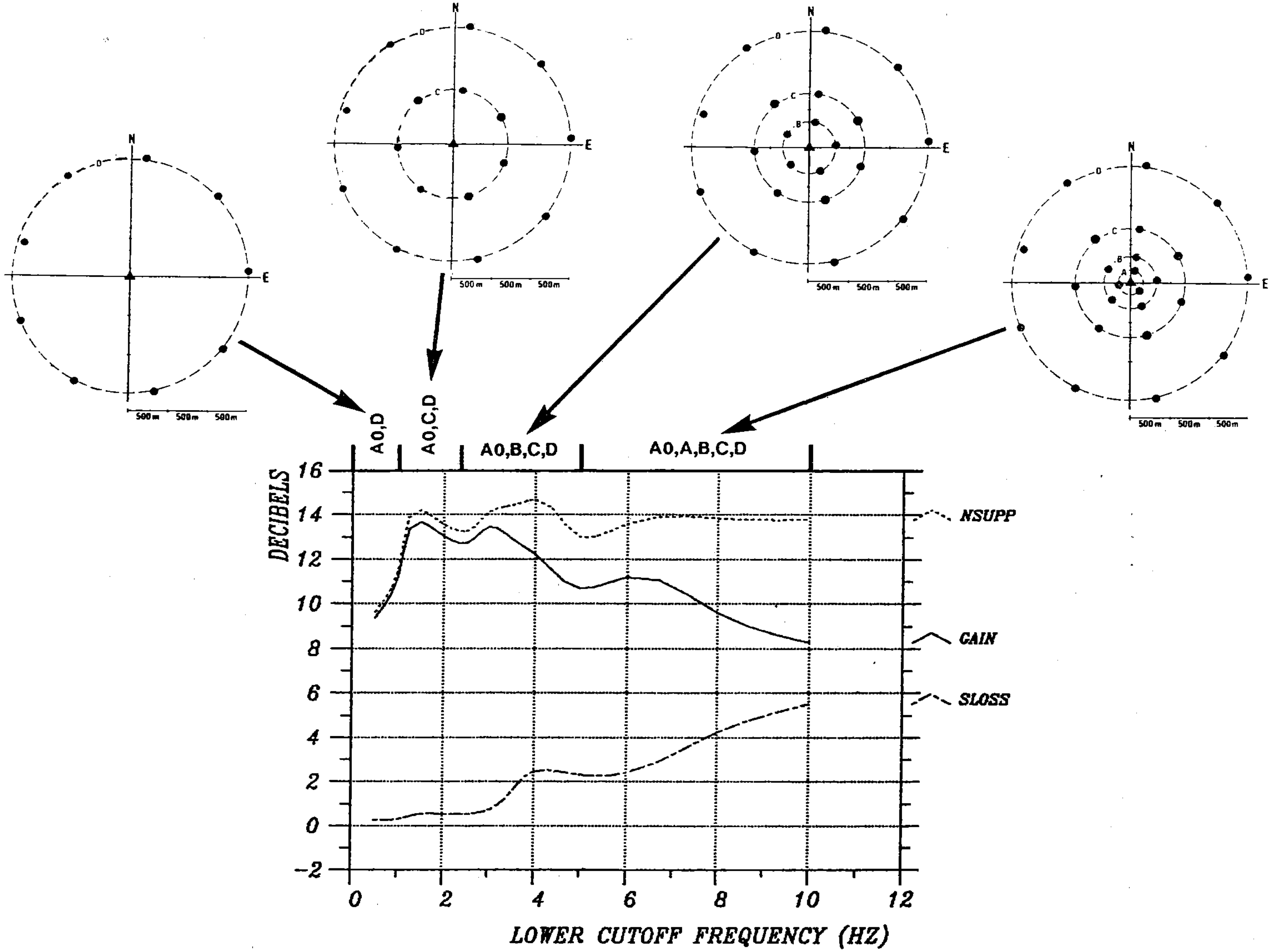

Fig. VII.1.4 The gain curve shown in this figure represents the best gain values produced by any of the ten sub-geometries. In addition, we have also given the corresponding noise suppresion (NSUPP) and signal loss (SLOSS). The best sub-geometries are shown above, and the arrows point to the frequency interval where they provide the highest SNR gain.

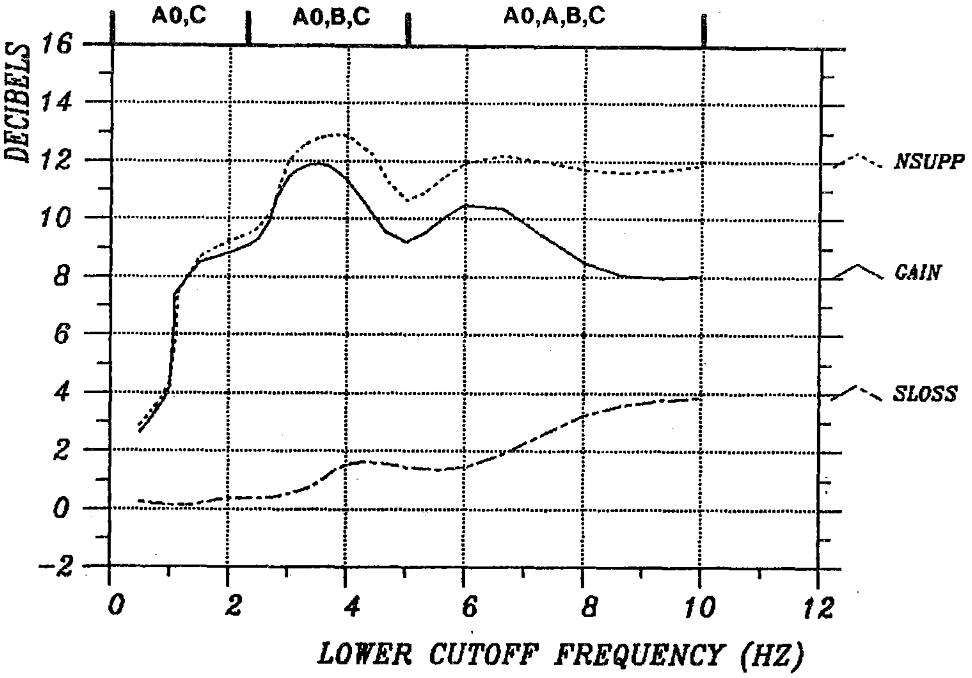

Fig. VII.1.5a The gain curve represents the best gain values when searching from sub-geometries with the D-ring excluded. In addition, the corresponding noise suppression (NSUPP) and signal loss (SLOSS) are given. The best sub-geometries and their frequency interval (A0Z,C denotes A0Z, C-ring) are given above.

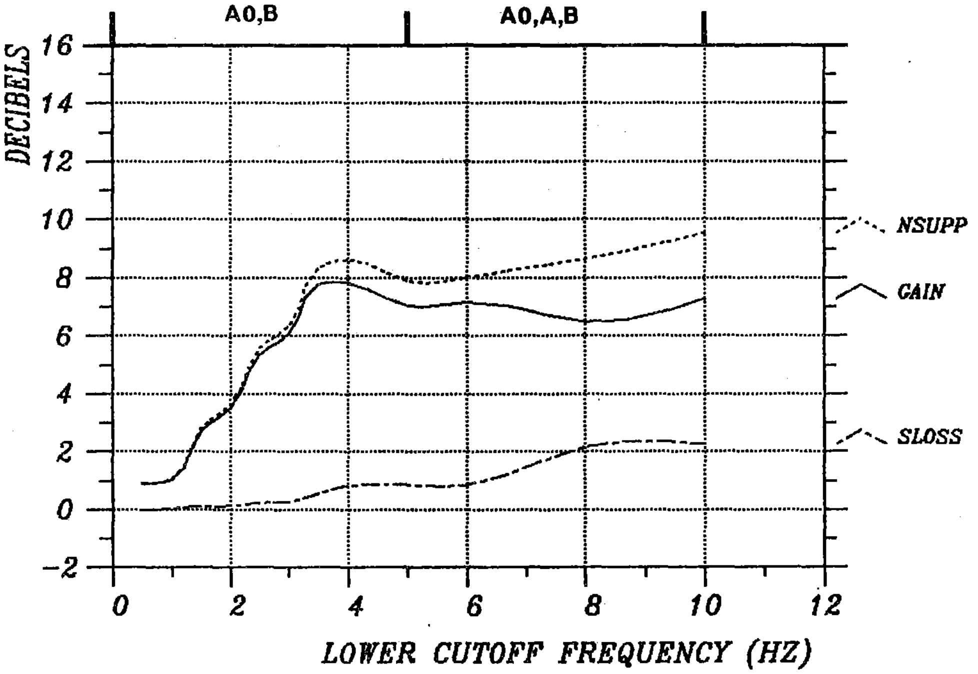

Fig. VII.1.5b Same as Fig. VII.1.5a, but now with both C-ring and D-ring excluded.

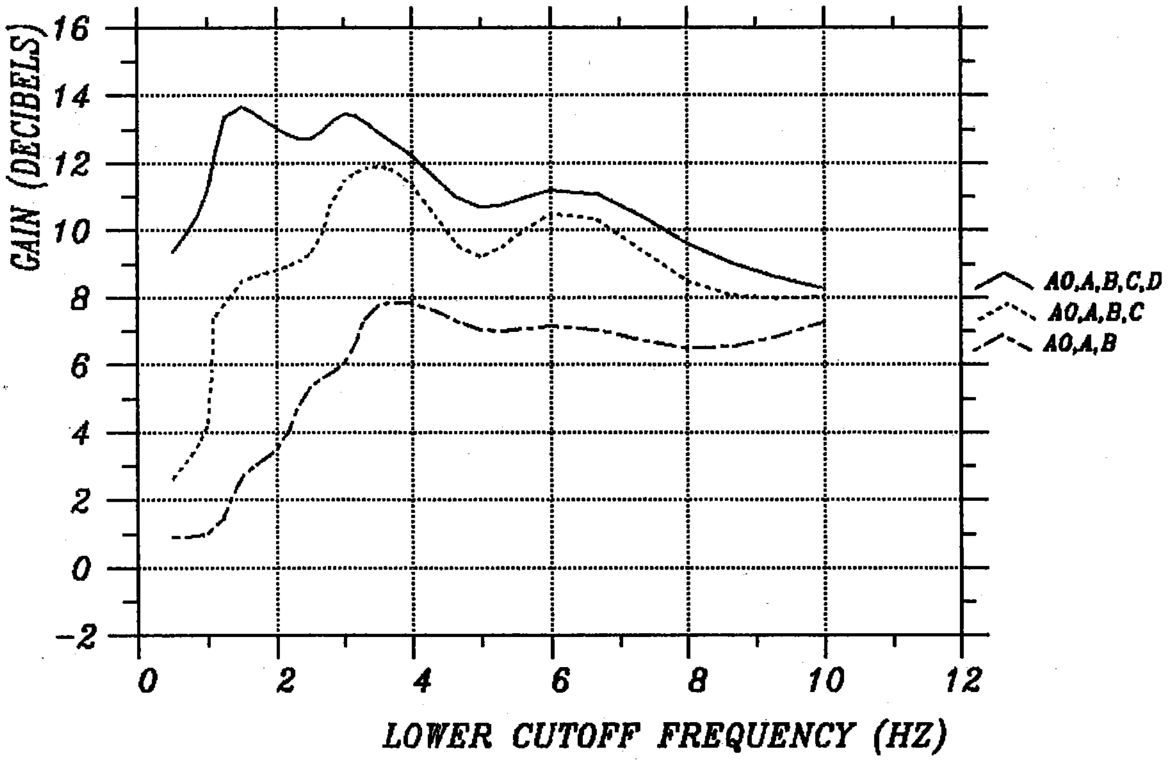

Fig. VII.1.6 The best gain curve based on the full NORESS geometry and also shown in Fig. VII.1.4, is given by the upper solid curve. The gain produced with the D-ring excluded is given by the dotted curve in the middle. We can see that up to about 3 Hz, the gain is well below the best, but for frequencies above 3 Hz, it stays only 1 to 2 dB below. The gain produced with both the C- and D-rings excluded is given by the lower closed dotted curve. As seen from the figure, it is more than 3 dB below the best for all frequencies up to 8 Hz, but between 8 and 10 Hz it comes closer to the best values.

## VII.2 Sources of short-term fluctuations in the seismic noise level at NORESS

The small-aperture array NORESS in southern Norway provides a unique tool to investigate the spatial coherence and directionality of the ambient seismic noise field. By using techniques such as narrow-band and wide-band frequency-wavenumber analysis, both apparent velocity and azimuth of the noise as well as signals can be reliably determined. Three years of operation of an automatic short-term to long-term (STA/LTA) detector algorithm has further offered the possibility of an extensive study of the short-term variability of the seismic noise field (i.e., noise bursts of a few seconds length). In conjunction with the associated automatic determination of apparent velocity and azimuth, this detector system provides a unique data base for detailed characterization of propagating noise phases.

An abrupt increase in the seismic noise level will cause an STA/LTA detector algorithm to delare a detection. The three-year period of continuous processing of data from from NORESS, has shown that this kind of detections sometimes completely dominates the output report from the real-time processor. In most cases these noise bursts can be separated from the local and regional S-phases on the basis of their relatively low apparent velocity estimates. But there is clearly a need to understand the mechanisms causing these phenomena and their implications on real-time array processing. Several studies have during the past fifteen years been conducted on the seismic noise field at the NORSAR / NORESS array sites. These investigations have revealed systematic diurnal and seasonal variations in the seismic noise level (Fyen, 1988; Ringdal and Bungum, 1977). Bungum et al (1985) found that the short-period noise field at NORSAR was dominated by westerly directions for frequencies at 1 Hz and below, whereas easterly directions dominated the noise field above 2 Hz. It has also been shown that from time to time there is a significant increase in the noise variance which results in an increased number of false alarms triggered by the automatic signal detector (Steinert et al, 1975). In this study we will report on the directional and temporal distribution of the short-term noise fluctuations. We will correlate the temporal distribution with environmental factors and attempt to locate possible noise sources.

**Real-time processing results**

The algorithm for real-time processing of data from the NORESS array has been described in detail by Mykkeltveit and Bungum (1984). A conventional STA/LTA detector is applied to a set of 17 coherent and 3 incoherent filtered array beams. For further information on incoherent beamforming, see Ringdal et al (1975). When a detection is declared, the refined arrival time and the dominant signal frequency are estimated. Narrow-band frequency-wavenumber analysis (Capon, 1969) is then performed to estimate the apparent velocity and azimuth of the detected phase. The automatic event location procedure is based on the S-P travel time difference and the azimuth of one of the phases. The P- and S-phases are automatically separated by their apparent velocity estimates (above and below 6.0 km/s, respectively), and are associated to the same event if the estimated azimuths differ by less than a predefined value. The data investigated in this paper are the reports produced by the real-time processor, which contain arrival time, definition of the detection beam, dominant frequency, signal-to-noise ratio, apparent velocity and azimuth for each detected phase. The main topic of interest in the context of this study is the occasional occurrence of a vast increase (sometimes lasting for several days) in the number of detections on the incoherent beams.

In most cases the associated apparent velocities are less than 3.0 km/s and unlike the local and regional S-waves, there is no sign of P-detections preceding these phases. When sorting the processing reports according to the apparent velocities of the detected phases, we found for the year 1986 that 15406 out of a total number of 49891 detections had apparent velocities less than 3.0 km/s. The numbers for the year

1987 were 22087 and 50665, respectively. The majority of the low-velocity detections have low signal-to-noise ratios and could be avoided if the detection threshold on the incoherent beams were raised. But the incoherent beams are our best tool for detecting local and regional secondary phases, so raising the threshold would imply missing a lot of interesting secondary phases.

**Azimuthal distribution**

Figs. VII.2.1a and 1b are histograms showing the azimuthal distribution of the low-velocity detections for 1986 and 1987. The distributions are very similar with a dominant region between 5 and 120 degrees azimuth and a peak between 95 and 105 degrees. Few low-velocity arrivals come from the southern direction, and two minor peaks show up at about 250 and 320 degrees azimuth. It should also be emphasized that 1987 had about 6500 more low-velocity detections than 1986 and that most of these 6500 were confined to the major dominant azimuth range (95-105 degrees).

**Temporal distribution**

The majority of the low-velocity detections have peak frequencies between 2 and 3 Hz. Fyen (1988) found that there was an increase in the 3 Hz noise level coinciding with increased water flow in the nearby river Glomma. Fig. VII.2.2 shows a map of the NORESS site, the nearby populated areas and the river Glomma. In Fig. VII.2.3a we have displayed the distribution within the year 1986 of the low-velocity detections with azimuths between 95 and 105 degrees, and in Fig. VII.2.3b the corresponding distribution of the water flow in river Glomma. The correlation between these histograms is obvious. The maxima at about day 230 and day 300 coincide, but the major detection peak starting at day 130 is somewhat delayed relative to the water flow maximum. The equivalent annual distributions for 1987 are given in Figs. VII.2.4a and 4b. In contrast to 1986, there was during the autumn of 1987 a large flood due to heavy rain for more than a week, and this is also reflected in a peak in the number of detections. Also in this case, the largest detection peaks at about day 190 and day 300 are delayed relative to the water flow maxima and they seem to occur with the decrease in the water flow.

In order to investigate further the stability of the noise field, a 6-hour interval containing numerous low-velocity detections were subjected to additional analysis by the wide-band frequency-wavenumber method desribed by Kværna and Doornbos (1986). A total of 720 time samples, each of 25 seconds length, were processed in the frequency band 2.5 to 2.9 Hz. Excluding the relatively few time samples with other types of signals, we obtained a mean azimuth of 99.5 degrees with a standard deviation of 0.8 degrees. The mean apparent velocity was 2.83 km/s with a standard deviation of 0.03 km/s. Thus, there is a continuous background noise field within this frequency band with fluctuations causing the low-velocity detections.

We also investigated the time-dependency of low-velocity detections at other azimuths. We found that the temporal distributions of low-velocity detections with azimuths between 0 and 95 degrees were rather flat and did not reveal any particular peaks during the year. The same applies to the detections with azimuths between 300 and 330 degrees. Thus the only definite correlation with water flow occurred in the 95-105 degree range.

## Discussion and conclusions

The short term variability of seismic noise recorded at NORESS has been characterized in this paper by observing the distribution of array detections triggered by the short-term to long-term "linear power" ratio. The cumulative frequency distribution of these detections has been computed as a function of signal-to-noise ratio. The slope of the log(SNR) versus log (number of detections) relationship at low SNR values is 6.7 for the year 1987, see Fig. VII.2.5. This is significantly greater than the value near 1.0 normally associated with earthquakes (see, e.g., Steinert et al, 1975). This observation, in conjunction with the observed low apparent velocities and the absence of associated P-phase detections, indicates that these low SNR detections generally do not originate from tectonic events or explosions, and are thus part of the ambient noise field.

Our results show typical Rayleigh wave velocities (2.5-3.0 km/s) and dominant frequencies between 2 and 3 Hz for the vast majority of these detections. The azimuthal distribution of the detections is remarkably similar for the two years 1986 and 1987, with a dominance of phases from the easterly direction. This corresponds to the direction to the large nearby river Glomma, and thus indicates that the water flow in this river directly or indirectly is strongly associated with such noise fluctuations.

A particularly good correlation has been found between the number of Rayleigh wave detections in the azimuth range 95-105 degrees (which has the most detections for either year) and the Glomma water flow. In fact, during periods of heavy water flow, the noise field is continuously dominated by propagating Rayleigh waves from this particular direction. This implies that there is a continuous source of these disturbances. Tracing in the previously found direction of 99.5 degrees from NORESS, we find at the river Glomma, near the town of Braskereidfoss, a dam construction and a hydroelectric power plant.

Bungum et al (1977) conducted a study of propagating seismic phases from a similar source, the hydroelectric power plant at Hunderfossen near NORSAR subarray 14C. The concluded that this plant produced continuous strong seismic energy at 2.778 Hz frequency and S-phase velocity (3-5 km/s). It is interesting that in our case we observe similar signal frequencies, but significantly lower phase velocities. In fact, one of the unique capabilities of the NORESS system is the ability to provide very reliable phase velocity and directional measurements, and the uncertainty in our phase velocity estimates is extremely small (only 0.03 km/s for the 6-hour period analyzed in detail). We also note that apart from the mentioned azimuth range, we have found no particular correspondence between water flow and the number of detections. Also an unresolved question is why the majority of detections in the azimuth range 95-105 degrees occur with a slight delay (3-5 days) after the Glomma water flow peaks. The diurnal distribution of the low-velocity detections have minima during working hours. This can be explained in terms of the increased noise level at these time intervals, as documented by Fyen (1988).

In conclusion, this study has documented that the main source of short-term variability in the seismic noise at NORESS, i.e., noise bursts of a few seconds duration, are propagating Rayleigh waves of frequencies between 2 and 3 Hz. In contrast to the lower frequency noise which is dominated by microseisms associated with storm activity in the North Atlantic Ocean in the westerly direction from NORESS, these Rayleigh waves mostly originate east of the array. To a large extent, the observed detections are strongly correlated with the water flow in the nearby river Glomma, but the exact determination of the actual source and the generation mechanisms will require further study.

T. Kværna

## References

Bungum, H., S. Mykkeltveit and T. Kværna (1985): Seismic noise in Fennoscandia, with emphasis on high frequencies. Bull. Seism. Soc. Am., 75, 1489-1513.

Bungum, H., T. Risbo and E. Hjortenberg (1977): Precise continuous monitoring of seismic velocity variations and their possible connection to solid earth tides. J. Geophys. Res., 82, 5365-5373.

Capon, J. (1969): High-resolutiohn frequency-wavenumber spectrum analysis. Proc. IEEE, 57, 1408-1418.

Fyen, J. (1988): Diurnal and seasonal variations in the microseismic noise level observed at the NORESS array. Manuscript submitted to Phys. Earth Planet. Inter.

Kværna, T. and D.J. Doornbos (1986): An integrated approach to slowness analysis with arrays and three-component stations. Semiann. Tech. Summary, 1 Oct 1985 - 31 Mar 1986, NORSAR Sci. Rep. No. 2-85/86, Kjeller, Norway.

Kværna, T., S. Kibsgaard and F. Ringdal (1987): False alarm statistics and threshold determination for regional event detection. Semiann. Tech. Summ., 1 Apr - 30 Sep 1987, NORSAR Sci. Rep. No. 1-87/88, Kjeller, Norway.

Mykkeltveit, S. and H. Bungum (1984): Processing of regional events using data from small-aperture arrays. Bull. Seism. Soc. Am., 74, 2313-2333.

Ringdal, F. and H. Bungum (1977): Noise level variation at NORSAR and its effect on detectability. Bull. Seism. Soc. Am., 67, 479-492.

Ringdal, F., E.S. Husebye and A. Dahle (1975): P-wave envelope representation in event detection using array data. In: K.G. Beauchamp (ed.), Exploitation of Seismograph Networks. Nordhoff-Leiden, The Netherlands, 353-372.

Steinert, O., E.S. Husebye and H. Gjøystdal (1975): Noise variance fluctuations and earthquake detectability. Geophys. J. R. astr. Soc., 41, 298-302.

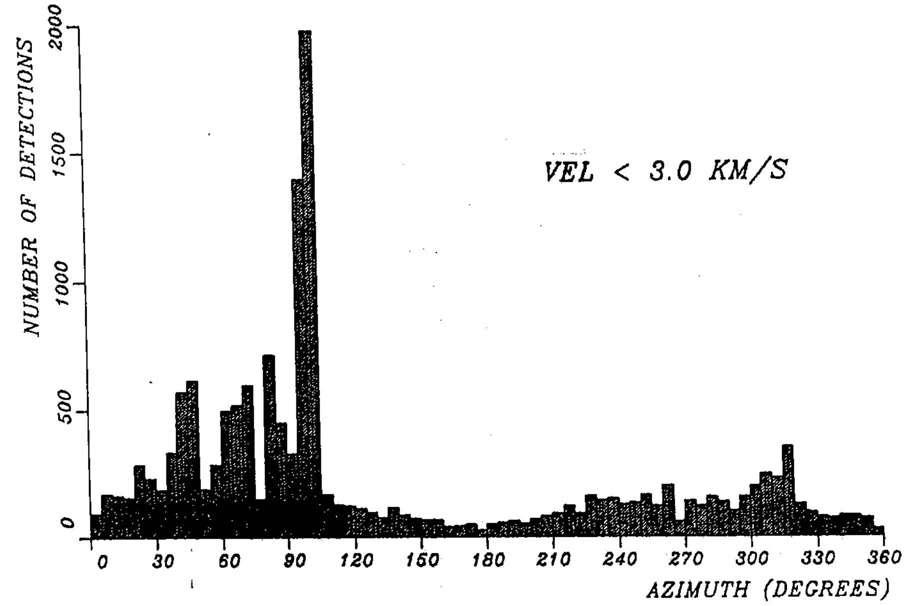

Fig. VII.2.1a Histogram showing the azimuthal distribution of NORESS low-velocity detections for the year 1986. The azimuth solutions have been estimated by the frequency-wavenumber method of Capon (1969). The bar width is five degrees.

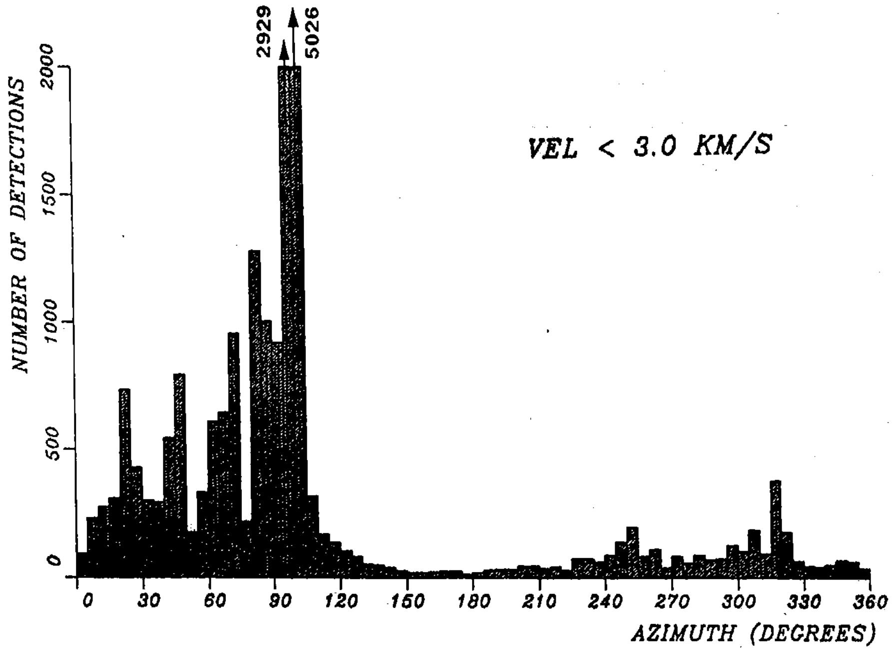

Figure VII.2.1b Same as Fig. VII.2.1a, but for the year 1987.

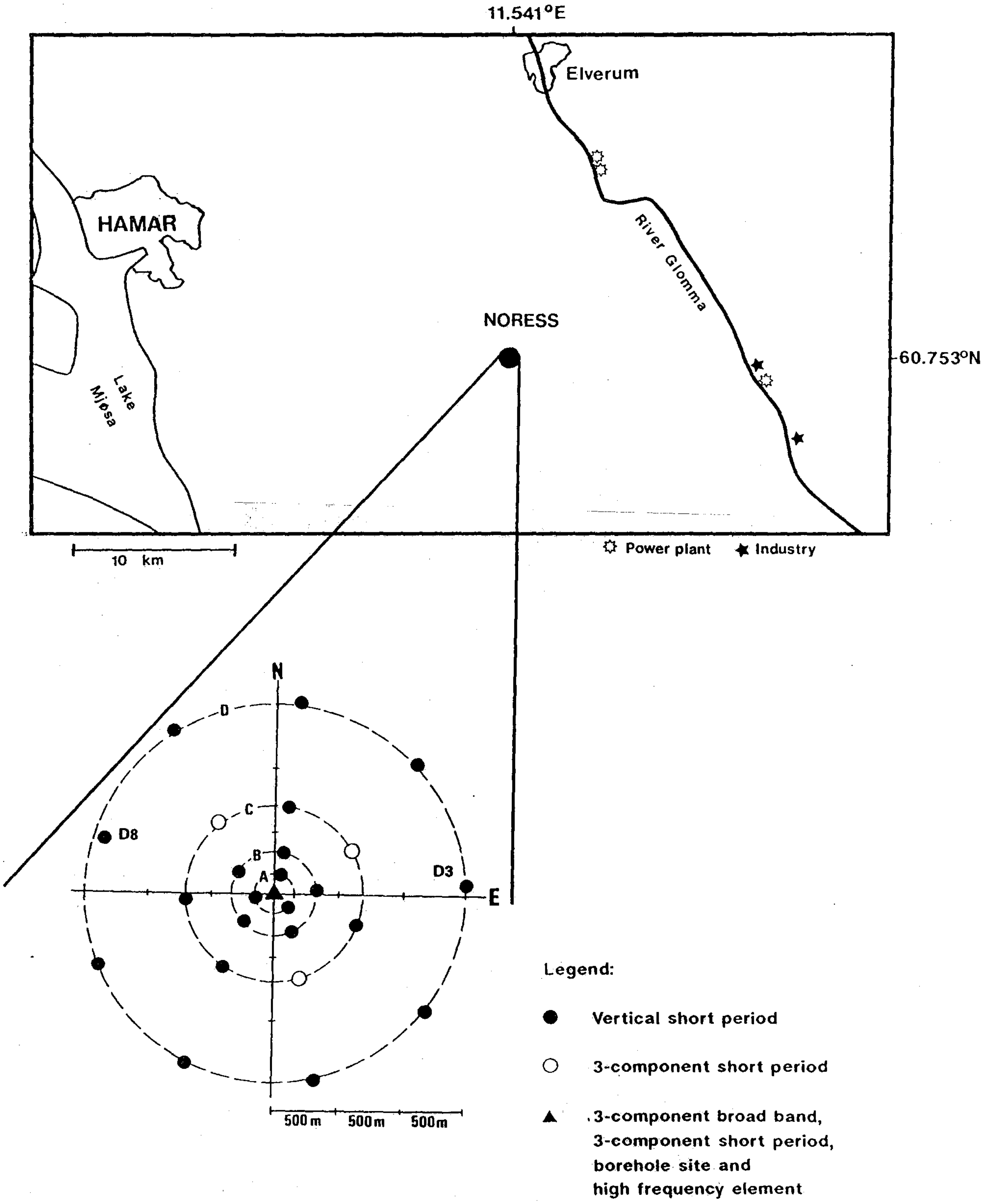

Fig. VII.2.2 Map of the area surrounding the NORESS array, with nearby populated areas, industry sites and the river Glomma specially marked. The geometry of NORESS is also shown.

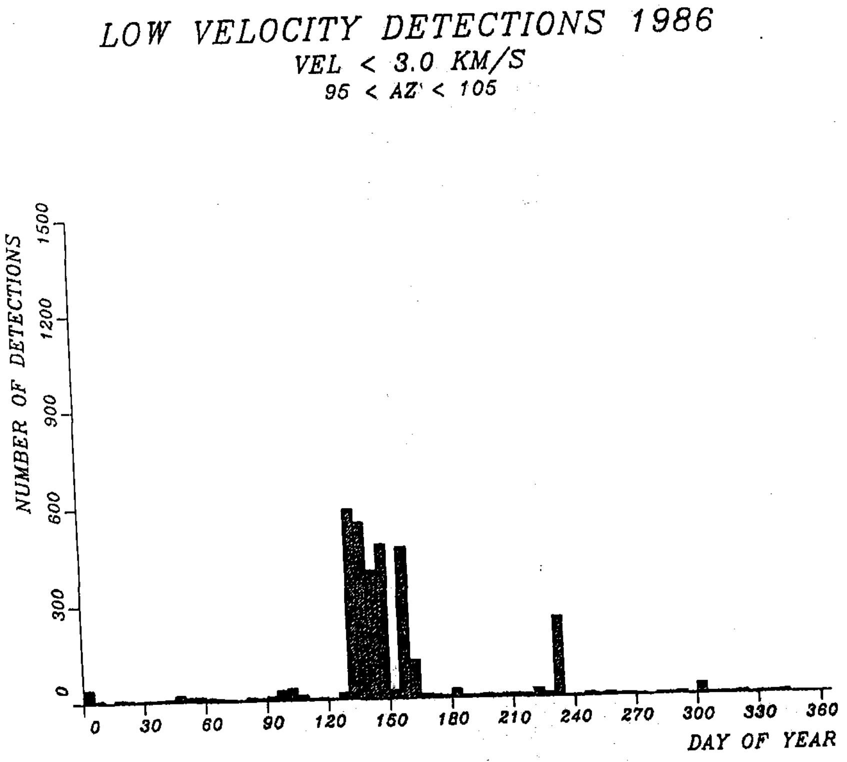
LOW VELOCITY DETECTIONS 1986
VEL < 3.0 KM/S
95 < AZ < 105

Fig. VII.2.3a Histogram showing the distribution of NORESS low-velocity detections in the azimuth range 95-105 degrees during the year 1986. Each bar gives the number of detections in a five-day period.

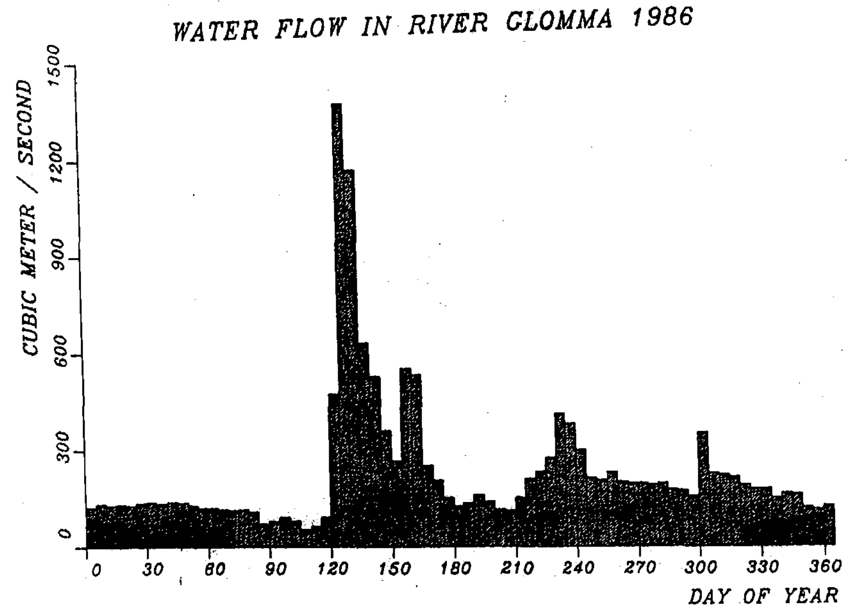
WATER FLOW IN RIVER GLOMMA 1986

Fig. VII.2.3b Histogram showing the distribution of water flow in river Glomma measured at the town of Elverum (see Fig. VII.2.2) for the year 1986. Each bar corresponds to a five-day average value.

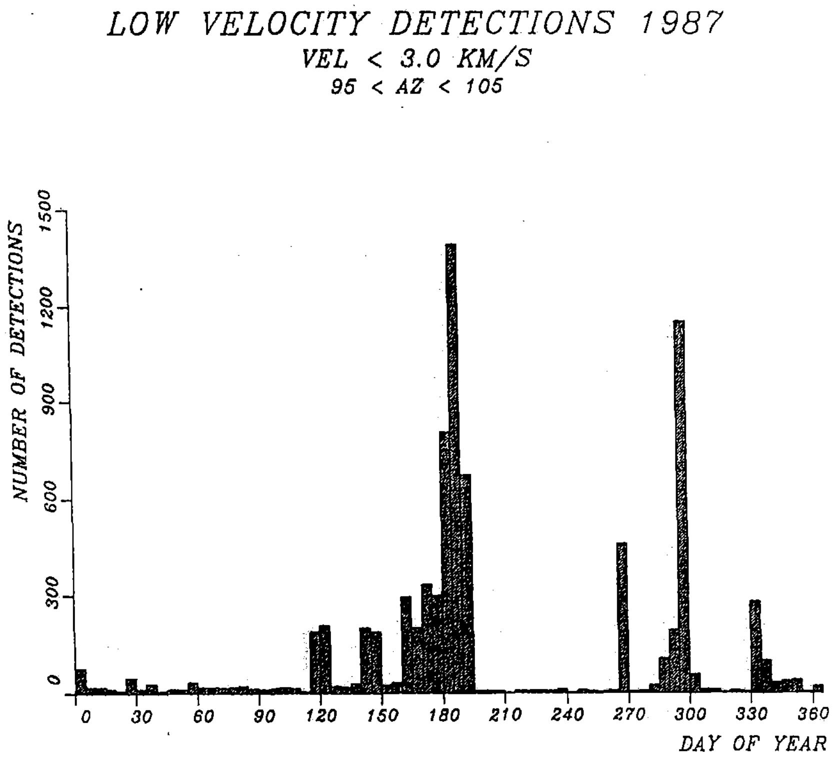

Fig. VII.2.4a The same as for Fig. VII.2.3a, but for the year 1987.

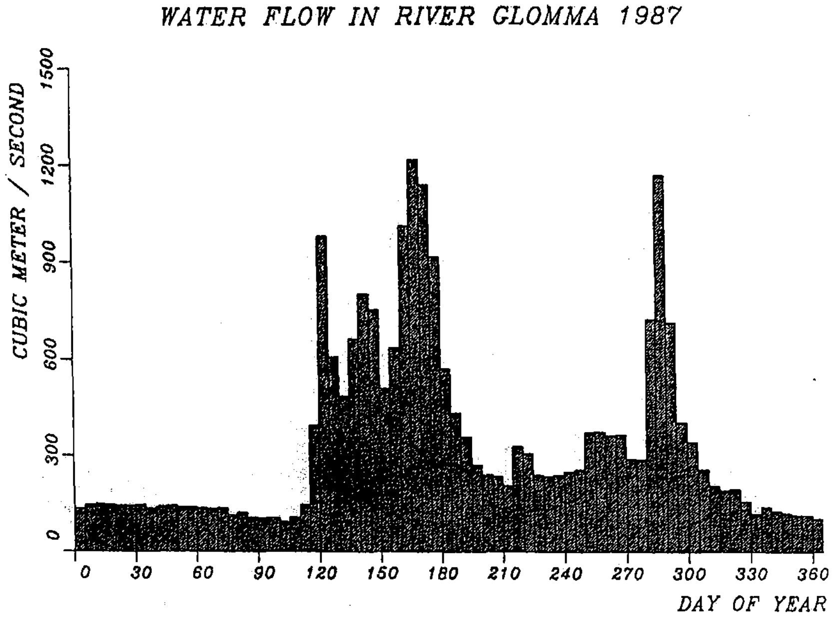

Fig. VII.2.4b The same as for Fig. VII.2.3b, but for the year 1987.

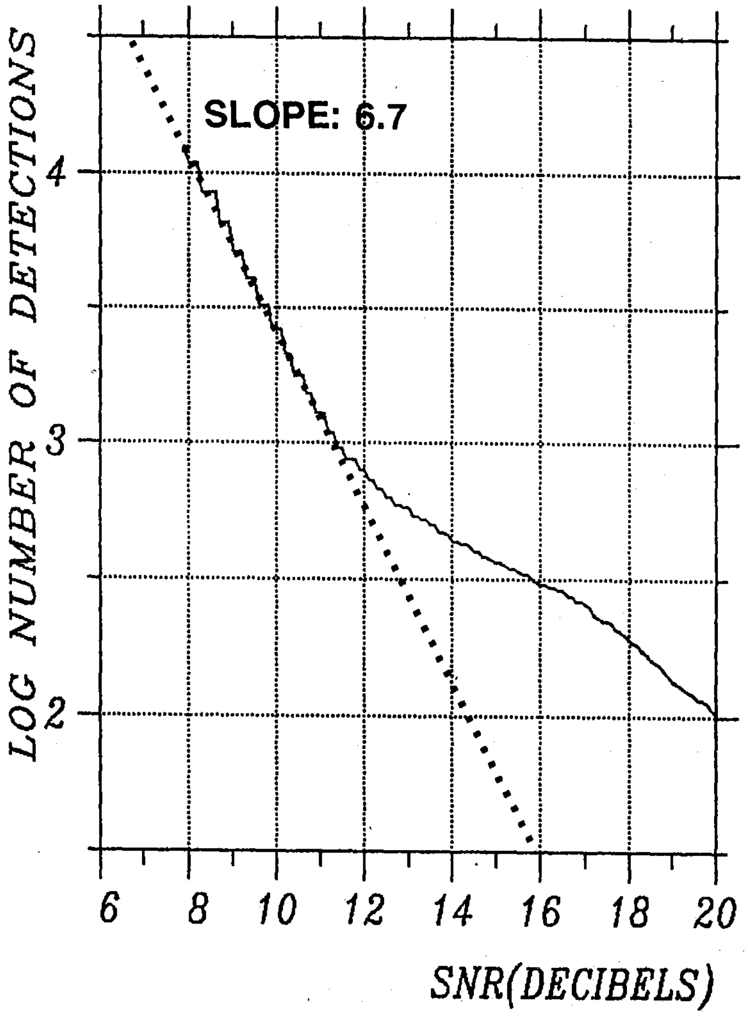

Fig. VII.2.5 Cumulative distribution during 1987 of number of detections versus signal-to-noise ratio for an incoherent NORESS beam filtered in the frequency band 2.0-3.0 Hz. The slope of the log(SNR) versus log(number of detections) relationship at low SNR give some indication on the mechanisms causing these detections (see Steinert et al, 1975; Kværna et al, 1987).

## VII.3 Surface topographic effects on arrays and three-component stations

A recent analysis of the location capabilities by the NORESS array and by the 3-component stations within the array has led to the following conclusions concerning 3-component slowness solutions for regional P waves (Kværna and Doornbos, 1986): 1) There is a relatively large scatter in the solutions for events from the same source region, and 2) there are significant differences between the solutions at the different stations. The differences are systematic, and for a proper evaluation of NORESS and similar arrays it is important to understand their cause. Here we report on an investigation of the effects of surface topography.

The usual correction for surface topography implies an arrival time correction for elevation, and possibly a particle motion correction for surface slope. These corrections are consistent with geometrical ray theory, which requires that topographic relief be smooth on the scale of a wavelength. If this is not the case, wave scattering by topographic relief will be important. We have digitized a topographic map of the NORESS array area. The data are displayed in the form of elevation in Fig. VII.3.1, and in the form of surface gradients in Fig. VII.3.2. These figures demonstrate that topographic relief is not smooth on the scale of the wavelengths involved ($\sim 2$ km). To evaluate the scattering we have applied a recently developed multiple scattering method (Doornbos, 1988). For the present purpose, we need to determine only the displacement vector at the surface, say $\underline{u}$. In the above method, the solution for $\underline{u}$ is obtained recursively in wavenumber space. If the topography is described by a function $f(x,y)$, and $\underline{U}(k_x,k_y)$ is the Fourier transform of $\underline{u}(x,y)$, then a trial solution in the form of a perturbation series is

$$\underline{U}(k_x,k_y) = \sum_{n=0}^{\infty} \underline{U}^{(n)}(k_x,k_y)$$

and $\underline{U}^{(n)}$ is a function of $\underline{U}^{(n-m)}$, $1 < m < n$, of the surface topography $f(x,y)$, and of the surface gradients $\partial f/\partial x$, $\partial f/\partial y$. The zeroth order term $\underline{U}^{(0)}$ gives the conventional free surface response for a plane, the first order term $\underline{U}^{(1)}$ includes the Born approximation, and the higher order terms account for multiple scattering.

Kværna and Doornbos (1986) analyzed in detail the P waves from a suite of mining events in the same location near Leningrad. The slowness solution based on wide-band signals (2-4 Hz) from the complete vertical-component array, was very stable. The solution differs from that expected for $P_n$ from this source region, but the difference cannot be attributed to near-receiver structure. Hence we associate the observed slowness with that of an incident plane P wave. Three-component slowness solutions were obtained at 4 sites. The average of solutions for the 4 sites coincides reasonably well with the array solution, but there are significant differences between the individual sites, and there is also a relatively large scatter in the solutions at each site. We have synthesized the free surface response in the frequency range 2-4 Hz, and applied Kværna and Doornbos' method to determine the apparent slowness of the synthetics. The procedure was applied to the 3-component sites A0 and C7. The other 3-component sites C2 and C4 are located too close to the boundaries of the available topographic map to yield reliable synthetics. The results for discrete frequencies between 2 and 4 Hz are displayed in Fig. VII.3.3 for station A0, and in Fig. VII.3.4 for station C7. The results show a significant variation with frequency, but the average over the frequency band explains about half of the observed anomaly. We speculate that shallow subsurface structure may enhance the surface topographic effect. The variation with frequency is in agreement with the notion of surface response as an interference pattern. One consequence is that the slowness solutions for P from two events will be different if the source spectra are different. This is in agreement with the observed scatter of 3-component slowness solutions at each site. We have calculated the response at 10 other array sites for which the topographic map provides adequate information, even though there are no 3-component stations at these sites. The results for all 12 sites are summarized in Fig. VII.3.5, in the form of average azimuth angle and incidence angle. The results suggest that the particle motion vector varies smoothly across the array. An important mechanism for the perturbation of particle motion is scattering into S motion, and this modifies especially the horizontal components. The vertical components are more stable. Since the array slowness solution is based on phase differences between stations, we have also calculated the vertical component phase perturbations due to topographic relief. The corresponding delay time perturbations are included in Fig. VII.3.5. These perturbations are negligible, hence the array slowness solution appears to be relatively insensitive to topographic relief.

In summary, our results suggest that surface topographic relief significantly perturbs the surface particle motion and hence 3-component slowness solutions. The perturbation varies from site to site within the NORESS array, and it also depends on details of the input signal spectrum. On the other hand, the array slowness solution based on vertical component phase delays is relatively stable since the additional phase perturbations are negligible.

E. Ødegaard, Univ. of Oslo
D.J. Doornbos

## References

Doornbos, D.J. (1988): Multiple scattering by topographic relief, with application to the core-mantle boundary. Geophys. J., 92, 465-478.

Kværna, T. and D.J. Doornbos (1986): An integrated approach to slowness analysis with arrays and three-component stations. Semiannual Technical Summary, 1 October 1985 - 31 March 1986. NORSAR Sci. Rep. No. 1-85/86, Kjeller, Norway.

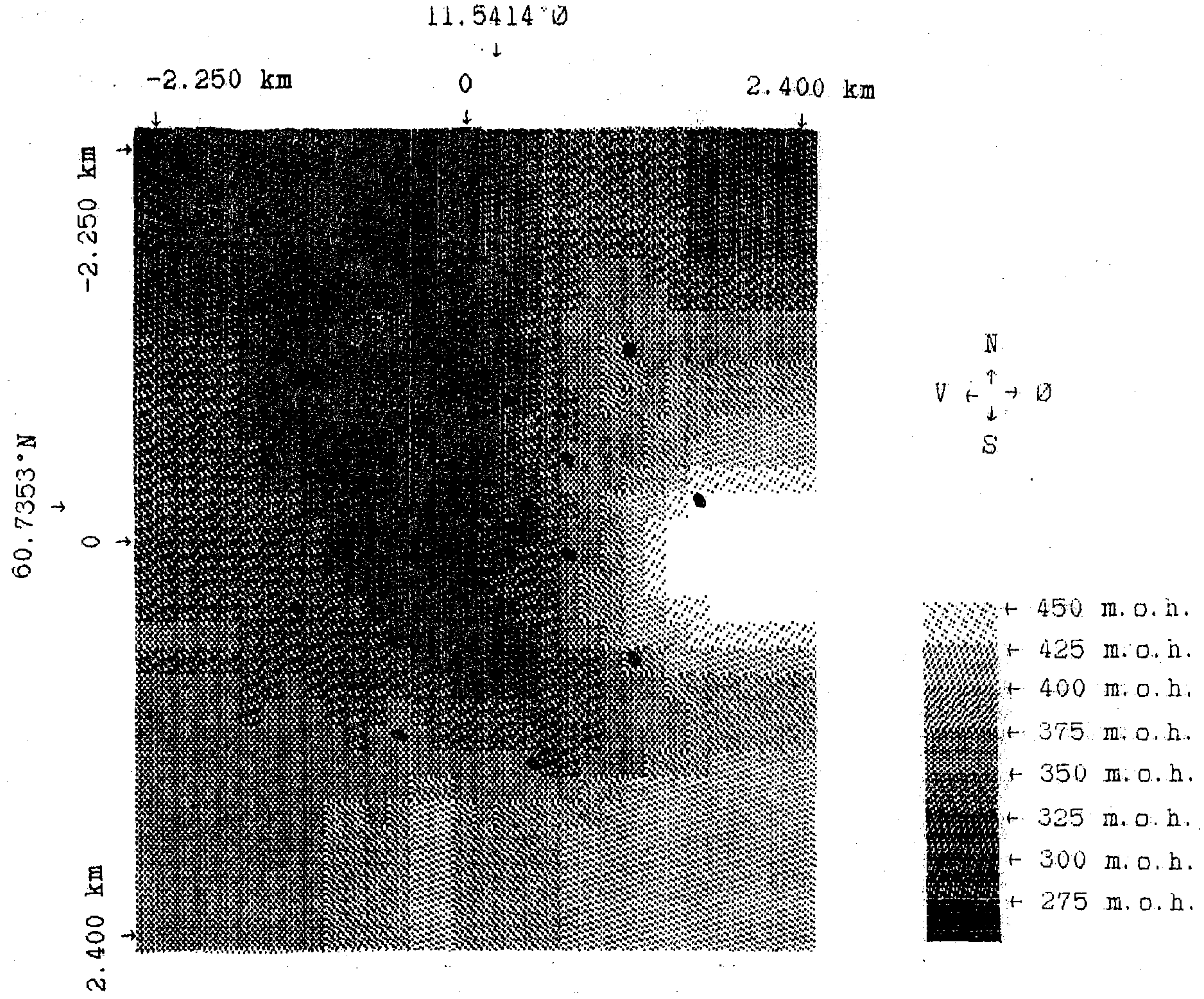

Fig. VII.3.1 Topographic map of the NORESS array area between 60.71 - 60.76°N and 11.50 - 11.58°E.

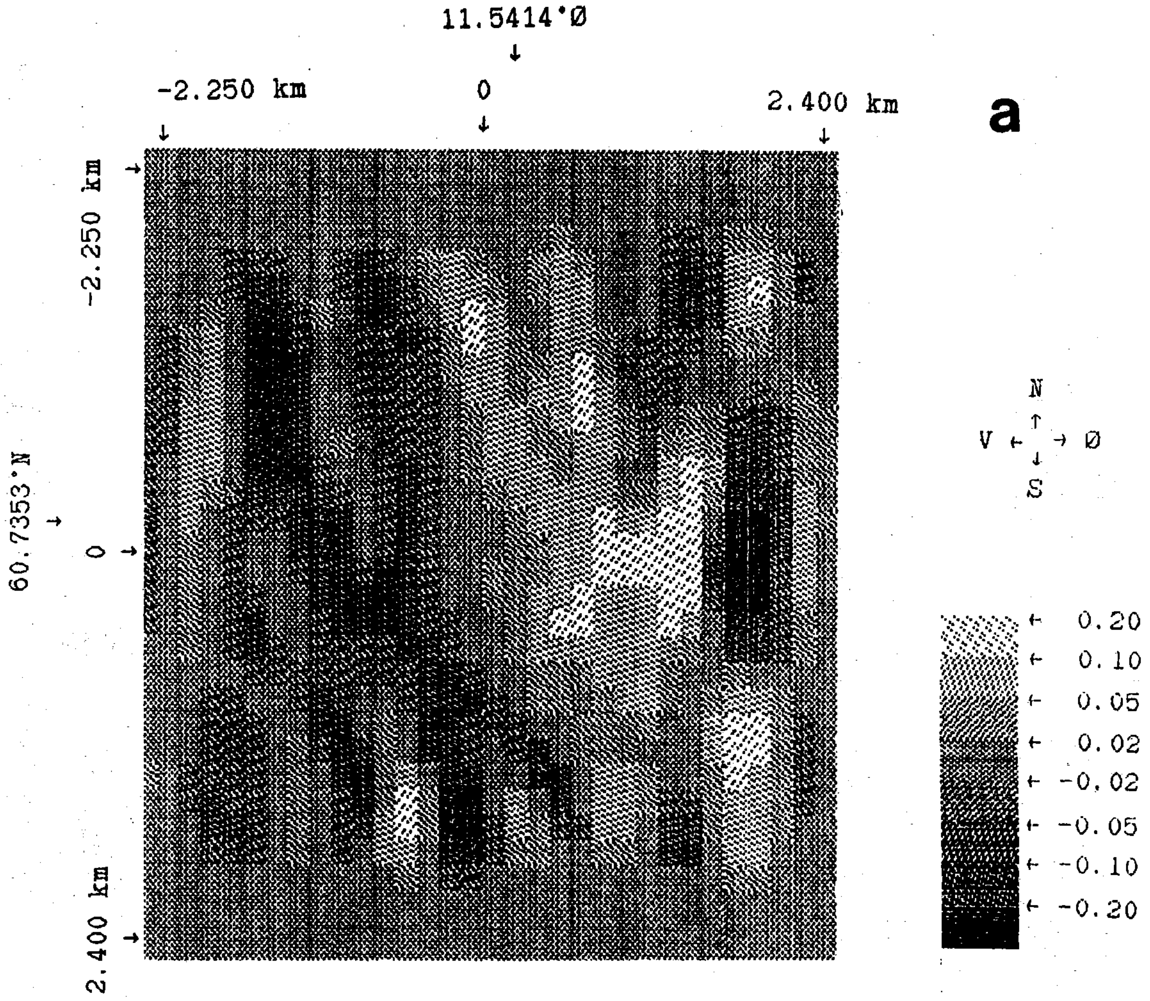

Fig. VII.3.2 Surface gradients of topography in Fig. VII.3.1. (a) Gradient toward East ( $\partial f/\partial x$). (b) Gradient toward south ( $\partial f/\partial y$). Here f(x,y) represents the topography.

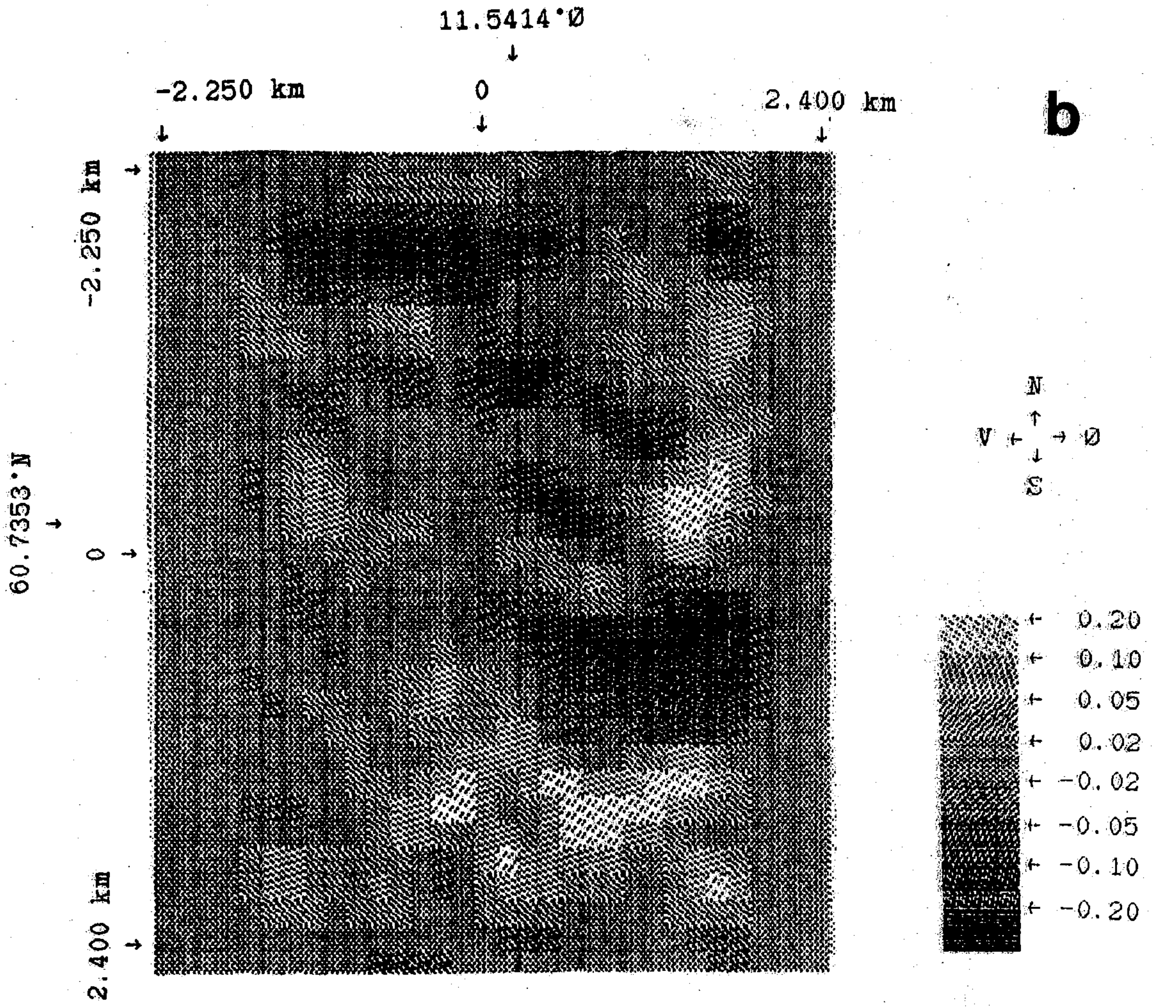

Fig. VII.3.2 (cont.)

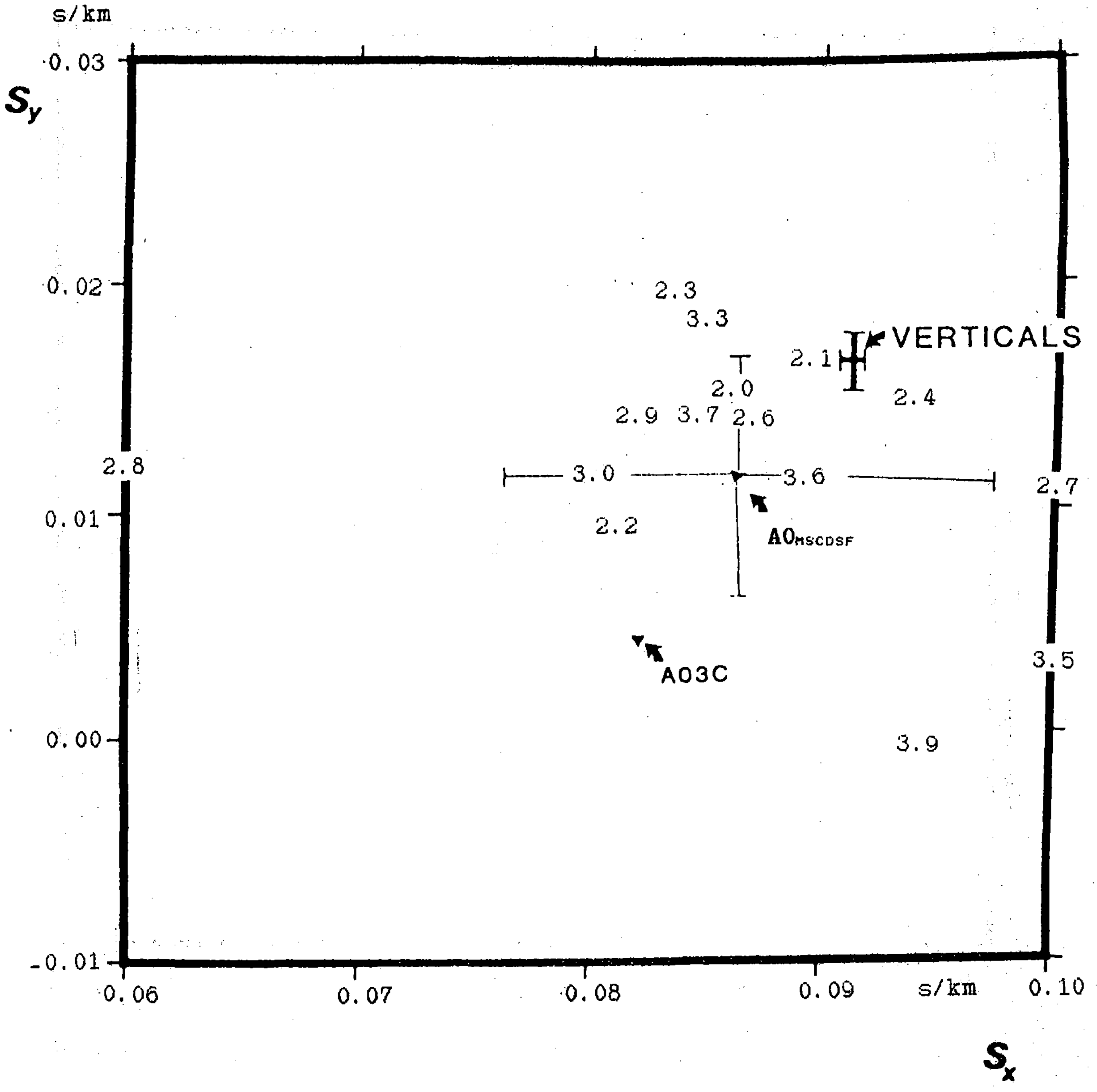

Fig. VII.3.3 Slowness solutions at site AO, based on synthetic response in the frequency range 2-4 Hz. Slowness components in s/km. The incident plane wave slowness is labelled "VERTICALS". Solutions at single frequencies are labelled by the frequency in Hz. The averaged solution over the band 2-4 Hz is labelled "AO" with standard deviations indicated. The averaged solution from real data is "A03C".

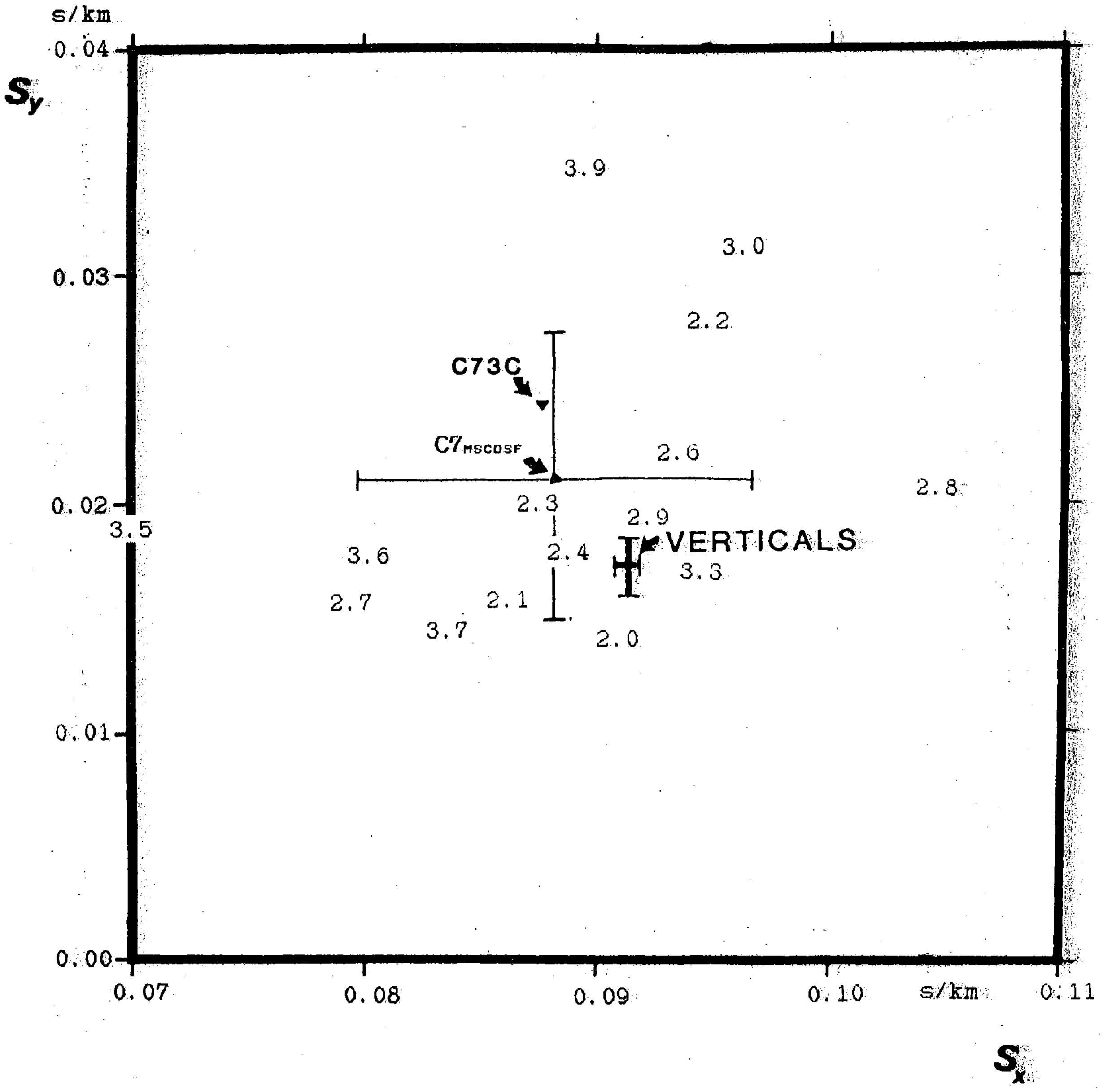

Fig. VII.3.4 Slowness solutions at site C7, based on synthetic response in the frequency range 2-4 Hz. Other details as in Fig. VII.3.3.

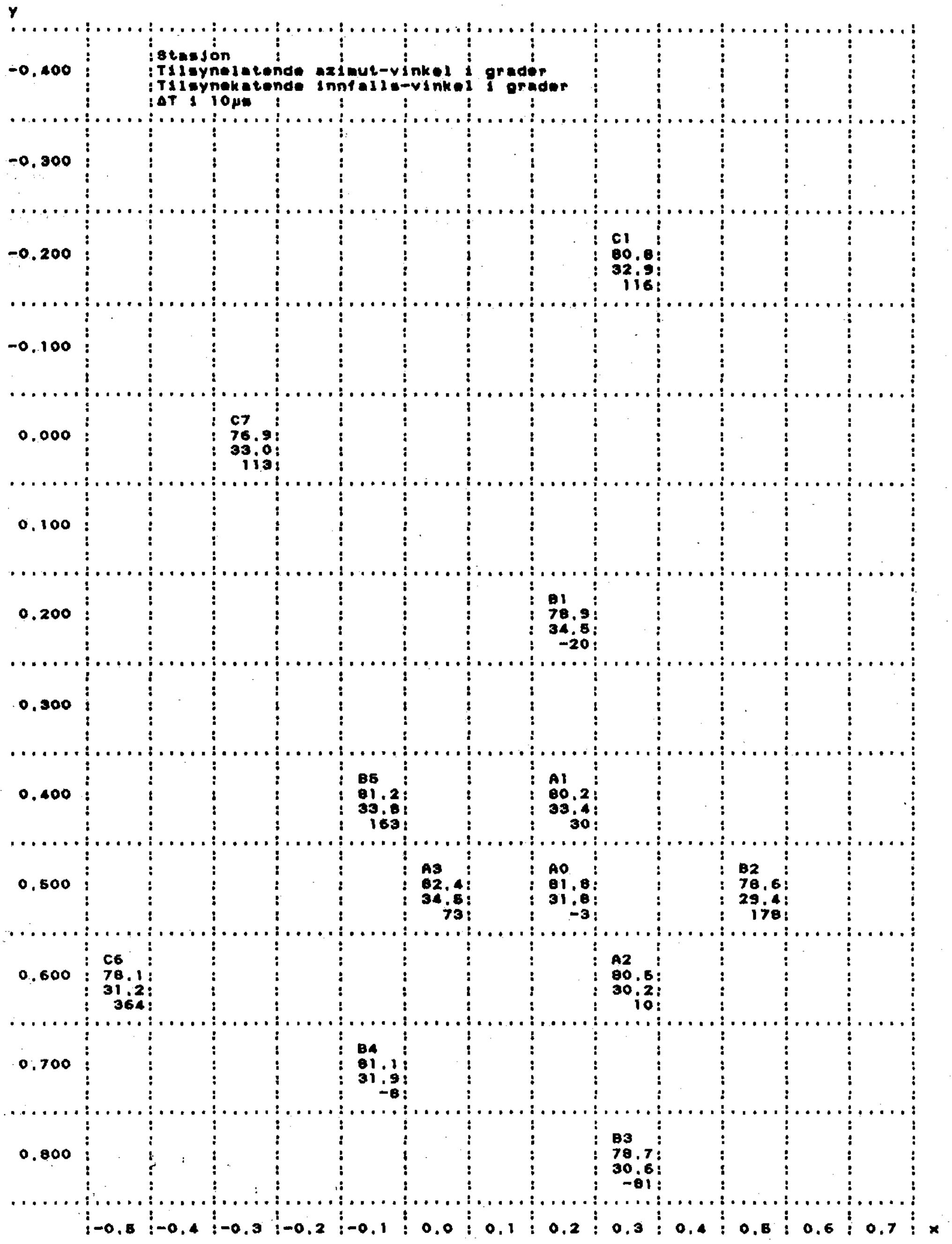

Fig. VII.3.5 Synthetic particle motion direction and delay time perturbation at 12 sites within the NORESS array. The 3 numbers given for each site denote azimuth (in $^{o}$), incidence angle (in $^{o}$), and delay time perturbation (in units of 10 $\mu$s). The theoretical numbers for a plane surface are: azimuth 79.4$^{o}$ and incidence angle 33.8$^{o}$.

## VII.4 Coupling of short period surface wavetrains across the North Sea Graben

In the previous semiannual technical report (Maupin, 1987), we briefly presented a coupling method aiming at modelling surface wave propagation in 2-D structures, and some preliminary results. The method is now applied to a model of the North Sea Graben. We examine how a large-scale and very strong lateral variation of the crustal structure affects the propagation of the short-period surface wave trains.

### Model

We use a simplified 2-D model of the North Sea Graben devised by Kennett and Mykkeltveit (1984), based on seismic refraction profiling experiments reported by Wood and Barton (1983). The model consists of purely elastic homogeneous layers of laterally varying thicknesses (Fig. VII.4.1). It is extended at depth with a 60 km thick lid, having S-wave velocities increasing from 4.65 to 4.71 km/s. The Rg, Lg and Sn wavetrains that we aim to study are supported by these crustal and lid waveguides. Due to the lateral variation of the waveguides, the wavetrains may radiate body waves, which leave the structure to propagate deeper in the mantle. The body waves can be represented by a sum of surface wave modes, as required by the coupling method, by extending the model to depths where the S-velocity is as large as the largest horizontal apparent velocity of the radiated body waves. The mantle underneath the North Sea presents a low-velocity zone (Stuart, 1978). In such a structure, a large number of modes propagate, many of them having very little energy in crustal and lid waveguides. Thus using a realistic model of the mantle requires to use a large number of modes to model the body wavefield propagating in the crust and in the lid, most of the modes having a very small contribution to the wavefield. A least-cost approximation is available with the locked mode method (Harvey, 1981); the introduction of a half-space with a very high S-wave velocity underneath the structure of interest creates trapped modes with high phase velocities able to represent the body waves with a minimum number of modes. We thus introduce a halfspace with an S-wave velocity of 7.0 km/s underneath the lid to complete the model.

The model is divided into 51 zones, 25 equally wide zones in each laterally heterogeneous outer part of the Graben, and one 50 km wide zone in the central part of the Graben. The 26 first Rayleigh wave modes and the 26 first Love wave modes are calculated in each zone at a period of 1.0 s using the subroutine package of Saito (1988). The vertical displacement with depth of the Rayleigh wave local modes at the outskirts of the Graben are plotted on Fig. VII.4.2, where they are classified according to the wavetrain they belong to. The necessity to retain only a reasonable amount of modes leads us to neglect body waves with higher apparent phase velocities than 5.1 km/s. The phase velocities of the different modes are plotted as a function of horizontal distance in the Graben on Fig. VII.4.3 for Rayleigh wave modes and on Fig. VII.4.4 for Love wave modes. The zonal phase velocities are superimposed on the local phase velocities, issued as a subproduct of the coupling method. We can notice the good agreement between the velocities calculated with the two methods. The very fine zoning in the laterally varying parts of the model is required by the non-linearity of the sedimentary layer influence, specially on the Rayleigh wave modes, testified by the oscillatory behavior of the phase velocities with distance on Fig. VII.4.3.

**Transmission properties**

Through propagation across the Graben, the different modes are coupled by the lateral heterogeneity. Due to the large scale of the model compared to the wavelengths of the modes involved in this study, the coupling in reflection is very small. For Rayleigh waves propagating perpendicularly to the Graben for example, only 0.02% of the incoming energy is reflected by the structure. We will therefore concentrate our attention on the transmission properties of the structure.

We study the transmission properties for 2 different wave propagation directions. First for waves propagating in the x-direction of the structure lateral variation. And second for waves propagating at an angle with respect to this direction. Since coupling occurs between modes having a common slowness in the y-direction parallel to the Graben structure, and that the modes involved in the coupling have different total slownesses, they all propagate in slightly different directions in the second case. As an example, we have chosen to treat the case of a slowness in the y-direction equal to 1 s/km. This corresponds to propagation with respect to the x-direction at 22° for the Rg-wavetrain, 25 to 45° for the Lg-wavetrain, around 48° for the Sn wave, and from 49 to 58° for the body waves.

The transmission matrices express how the energy of an incoming mode is distributed on the different modes of the system after propagation across the Graben. The matrix elements on Figs. VII.4.5 to VII.4.8 are the absolute values of the amplitude transmission coefficients expressed in %, for modes normalized to a unit energy flux. The square elements thus represent energy transmission coefficients. Each column of the matrix corresponds to a different incoming wave.

For propagation at right angle across the Graben, the Rayleigh and Love wave modes are decoupled. On Fig. VII.4.5 is plotted the transmission matrix for the Rayleigh wave modes, and on Fig. VII.4.6 for the Love wave modes. In this model, the fundamental mode of the Rayleigh waves, or the Rg wavetrain, is little affected by the lateral heterogeneity. It has hardly any coupling with adjacent modes (Fig. VII.4.5). We should notice that this results from the homogeneous velocities of the sedimentary layer of this model, where the Rayleigh wave fundamental mode at 1 Hz is confined. With a refined representation of the sediments, the Rg wavetrain might be more affected by the Graben structure. Among the other Rayleigh wave modes of Fig. VII.4.5, the Lg modes are strongly coupled to each other as well as to the Sn modes. Their coupling is weaker with the body wave modes. The Sn modes are strongly coupled both to the Lg modes and to the body waves. And symmetrically, the SV body waves are strongly coupled to the Sn modes, but weakly to the Lg ones. The partition of the modal set into different wavetrains associated with different waveguides is clearly mirrored by the transmission matrix. The strongest couplings appear to be restricted to neighboring waveguides. The coupling pattern is somewhat more complex for the Love wave modes (Fig. VII.4.6). For the Love waves, the coupling of the Lg wave modes is fairly strong both with the Sn wave and the body waves, and the Sn wave modes are strongly coupled with Lg as well as with body wave modes.

Figs. VII.4.7 and VII.4.8 display the transmission matrices for Rayleigh and Love waves propagating at an angle with respect to the x-direction. The shift of the propagation direction away from the direction of lateral variation of the structure does not strongly alter the coupling among the Rayleigh wave modes or among the Love wave modes. The new feature is the coupling between the Love and Rayleigh wave modes, which remains nonetheless very small.

In order to summarize the results quantitatively, we transform the transmission matrices, expressed as mode to mode coupling coefficients, into energy transfers from wavetrain to wavetrain. Since the coupling between two wavetrains depends on the modal content, both in amplitude and in phase, of the incoming wavetrain, we average out over amplitudes and phases in order to obtain a mean coupling, comparable to a general trend in a set of seismograms. Averaging out the amplitudes is equivalent to using a wavetrain where the energy is equally distributed among the different modes. The energy carried by a mode or a wavetrain is also distributed with depth differently from one mode to another, and therefore does not directly predict the amplitude of its surface displacement. The energy transfers need thus also to be converted into wavetrain amplitudes at the surface of the model to be directly comparable to observed seismograms.

In Table VII.4.1, we give the percentage of energy distributed on the different wavetrains of the system (1st column) after propagation across the Graben, for different incoming wavetrains. The energy distribution is also transcribed into surface amplitudes (2nd column) scaled to the surface amplitude of the incoming wavetrain. We use the vertical displacement for the Rayleigh waves. The two first parts of the table deal with Rayleigh and Love waves propagating at right angle across the Graben. The lower part of the table displays the coupling among wavetrains propagating across the North Sea Graben in a direction non-perpendicular to the symmetry direction of the structure. The most significant features of the table are expressed as diagrams on Figs. VII.4.9 to VII.4.11.

The properties of the transmission matrices are of course mirrored into the parts of the table and diagrams related to energy transmission. We recognize the independence of Rg wavetrain (Fig. VII.4.9a). Whether they are of Rayleigh or Love type, and whether they propagate in a direction perpendicular or not to the structure, the Lg wavetrains leak only a small fraction of their energy in the Sn wave and in the body waves (Fig. VII.4.9b, 9c and 10). The energy transferred from Rayleigh to Love wave modes (Fig. VII.4.9c) or conversely (Fig. VII.4.10b) when the propagation direction is at an angle with respect to the structure, is very small. Fig. VII.4.11 displays the strong transfer from Sn to Lg and body-wave energy.

If we now turn to the transcription of these energy transfers into surface displacement amplitudes, we notice that the transfers from Lg to Sn waves, which shift some energy depthward, reduce the total amplitude of the signal (see Fig. VII.4.9b and 10a, where the amplitude of the body waves, transferred into deeper parts of the earth, should not be considered as part of the signal). On the other hand, the strong conversion from Sn to Lg produces an Lg surface signal at the exit of the Graben 2.5 times larger than the original surface displacement for Rayleigh waves (Fig. VII.4.11) and 3 times larger for Love waves.

Similarly, and despite the small amount of energy involved, transfers from Rayleigh to Love modes enhance the surface displacement significantly. For example, we observe on Fig. VII.4.9c that the total Lg wavetrain at the exit of the Graben presents a transversal displacement (associated with Love wave modes) up to 0.3 times the vertical displacement (associated with Rayleigh wave modes). Conversely, transfers from Love to Rayleigh wave modes does not produce such a significant vertical surface displacement (Fig. VII.4.10b). This results from the general property of the surface displacements around 1 Hz, which are on the average twice as large for Lg Love wave modes as for Lg Rayleigh wave modes, for a similar amount of energy at depth. This property predicts that, if after some strong couplings, the energy becomes equally distributed among Love and Rayleigh modes, the transversal component of the Lg wavetrain is twice as large as the vertical one.

## Conclusion

We find a mean energy transmission across the North Sea Graben of 80% for an Lg wavetrain at 1 Hz. This is in apparent contradiction with the extinction of the Lg phase across this structure, as observed by Kennett and Mykkeltveit (1984). Even if we include more modes in order to better account for the body waves propagating in the mantle, and thereby decrease the amount of energy confined in the waveguides, it seems unlikely that this will prove sufficient to reconcile modelling results and observations. These results deal only with the amplitude of the transmission matrix at a given period. The phase behavior of the wave as a function of period is a key-element to the effective build-up of a wavetrain. Further tests need thus to be performed to study how the phase of the transmission matrix varies with period. If rapid variations are observed, destructive interferences between neighboring periods might explain the disappearance of the Lg wavetrain. Furthermore, our modelling accounts only for the gross features of the Graben. Other phenomena, such as a strong attenuation or particularly important small-scale heterogeneities able to reflect energy, might be associated with the sedimentary thickening and the Moho uprising to explain the extinction of the Lg phase.

On the other hand, our results concerning Rayleigh-Love couplings are in better agreement with observations of anomalously high transversal motions on Lg wavetrains (Kennett and Mykkeltveit, 1984) for explosive sources. Despite a level of coupling rather low in the above example, we show how the couplings from Rayleigh to Love waves enhance the total displacement, whereas couplings from Love to Rayleigh waves lower it, and that strong couplings produce Lg transversal surface displacement twice as large as the vertical one.

V. Maupin, Postdoctorate
Fellow

References

Harvey, D.J. (1981): Seismogram synthesis using normal mode superposition: the locked mode approximation. Geophys. J.R. astr. Soc., 66, 37-70.

Kennett, B.L.N. and S. Mykkeltveit (1984): Guided wave propagation in laterally varying media. II: Lg waves in northwestern Europe. Geophys. J.R. astr. Soc., 79, 257-267.

Maupin, V. (1987): Preliminary tests for surface waves in 2-D structures. Semiann. Tech. Summary, 1 Apr - 30 Sep 1987, NORSAR Sci. Rep. No. 1-87/88, Kjeller, Norway.

Saito, M. (1988): Disper80: a subroutine package for the calculation of seismic normal mode solutions. In: D.J. Doornbos (ed.), Seismological Algorithms, Academic Press.

Stuart, G.W. (1978): The upper mantle structure of the North Sea region from Rayleigh wave dispersion. Geophys. J.R. astr. Soc., 52, 367-382.

Wood, R. and P. Barton (1983): Crustal thinning and subsidence in the North Sea. Nature, 302, 134-136.

Propagation perpendicular to the Graben

Rayleigh waves

| Input<br>Output | Rg | | Lg | | Sn | |
|---|---|---|---|---|---|---|
| Rg | 99.667 | 0.9983 | 0.026 | 0.0297 | 0.002 | 0.0826 |
| Lg | 0.281 | 0.0278 | 79.172 | 0.8837 | 37.043 | 2.4583 |
| Sn | 0.007 | 0.0004 | 10.071 | 0.0347 | 18.139 | 0.2903 |
| P/Sv | 0.038 | 0.0012 | 10.735 | 0.0436 | 44.810 | 0.8721 |

Love waves

| Input<br>Output | | | Lg | | Sn | |
|---|---|---|---|---|---|---|
| Lg | | | 78.560 | 0.9038 | 22.100 | 3.0854 |
| Sn | | | 3.692 | 0.0242 | 48.885 | 0.6393 |
| Sh | | | 17.751 | 0.1899 | 29.021 | 1.7655 |

Propagation at an angle with the Graben

| Input<br>Output | R Rg | | R Lg | | R Sn | |
|---|---|---|---|---|---|---|
| R Rg | 99.737 | 0.9987 | 0.015 | 0.0229 | 0.001 | 0.0402 |
| R Lg | 0.168 | 0.0206 | 76.146 | 0.8628 | 33.267 | 4.9471 |
| R Sn | 0.002 | 0.0002 | 9.083 | 0.0327 | 11.992 | 0.3345 |
| R P/Sv | 0.027 | 0.0008 | 12.774 | 0.0489 | 53.874 | 0.8546 |
| L Lg | 0.048 | 0.0295 | 1.325 | 0.2538 | 0.601 | 1.1842 |
| L Sn | 0.004 | 0.0010 | 0.207 | 0.0128 | 0.065 | 0.0655 |
| L Sh | 0.012 | 0.0054 | 0.446 | 0.0616 | 0.193 | 0.3828 |

| Input<br>Output | | | L Lg | | L Sn | |
|---|---|---|---|---|---|---|
| R Rg | | | 0.004 | 0.0052 | 0.002 | 0.0302 |
| R Lg | | | 1.214 | 0.0477 | 1.143 | 0.3451 |
| R Sn | | | 0.151 | 0.0019 | 0.098 | 0.0122 |
| R P/Sv | | | 0.688 | 0.0045 | 0.284 | 0.0222 |
| L Lg | | | 77.177 | 0.8926 | 26.910 | 3.5245 |
| L Sn | | | 4.459 | 0.0266 | 42.850 | 0.6438 |
| L Sh | | | 16.311 | 0.1756 | 28.719 | 1.6148 |

Table VII.4.1 Wavetrain coupling at 1 Hz by propagation across the North Sea Graben. The left columns give the energy distribution in %, and the right columns give the surface displacement amplitudes, normalized to the surface displacement of the incoming wave, of the different wavetrains, at the exit of the model. Rayleigh wavetrains are noted R and Love wavetrains are noted L.

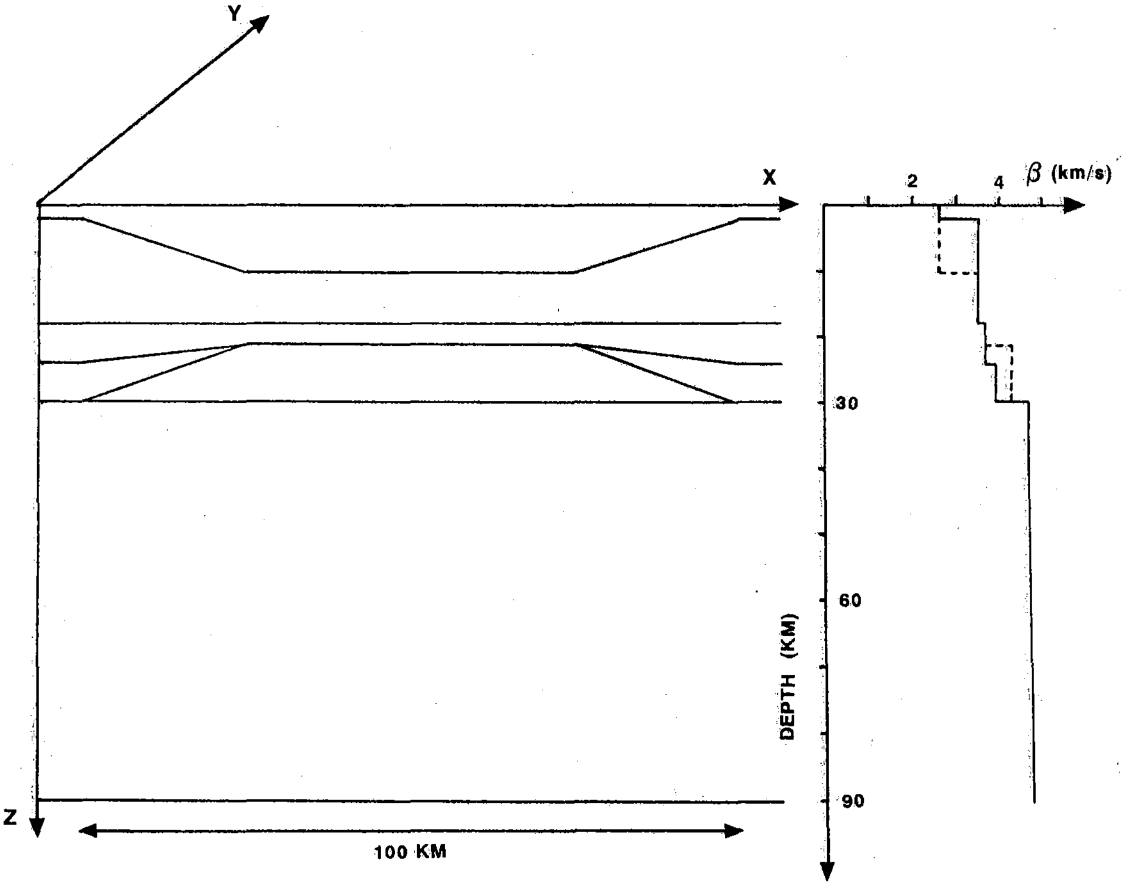

Fig. VII.4.1 Model of the North Sea Graben (after Kennett and Mykkeltveit, 1984).

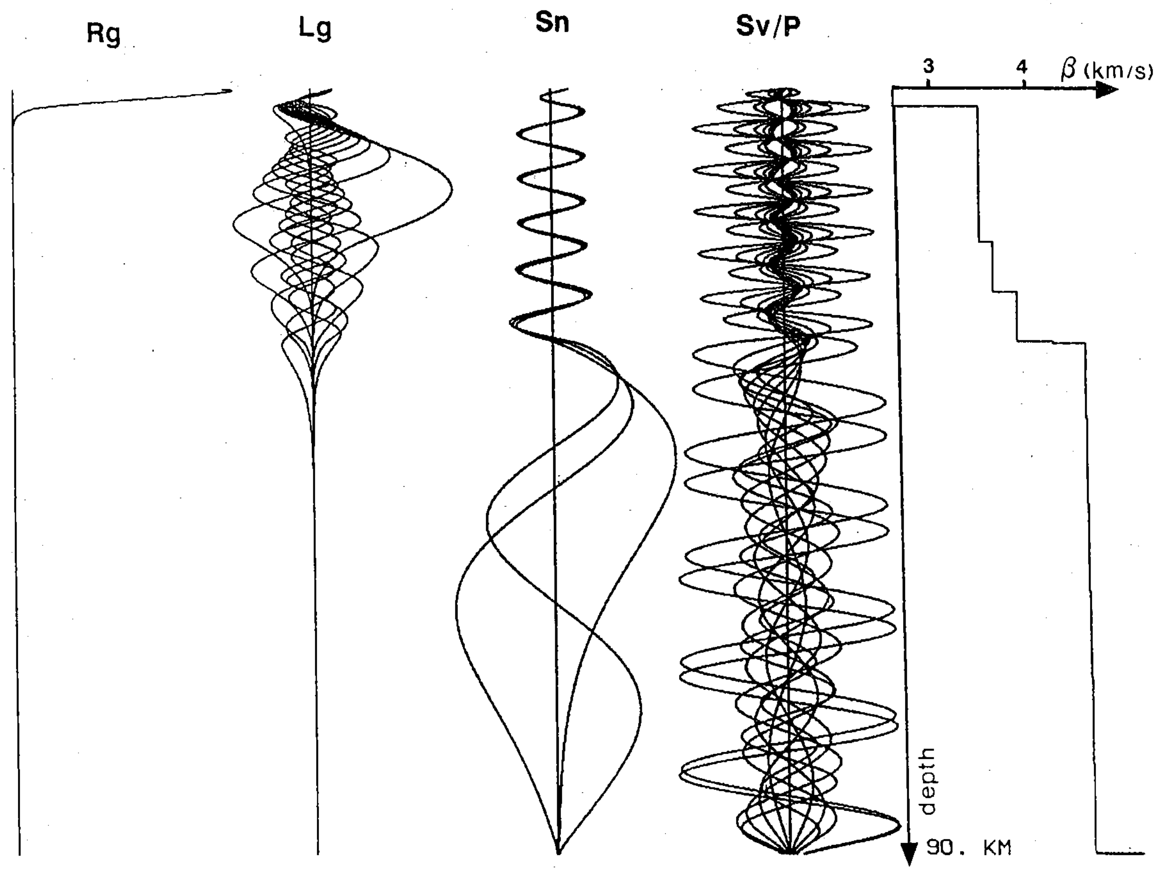

Fig. VII.4.2 Vertical displacement as a function of depth of the 26 first Rayleigh wave modes at 1 Hz at the outskirts of the North Sea Graben. The modes are classified according to the wavetrain they belong to. The S-wave velocity as a function of depth is plotted for reference.

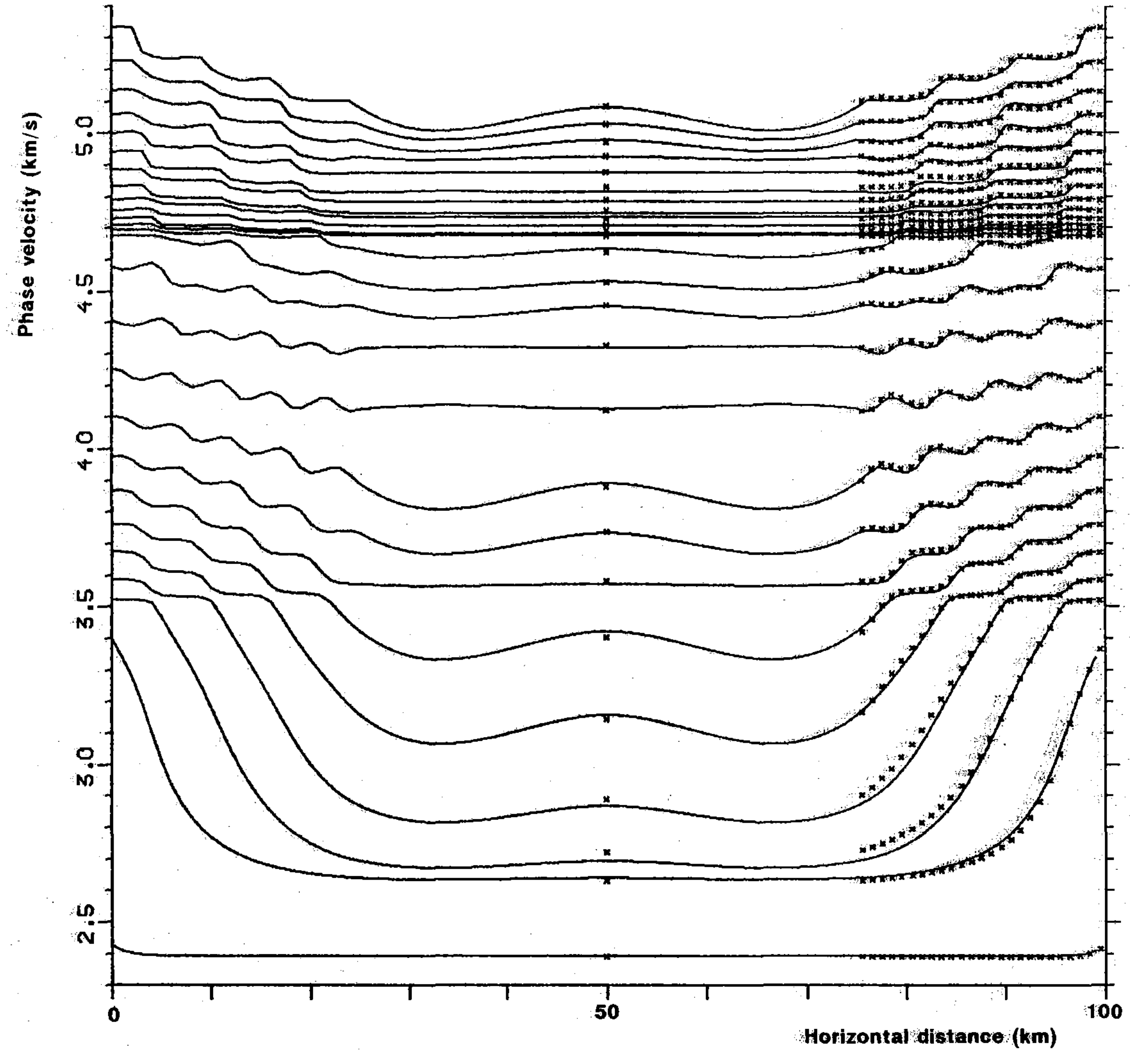

Fig. VII.4.3 Phase velocities of the 26 first Rayleigh wave modes as a function of horizontal distance in the North Sea Graben model, at 1 Hz. The lines represent the phase velocities integrated by the coupling method, and the crosses represent the zonal phase velocities (with omission of the left side crosses).

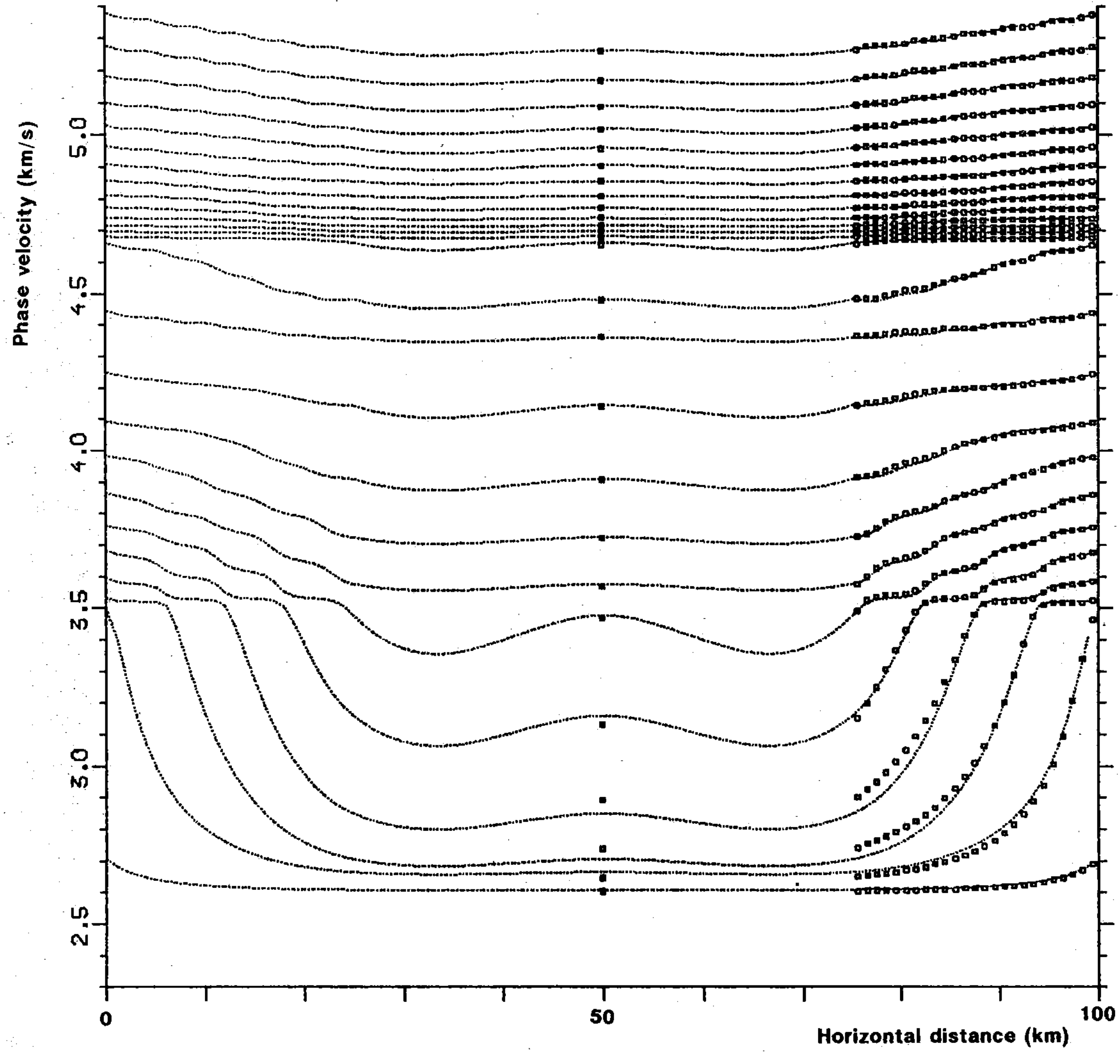

Fig. VII.4.4 Figure caption as for Fig. VII.4.3, for Love wave modes.

| | | Rg | Lg | | | | | | | | | | | Sn | | | P and Sv | | | | | | | | | | |
|---|---|---|---|---|---|---|---|---|---|---|---|---|---|---|---|---|---|---|---|---|---|---|---|---|---|---|---|
| | | 0 | 1 | 2 | 3 | 4 | 5 | 6 | 7 | 8 | 9 | 10 | 11 | 12 | 13 | 14 | 15 | 16 | 17 | 18 | 19 | 20 | 21 | 22 | 23 | 24 | 25 |
| Rg | 0 | 99 | 3 | 0 | 1 | 1 | 1 | 0 | 1 | 1 | 0 | 1 | 0 | 0 | 0 | 0 | 0 | 0 | 0 | 0 | 0 | 0 | 0 | 0 | 0 | 0 | 0 |
| | 1 | 3 | 45 | 7 | 40 | 42 | 47 | 20 | 9 | 13 | 5 | 7 | 6 | 11 | 11 | 15 | 11 | 2 | 9 | 11 | 3 | 4 | 10 | 10 | 13 | 5 | 9 |
| | 2 | 0 | 7 | 17 | 8 | 7 | 12 | 56 | 43 | 4 | 28 | 22 | 21 | 20 | 15 | 17 | 15 | 5 | 9 | 19 | 10 | 4 | 6 | 5 | 12 | 14 | 13 |
| | 3 | 1 | 40 | 8 | 56 | 20 | 28 | 17 | 29 | 23 | 17 | 21 | 3 | 11 | 11 | 13 | 12 | 4 | 9 | 15 | 7 | 1 | 3 | 6 | 11 | 8 | 6 |
| | 4 | 1 | 42 | 7 | 20 | 40 | 29 | 14 | 36 | 35 | 17 | 32 | 22 | 8 | 15 | 1 | 6 | 4 | 3 | 7 | 2 | 3 | 4 | 3 | 8 | 2 | 3 |
| | 5 | 1 | 47 | 12 | 28 | 29 | 27 | 34 | 26 | 11 | 29 | 21 | 10 | 4 | 25 | 20 | 7 | 8 | 10 | 6 | 3 | 1 | 9 | 4 | 6 | 10 | 5 |
| Lg | 6 | 0 | 20 | 56 | 17 | 14 | 34 | 14 | 24 | 32 | 13 | 13 | 12 | 6 | 33 | 19 | 14 | 6 | 13 | 7 | 2 | 2 | 6 | 5 | 5 | 12 | 2 |
| | 7 | 1 | 9 | 43 | 29 | 36 | 26 | 24 | 50 | 16 | 3 | 5 | 18 | 3 | 12 | 22 | 3 | 6 | 8 | 9 | 3 | 2 | 5 | 10 | 6 | 10 | 3 |
| | 8 | 1 | 13 | 4 | 23 | 35 | 11 | 32 | 16 | 47 | 35 | 24 | 14 | 2 | 14 | 30 | 10 | 5 | 1 | 8 | 8 | 1 | 6 | 14 | 13 | 17 | 6 |
| | 9 | 0 | 5 | 28 | 17 | 17 | 29 | 13 | 3 | 35 | 48 | 16 | 34 | 12 | 33 | 10 | 12 | 7 | 9 | 4 | 7 | 5 | 3 | 13 | 16 | 8 | 10 |
| | 10 | 1 | 7 | 22 | 21 | 32 | 21 | 13 | 5 | 24 | 16 | 45 | 16 | 34 | 16 | 22 | 5 | 27 | 16 | 20 | 8 | 11 | 11 | 3 | 8 | 6 | 9 |
| | 11 | 0 | 6 | 21 | 3 | 22 | 10 | 12 | 18 | 14 | 34 | 16 | 59 | 22 | 21 | 8 | 16 | 20 | 19 | 6 | 7 | 15 | 5 | 12 | 19 | 12 | 7 |
| | 12 | 0 | 11 | 20 | 11 | 8 | 5 | 6 | 3 | 2 | 12 | 34 | 22 | 37 | 22 | 9 | 13 | 28 | 28 | 32 | 24 | 12 | 28 | 10 | 23 | 11 | 9 |
| Sn | 13 | 0 | 11 | 15 | 11 | 15 | 25 | 32 | 12 | 13 | 33 | 16 | 21 | 22 | 4 | 35 | 29 | 21 | 12 | 27 | 9 | 15 | 12 | 21 | 9 | 18 | 2 |
| | 14 | 0 | 15 | 17 | 13 | 1 | 20 | 19 | 22 | 30 | 10 | 23 | 8 | 9 | 35 | 19 | 15 | 11 | 13 | 28 | 15 | 10 | 14 | 29 | 27 | 29 | 10 |
| | 15 | 0 | 11 | 15 | 13 | 6 | 7 | 14 | 3 | 10 | 12 | 5 | 16 | 14 | 28 | 14 | 63 | 25 | 26 | 5 | 13 | 24 | 16 | 9 | 14 | 19 | 10 |
| | 16 | 0 | 2 | 5 | 4 | 4 | 8 | 7 | 6 | 6 | 7 | 27 | 20 | 28 | 21 | 10 | 24 | 66 | 21 | 15 | 23 | 21 | 7 | 0 | 9 | 11 | 2 |
| | 17 | 0 | 9 | 9 | 9 | 3 | 10 | 13 | 8 | 1 | 9 | 16 | 19 | 28 | 12 | 13 | 26 | 20 | 52 | 28 | 35 | 26 | 8 | 9 | 20 | 14 | 3 |
| P | 18 | 0 | 11 | 19 | 15 | 7 | 6 | 7 | 9 | 8 | 4 | 20 | 6 | 32 | 27 | 29 | 4 | 15 | 28 | 36 | 21 | 6 | 25 | 21 | 29 | 26 | 13 |
| | 19 | 0 | 3 | 10 | 7 | 2 | 3 | 2 | 3 | 8 | 7 | 8 | 7 | 24 | 10 | 15 | 13 | 23 | 35 | 21 | 69 | 9 | 7 | 18 | 17 | 17 | 14 |
| and | 20 | 0 | 4 | 4 | 1 | 3 | 1 | 2 | 2 | 1 | 5 | 11 | 15 | 12 | 15 | 10 | 25 | 21 | 26 | 6 | 9 | 76 | 16 | 20 | 17 | 11 | 8 |
| | 21 | 0 | 10 | 5 | 3 | 4 | 9 | 6 | 5 | 6 | 3 | 11 | 5 | 28 | 11 | 14 | 16 | 7 | 9 | 25 | 7 | 16 | 81 | 5 | 8 | 11 | 4 |
| Sv | 22 | 0 | 10 | 5 | 6 | 3 | 4 | 5 | 10 | 14 | 13 | 3 | 12 | 10 | 21 | 29 | 9 | 0 | 9 | 21 | 18 | 20 | 5 | 59 | 43 | 24 | 14 |
| | 23 | 0 | 13 | 12 | 11 | 8 | 6 | 5 | 6 | 13 | 16 | 8 | 19 | 23 | 9 | 27 | 15 | 9 | 20 | 29 | 17 | 17 | 8 | 43 | 26 | 19 | 41 |
| | 24 | 0 | 5 | 14 | 8 | 2 | 10 | 12 | 10 | 17 | 8 | 6 | 12 | 11 | 18 | 29 | 19 | 11 | 14 | 26 | 17 | 11 | 11 | 24 | 19 | 62 | 21 |
| | 25 | 0 | 9 | 13 | 6 | 3 | 5 | 2 | 3 | 6 | 10 | 9 | 7 | 9 | 2 | 10 | 10 | 2 | 3 | 13 | 14 | 8 | 4 | 14 | 42 | 21 | 78 |

Fig. VII.4.5 Transmission matrix in % for the 26 first Rayleigh wave modes at 1 Hz, after crossing the North Sea Graben perpendicularly. The matrix elements are the absolute values of amplitude transmission coefficients which carry a unit energy flux.

```
                              Lg                                  Sn                          Sh

          0   1   2   3   4   5   6   7   8   9  10  11     12  13     14  15  16  17  18  19  20  21  22  23  24  25
                                                         .          .                                                .
     0   78   9  41  31  12  15   5   6   3   2   9   6 .   9   5 .   0   3   5   4   1   6   7   6   5   3   1   3 .
     1    9  46  23  38  28  54   7  14  12   7  23   6 .   8   5 .   1   1   4   3   5  12  14  12   8   2   5   9 .
     2   41  23  43  15  21  11  28   5   3  20  21  22 .  31  17 .   0   9  15  11   3  12  14  14  16  12   5   4 .
     3   31  38  15  43  30  26  18   9  30  16   4   1 .  17   7 .   1   4   8   7   3  15  19  18  18  11   8   7 .
     4   12  28  21  30  13  41  17  29  32  27  40  19 .  12   3 .   4   2   1   4   4   4   9  11  10   4   2   5 .
     5   15  54  11  26  41  13  19  14  21  22  15   9 .  16   6 .   4   2   2   5   3  11  19  21  18  10  12  14 .
Lg   6    5   7  28  18  17  19  57  40  21  10  23  27 .  10   4 .   1   2   7   6   3  14  17  13  10   7   6   9 .
     7    6  14   5   9  29  14  40  47  28  43   4   1 .   7   4 .   9  10   8   3   5   9  14  16  12   8  14  21 .
     8    3  12   3  30  32  21  21  28  43  27  39   8 .   9   9 .   6   6   7   6   6   5   9  12  10  10  16  25 .
     9    2   7  20  16  28  23  10  43  27  14   8  31 .  16  13 .  12  11  15  18  11   3   1   5   9  14  26  36 .
    10    9  23  21   4  40  14  23   4  39   8  21  20 .  20  20 .  15  13  13  20  24  14   2  10  14  12  12  24 .
    11    6   6  22   1  19   9  27   1   7  31  20  50 .  10  16 .  14  12   9  10  15  31  25   1  22  25  11   9 .
        ...........................................................................................................
Sn  12    9   8  31  17  12  16  10   7   9  17  20  10 .  39  23 .  16  17  26  30  24  18  16  17  18  17  17  13 .
    13    5   4  17   7   3   5   4   5   9  13  20  16 .  24  84 .  10   6   9  11   5   3   7   5   5  11  12   9 .
        ...........................................................................................................
    14    0   1   0   1   4   4   1   9   6  12  14  14 .  16  12 .  90  10  10   9   3   3   5   2   3   9  10   6 .
    15    3   1   9   4   2   2   2   9   6  11  12  12 .  17   6 .  11  90  12  10   4   6   6   2   3   9   9   5 .
    16    5   4  15   8   1   2   7   8   7  15  13   9 .  26   9 .  10  13  84  16  12   9   7   2   4   8   6   4 .
    17    4   3  11   7   4   5   6   3   6  18  20  10 .  29  11 .   9  10  16  80  19  11   4   3   7   9   6   4 .
    18    1   5   3   3   4   3   3   5   6  11  24  15 .  24   5 .   3   4  12  19  83  15   9   2   6  10  11   9 .
Sh  19    6  12  12  15   4  11  14   9   5   3  14  31 .  18   3 .   3   6   9  11  16  74  24  14   4   5  12  13 .
    20    7  14  14  19   9  19  17  14   9   1   2  25 .  15   7 .   5   6   7   4   9  24  70  26  19   7   7  12 .
    21    6  12  14  19  11  21  13  16  12   5  10   1 .  17   5 .   2   2   2   3   3  14  27  66  35  25  11   2 .
    22    5   8  16  18  10  18  10  12  10   9  14  22 .  18   5 .   3   3   4   7   6   4  19  36  53  42  26  11 .
    23    3   2  12  11   4  10   7   8  10  14  12  25 .  17  11 .   9   9   8   9  10   5   7  25  43  52  38  24 .
    24    1   5   5   8   2  12   6  14  17  26  12  11 .  17  12 .  10   9   6   6  11  12   7  11  26  38  58  37 .
    25    3   9   4   7   5  14   9  21  25  36  24   9 .  13   9 .   6   6   4   4   9  13  12   2  11  24  37  58 .
        ...........................................................................................................
```

Fig. VII.4.6 Figure caption the same as for Fig. VII.4.5, for the first 26 Love wave modes.

|  |  |  | Rg |  |  |  |  | Lg |  |  |  |  |  |  | Sn |  |  |  |  |  |  | P and Sv |  |  |  |  |
|---|---|---|---|---|---|---|---|---|---|---|---|---|---|---|---|---|---|---|---|---|---|---|---|---|---|---|
|  |  |  | 0 | 1 | 2 | 3 | 4 | 5 | 6 | 7 | 8 | 9 | 10 | 11 | 12 | 13 | 14 | 15 | 16 | 17 | 18 | 19 | 20 | 21 | 22 | 23 | 24 | 25 |
| Rayleigh modes | Rg | 0 | 99 | 2 | 0 | 0 | 0 | 1 | 2 | 0 | 0 | 0 | 0 | 0 | 0 | 0 | 0 | 0 | 0 | 0 | 0 | 0 | 0 | 0 | 0 | 0 | 0 | 0 |
|  |  | 1 | 2 | 46 | 16 | 43 | 17 | 49 | 31 | 23 | 3 | 5 | 5 | 13 | 5 | 7 | 9 | 1 | 5 | 5 | 1 | 2 | 8 | 11 | 11 | 6 | 7 | 12 |
|  |  | 2 | 0 | 16 | 26 | 21 | 46 | 39 | 6 | 2 | 39 | 19 | 10 | 23 | 12 | 23 | 13 | 2 | 13 | 4 | 4 | 5 | 9 | 12 | 7 | 2 | 13 | 12 |
|  |  | 3 | 0 | 43 | 21 | 61 | 4 | 38 | 21 | 26 | 16 | 5 | 4 | 13 | 10 | 2 | 6 | 5 | 1 | 0 | 8 | 5 | 1 | 4 | 7 | 4 | 3 | 2 |
|  |  | 4 | 0 | 17 | 46 | 4 | 54 | 31 | 33 | 19 | 11 | 16 | 22 | 8 | 5 | 13 | 5 | 3 | 12 | 3 | 3 | 5 | 6 | 11 | 10 | 2 | 3 | 9 |
|  |  | 5 | 1 | 49 | 39 | 38 | 31 | 16 | 5 | 11 | 18 | 15 | 22 | 9 | 7 | 23 | 3 | 4 | 15 | 3 | 4 | 6 | 10 | 14 | 10 | 6 | 4 | 17 |
|  | Lg | 6 | 2 | 31 | 6 | 21 | 33 | 5 | 64 | 25 | 15 | 16 | 7 | 9 | 7 | 23 | 11 | 6 | 17 | 7 | 4 | 4 | 7 | 12 | 9 | 8 | 7 | 14 |
|  |  | 7 | 0 | 23 | 2 | 26 | 19 | 11 | 25 | 42 | 11 | 41 | 27 | 26 | 28 | 11 | 22 | 8 | 8 | 7 | 18 | 6 | 1 | 6 | 8 | 10 | 9 | 7 |
|  |  | 8 | 0 | 3 | 39 | 16 | 11 | 18 | 16 | 11 | 47 | 28 | 14 | 34 | 18 | 30 | 24 | 5 | 9 | 10 | 12 | 3 | 1 | 5 | 5 | 8 | 16 | 8 |
|  |  | 9 | 0 | 5 | 19 | 5 | 16 | 15 | 16 | 41 | 28 | 54 | 23 | 3 | 4 | 31 | 19 | 13 | 15 | 5 | 5 | 4 | 6 | 11 | 7 | 5 | 14 | 12 |
|  |  | 10 | 0 | 5 | 10 | 4 | 22 | 22 | 7 | 27 | 14 | 23 | 45 | 19 | 20 | 22 | 11 | 29 | 34 | 20 | 6 | 12 | 0 | 9 | 12 | 10 | 19 | 13 |
|  |  | 11 | 0 | 13 | 23 | 13 | 8 | 9 | 9 | 26 | 34 | 3 | 19 | 46 | 9 | 17 | 31 | 14 | 30 | 24 | 13 | 14 | 10 | 3 | 12 | 20 | 0 | 8 |
|  |  | 12 | 0 | 5 | 12 | 10 | 5 | 7 | 7 | 28 | 18 | 4 | 21 | 9 | 17 | 11 | 7 | 32 | 12 | 40 | 41 | 17 | 12 | 34 | 4 | 21 | 14 | 18 |
|  | Sn | 13 | 0 | 7 | 23 | 2 | 13 | 23 | 23 | 11 | 30 | 31 | 22 | 16 | 11 | 37 | 22 | 19 | 22 | 1 | 25 | 11 | 2 | 8 | 7 | 27 | 12 | 19 |
|  |  | 14 | 0 | 9 | 14 | 6 | 5 | 3 | 11 | 22 | 24 | 18 | 11 | 32 | 6 | 21 | 22 | 14 | 17 | 11 | 42 | 3 | 10 | 29 | 20 | 23 | 31 | 17 |
|  |  | 15 | 0 | 1 | 2 | 5 | 3 | 5 | 6 | 9 | 5 | 13 | 29 | 14 | 32 | 18 | 14 | 61 | 23 | 25 | 10 | 17 | 31 | 11 | 6 | 8 | 4 | 12 |
|  |  | 16 | 0 | 5 | 13 | 1 | 12 | 15 | 17 | 8 | 9 | 15 | 33 | 30 | 12 | 22 | 17 | 24 | 54 | 8 | 8 | 15 | 21 | 6 | 17 | 18 | 13 | 16 |
|  |  | 17 | 0 | 5 | 4 | 0 | 3 | 3 | 7 | 7 | 10 | 5 | 20 | 23 | 40 | 1 | 11 | 26 | 8 | 37 | 12 | 34 | 28 | 10 | 44 | 7 | 17 | 3 |
|  | P | 18 | 0 | 1 | 4 | 8 | 3 | 4 | 4 | 18 | 12 | 5 | 7 | 13 | 41 | 26 | 42 | 10 | 8 | 13 | 32 | 17 | 13 | 39 | 17 | 14 | 20 | 20 |
|  |  | 19 | 0 | 2 | 5 | 5 | 5 | 6 | 4 | 6 | 3 | 4 | 12 | 14 | 17 | 11 | 3 | 17 | 15 | 34 | 17 | 66 | 12 | 24 | 17 | 24 | 19 | 19 |
|  | and | 20 | 0 | 8 | 9 | 1 | 6 | 11 | 7 | 1 | 1 | 6 | 0 | 10 | 12 | 2 | 10 | 31 | 21 | 28 | 13 | 11 | 57 | 31 | 44 | 3 | 12 | 5 |
|  |  | 21 | 0 | 11 | 12 | 4 | 11 | 14 | 12 | 7 | 5 | 11 | 10 | 3 | 34 | 9 | 29 | 11 | 6 | 11 | 39 | 24 | 30 | 31 | 38 | 19 | 13 | 11 |
|  | Sv | 22 | 0 | 11 | 7 | 7 | 10 | 10 | 9 | 8 | 5 | 7 | 12 | 12 | 5 | 7 | 20 | 6 | 17 | 44 | 17 | 16 | 44 | 39 | 34 | 5 | 23 | 13 |
|  |  | 23 | 0 | 6 | 2 | 4 | 2 | 6 | 8 | 10 | 8 | 5 | 10 | 20 | 21 | 27 | 23 | 8 | 18 | 7 | 14 | 24 | 3 | 19 | 6 | 38 | 32 | 54 |
|  |  | 24 | 0 | 7 | 13 | 3 | 3 | 4 | 7 | 9 | 16 | 14 | 19 | 1 | 14 | 11 | 32 | 4 | 13 | 17 | 20 | 19 | 12 | 13 | 23 | 32 | 52 | 33 |
|  |  | 25 | 0 | 12 | 12 | 2 | 9 | 17 | 14 | 7 | 8 | 12 | 13 | 8 | 18 | 19 | 17 | 12 | 16 | 3 | 20 | 20 | 5 | 11 | 13 | 54 | 33 | 40 |
| Love modes |  | 0 | 1 | 4 | 3 | 3 | 3 | 3 | 2 | 2 | 1 | 1 | 0 | 2 | 0 | 0 | 0 | 0 | 0 | 1 | 0 | 0 | 1 | 1 | 3 | 2 | 1 | 1 |
|  |  | 1 | 1 | 2 | 4 | 7 | 3 | 3 | 1 | 5 | 1 | 5 | 4 | 3 | 1 | 0 | 2 | 2 | 3 | 3 | 1 | 1 | 3 | 4 | 6 | 4 | 2 | 4 |
|  |  | 2 | 0 | 1 | 6 | 3 | 1 | 1 | 1 | 2 | 5 | 2 | 1 | 5 | 3 | 3 | 3 | 1 | 2 | 3 | 1 | 1 | 2 | 2 | 5 | 2 | 6 | 3 |
|  |  | 3 | 0 | 3 | 1 | 4 | 3 | 1 | 3 | 3 | 6 | 2 | 3 | 4 | 0 | 6 | 3 | 0 | 3 | 1 | 0 | 3 | 5 | 6 | 6 | 3 | 4 | 7 |
|  |  | 4 | 0 | 3 | 8 | 4 | 2 | 4 | 1 | 1 | 2 | 3 | 1 | 2 | 1 | 1 | 0 | 1 | 2 | 1 | 1 | 1 | 1 | 1 | 1 | 3 | 2 | 1 |
|  |  | 5 | 0 | 7 | 2 | 3 | 2 | 5 | 2 | 1 | 0 | 2 | 2 | 1 | 0 | 2 | 2 | 2 | 2 | 1 | 0 | 2 | 1 | 1 | 1 | 1 | 2 | 3 |
|  | Lg | 6 | 0 | 1 | 2 | 1 | 7 | 4 | 3 | 1 | 2 | 3 | 1 | 1 | 1 | 1 | 0 | 1 | 1 | 0 | 0 | 0 | 0 | 0 | 0 | 2 | 1 | 2 |
|  |  | 7 | 0 | 5 | 2 | 4 | 2 | 2 | 1 | 1 | 1 | 3 | 3 | 2 | 0 | 3 | 0 | 1 | 1 | 1 | 1 | 1 | 0 | 1 | 1 | 1 | 2 | 1 |
|  |  | 8 | 0 | 3 | 3 | 1 | 2 | 3 | 2 | 0 | 2 | 2 | 1 | 2 | 1 | 1 | 2 | 0 | 1 | 0 | 3 | 2 | 0 | 0 | 0 | 1 | 2 | 1 |
|  |  | 9 | 0 | 3 | 5 | 2 | 1 | 3 | 2 | 2 | 2 | 4 | 4 | 0 | 1 | 0 | 1 | 2 | 2 | 0 | 0 | 1 | 0 | 0 | 0 | 1 | 2 | 2 |
|  |  | 10 | 0 | 1 | 0 | 3 | 4 | 2 | 0 | 2 | 1 | 4 | 2 | 4 | 1 | 1 | 2 | 2 | 2 | 1 | 1 | 1 | 1 | 0 | 0 | 0 | 2 | 2 |
|  |  | 11 | 0 | 2 | 5 | 4 | 0 | 1 | 1 | 2 | 1 | 2 | 1 | 2 | 3 | 1 | 1 | 1 | 1 | 1 | 1 | 0 | 1 | 1 | 0 | 0 | 3 | 1 |
|  | Sn | 12 | 0 | 6 | 7 | 3 | 2 | 2 | 2 | 3 | 0 | 2 | 3 | 2 | 2 | 1 | 2 | 1 | 1 | 0 | 1 | 1 | 0 | 1 | 1 | 2 | 3 | 3 |
|  |  | 13 | 0 | 4 | 3 | 3 | 1 | 0 | 2 | 2 | 0 | 1 | 2 | 1 | 1 | 1 | 1 | 0 | 0 | 0 | 1 | 0 | 0 | 0 | 0 | 1 | 1 | 0 |
|  |  | 14 | 0 | 4 | 5 | 2 | 2 | 1 | 2 | 2 | 0 | 0 | 1 | 0 | 1 | 0 | 2 | 1 | 0 | 0 | 1 | 1 | 0 | 0 | 0 | 1 | 1 | 1 |
|  |  | 15 | 0 | 3 | 4 | 1 | 1 | 1 | 1 | 1 | 1 | 0 | 1 | 0 | 0 | 0 | 2 | 1 | 0 | 0 | 1 | 1 | 0 | 0 | 0 | 0 | 0 | 1 |
|  |  | 16 | 0 | 1 | 2 | 1 | 0 | 1 | 0 | 1 | 1 | 1 | 0 | 0 | 0 | 0 | 1 | 1 | 0 | 0 | 1 | 0 | 0 | 0 | 0 | 0 | 0 | 1 |
|  |  | 17 | 0 | 0 | 3 | 1 | 0 | 0 | 0 | 2 | 0 | 1 | 0 | 1 | 1 | 1 | 0 | 0 | 0 | 0 | 1 | 0 | 0 | 0 | 0 | 0 | 0 | 0 |
|  |  | 18 | 0 | 3 | 3 | 2 | 1 | 0 | 2 | 2 | 1 | 3 | 0 | 2 | 1 | 0 | 1 | 0 | 0 | 1 | 0 | 0 | 0 | 1 | 0 | 0 | 0 | 0 |
|  | Sh | 19 | 0 | 3 | 2 | 3 | 1 | 2 | 2 | 1 | 2 | 3 | 3 | 0 | 1 | 0 | 2 | 0 | 0 | 1 | 1 | 0 | 0 | 2 | 1 | 1 | 1 | 0 |
|  |  | 20 | 0 | 1 | 0 | 1 | 1 | 2 | 1 | 0 | 2 | 2 | 3 | 0 | 0 | 0 | 1 | 0 | 0 | 0 | 2 | 0 | 0 | 1 | 0 | 1 | 1 | 0 |
|  |  | 21 | 0 | 1 | 1 | 0 | 1 | 1 | 1 | 0 | 1 | 2 | 1 | 0 | 0 | 1 | 1 | 1 | 0 | 0 | 1 | 0 | 0 | 0 | 0 | 1 | 1 | 0 |
|  |  | 22 | 0 | 0 | 1 | 1 | 0 | 0 | 1 | 0 | 0 | 1 | 1 | 0 | 1 | 1 | 0 | 1 | 0 | 0 | 0 | 0 | 0 | 1 | 0 | 0 | 1 | 0 |
|  |  | 23 | 0 | 0 | 1 | 1 | 1 | 1 | 1 | 0 | 0 | 1 | 2 | 1 | 0 | 0 | 1 | 0 | 0 | 0 | 1 | 0 | 0 | 1 | 0 | 1 | 0 | 0 |
|  |  | 24 | 0 | 1 | 2 | 2 | 2 | 0 | 1 | 1 | 0 | 2 | 2 | 1 | 1 | 1 | 1 | 1 | 0 | 0 | 0 | 0 | 0 | 0 | 0 | 0 | 0 | 0 |
|  |  | 25 | 0 | 1 | 1 | 0 | 2 | 1 | 1 | 2 | 1 | 1 | 3 | 2 | 1 | 1 | 0 | 0 | 0 | 0 | 1 | 0 | 0 | 0 | 0 | 0 | 1 | 1 |

Fig. VII.4.7 Figure caption the same as for Fig. VII.4.5, for propagation at an angle across the North Sea Graben, with a slowness of 1.0 s/km in the y-direction.

| | | | Lg | | | | | | | | | | | | Sn | | Sh | | | | | | | | | | | |
|---|---|---|---|---|---|---|---|---|---|---|---|---|---|---|---|---|---|---|---|---|---|---|---|---|---|---|---|---|
| | | | 0 | 1 | 2 | 3 | 4 | 5 | 6 | 7 | 8 | 9 | 10 | 11 | 12 | 13 | 14 | 15 | 16 | 17 | 18 | 19 | 20 | 21 | 22 | 23 | 24 | 25 |
| Love modes | Lg | 0 | 89 | 8 | 13 | 29 | 13 | 13 | 5 | 12 | 5 | 5 | 1 | 8 | 6 | 3 | 3 | 2 | 1 | 1 | 3 | 3 | 0 | 0 | 0 | 1 | 0 | 1 |
| | | 1 | 8 | 42 | 31 | 31 | 13 | 46 | 33 | 6 | 8 | 6 | 1 | 21 | 23 | 15 | 15 | 12 | 5 | 2 | 10 | 15 | 4 | 3 | 1 | 2 | 4 | 2 |
| | | 2 | 13 | 31 | 26 | 26 | 44 | 24 | 20 | 15 | 28 | 11 | 9 | 33 | 26 | 14 | 15 | 12 | 5 | 6 | 6 | 13 | 9 | 2 | 0 | 0 | 2 | 2 |
| | | 3 | 29 | 31 | 26 | 68 | 25 | 10 | 14 | 2 | 15 | 7 | 7 | 8 | 19 | 11 | 13 | 10 | 5 | 4 | 1 | 2 | 1 | 1 | 0 | 2 | 3 | 1 |
| | | 4 | 13 | 13 | 44 | 25 | 22 | 50 | 18 | 36 | 21 | 11 | 21 | 8 | 16 | 14 | 11 | 7 | 4 | 4 | 4 | 3 | 7 | 3 | 0 | 3 | 1 | 4 |
| | | 5 | 13 | 46 | 24 | 10 | 50 | 9 | 25 | 17 | 10 | 17 | 12 | 13 | 27 | 20 | 19 | 15 | 6 | 6 | 15 | 12 | 4 | 1 | 1 | 4 | 7 | 1 |
| | | 6 | 5 | 33 | 20 | 14 | 17 | 25 | 41 | 15 | 32 | 45 | 21 | 22 | 12 | 10 | 9 | 9 | 5 | 1 | 11 | 12 | 5 | 6 | 2 | 5 | 5 | 8 |
| | | 7 | 12 | 6 | 15 | 2 | 36 | 17 | 15 | 38 | 33 | 36 | 18 | 23 | 8 | 5 | 4 | 6 | 5 | 6 | 27 | 32 | 16 | 7 | 6 | 6 | 15 | 1 |
| | | 8 | 5 | 8 | 28 | 15 | 21 | 10 | 32 | 33 | 51 | 4 | 18 | 23 | 13 | 3 | 7 | 8 | 5 | 5 | 20 | 24 | 15 | 13 | 8 | 9 | 17 | 9 |
| | | 9 | 5 | 6 | 11 | 7 | 11 | 17 | 45 | 36 | 4 | 11 | 17 | 28 | 14 | 5 | 8 | 8 | 8 | 7 | 3 | 13 | 27 | 23 | 15 | 23 | 25 | 28 |
| | | 10 | 1 | 1 | 9 | 7 | 22 | 12 | 21 | 19 | 18 | 17 | 55 | 10 | 7 | 11 | 7 | 7 | 7 | 8 | 19 | 12 | 14 | 8 | 13 | 28 | 20 | 41 |
| | | 11 | 8 | 21 | 33 | 8 | 8 | 13 | 22 | 23 | 23 | 29 | 10 | 53 | 19 | 10 | 9 | 4 | 3 | 5 | 12 | 16 | 8 | 13 | 10 | 13 | 19 | 22 |
| | Sn | 12 | 6 | 23 | 26 | 19 | 16 | 27 | 12 | 8 | 13 | 14 | 7 | 19 | 55 | 21 | 23 | 18 | 11 | 11 | 6 | 6 | 14 | 12 | 3 | 17 | 20 | 13 |
| | | 13 | 3 | 15 | 14 | 11 | 14 | 20 | 10 | 5 | 2 | 5 | 11 | 10 | 19 | 68 | 30 | 24 | 16 | 7 | 5 | 4 | 9 | 7 | 2 | 7 | 20 | 26 |
| | Sh | 14 | 3 | 16 | 15 | 13 | 11 | 19 | 10 | 4 | 7 | 8 | 7 | 9 | 24 | 28 | 73 | 25 | 17 | 7 | 4 | 6 | 6 | 3 | 2 | 2 | 5 | 19 |
| | | 15 | 2 | 12 | 12 | 10 | 8 | 15 | 9 | 6 | 8 | 8 | 7 | 4 | 19 | 24 | 23 | 77 | 21 | 12 | 6 | 6 | 4 | 0 | 0 | 2 | 4 | 21 |
| | | 16 | 1 | 5 | 5 | 5 | 4 | 7 | 5 | 5 | 5 | 8 | 7 | 3 | 11 | 16 | 16 | 20 | 86 | 18 | 10 | 6 | 2 | 4 | 4 | 2 | 5 | 19 |
| | | 17 | 1 | 2 | 6 | 4 | 4 | 6 | 1 | 6 | 5 | 7 | 8 | 5 | 11 | 7 | 7 | 12 | 18 | 90 | 14 | 8 | 2 | 9 | 9 | 1 | 8 | 12 |
| | | 18 | 3 | 10 | 6 | 1 | 4 | 15 | 11 | 27 | 21 | 3 | 20 | 12 | 7 | 5 | 4 | 6 | 10 | 14 | 79 | 20 | 4 | 9 | 10 | 0 | 12 | 6 |
| | | 19 | 3 | 15 | 13 | 2 | 3 | 12 | 12 | 32 | 24 | 13 | 12 | 16 | 6 | 4 | 6 | 6 | 6 | 8 | 20 | 70 | 23 | 15 | 6 | 7 | 11 | 9 |
| | | 20 | 0 | 4 | 9 | 1 | 7 | 4 | 5 | 16 | 15 | 27 | 14 | 8 | 14 | 9 | 6 | 4 | 2 | 2 | 4 | 23 | 58 | 43 | 30 | 23 | 19 | 6 |
| | | 21 | 0 | 3 | 2 | 1 | 4 | 1 | 6 | 7 | 13 | 23 | 8 | 13 | 12 | 8 | 3 | 0 | 4 | 9 | 9 | 15 | 43 | 46 | 49 | 31 | 22 | 12 |
| | | 22 | 0 | 1 | 0 | 0 | 0 | 1 | 2 | 6 | 8 | 15 | 12 | 10 | 3 | 2 | 2 | 0 | 4 | 9 | 10 | 6 | 30 | 49 | 62 | 37 | 14 | 10 |
| | | 23 | 1 | 2 | 0 | 2 | 3 | 4 | 5 | 6 | 9 | 23 | 28 | 13 | 17 | 7 | 2 | 2 | 2 | 1 | 0 | 7 | 23 | 31 | 37 | 49 | 47 | 11 |
| | | 24 | 0 | 4 | 2 | 3 | 1 | 7 | 5 | 15 | 17 | 25 | 20 | 19 | 20 | 20 | 5 | 4 | 5 | 8 | 12 | 11 | 19 | 22 | 14 | 46 | 37 | 43 |
| | | 25 | 1 | 2 | 2 | 1 | 4 | 1 | 8 | 1 | 9 | 29 | 41 | 22 | 13 | 26 | 19 | 21 | 19 | 12 | 6 | 9 | 6 | 12 | 10 | 11 | 43 | 44 |
| Rayleigh modes | Rg | 0 | 1 | 1 | 0 | 0 | 0 | 0 | 0 | 0 | 0 | 0 | 0 | 0 | 0 | 0 | 0 | 0 | 0 | 0 | 0 | 0 | 0 | 0 | 0 | 0 | 0 | 0 |
| | Lg | 1 | 4 | 2 | 1 | 3 | 3 | 7 | 1 | 4 | 3 | 3 | 1 | 3 | 6 | 4 | 4 | 3 | 1 | 0 | 3 | 3 | 1 | 1 | 0 | 0 | 1 | 1 |
| | | 2 | 3 | 4 | 6 | 1 | 8 | 2 | 2 | 1 | 3 | 5 | 0 | 5 | 7 | 3 | 5 | 4 | 2 | 3 | 3 | 2 | 0 | 1 | 1 | 1 | 2 | 1 |
| | | 3 | 3 | 7 | 3 | 4 | 4 | 3 | 1 | 4 | 1 | 2 | 3 | 4 | 3 | 3 | 2 | 1 | 1 | 1 | 2 | 3 | 2 | 0 | 1 | 1 | 2 | 0 |
| | | 4 | 3 | 3 | 1 | 3 | 2 | 2 | 7 | 2 | 2 | 1 | 4 | 0 | 2 | 1 | 2 | 1 | 0 | 0 | 1 | 1 | 1 | 1 | 0 | 1 | 2 | 2 |
| | | 5 | 3 | 3 | 1 | 1 | 4 | 5 | 4 | 2 | 3 | 3 | 2 | 1 | 2 | 0 | 1 | 1 | 1 | 0 | 0 | 2 | 2 | 1 | 0 | 1 | 0 | 1 |
| | | 6 | 2 | 1 | 1 | 3 | 1 | 2 | 3 | 1 | 2 | 2 | 0 | 1 | 2 | 2 | 1 | 1 | 0 | 0 | 2 | 2 | 1 | 1 | 1 | 1 | 1 | 1 |
| | | 7 | 2 | 5 | 2 | 3 | 1 | 1 | 1 | 1 | 0 | 2 | 2 | 2 | 3 | 2 | 1 | 1 | 1 | 2 | 2 | 1 | 0 | 0 | 0 | 0 | 1 | 2 |
| | | 8 | 1 | 1 | 5 | 6 | 2 | 0 | 2 | 1 | 2 | 2 | 1 | 1 | 0 | 0 | 0 | 1 | 1 | 0 | 1 | 2 | 2 | 1 | 0 | 0 | 0 | 1 |
| | | 9 | 1 | 5 | 2 | 2 | 3 | 2 | 3 | 3 | 2 | 4 | 4 | 2 | 2 | 1 | 0 | 0 | 1 | 1 | 3 | 3 | 2 | 2 | 1 | 1 | 2 | 1 |
| | | 10 | 0 | 4 | 1 | 3 | 1 | 2 | 1 | 3 | 1 | 4 | 2 | 1 | 3 | 2 | 1 | 1 | 0 | 0 | 0 | 3 | 3 | 1 | 1 | 2 | 2 | 3 |
| | | 11 | 2 | 3 | 5 | 4 | 2 | 1 | 1 | 2 | 2 | 0 | 4 | 2 | 2 | 1 | 0 | 0 | 0 | 1 | 2 | 0 | 0 | 0 | 0 | 1 | 1 | 2 |
| | Sn | 12 | 0 | 1 | 3 | 0 | 1 | 0 | 1 | 0 | 1 | 1 | 1 | 3 | 2 | 1 | 1 | 0 | 0 | 1 | 1 | 1 | 0 | 0 | 1 | 0 | 1 | 1 |
| | | 13 | 0 | 0 | 3 | 5 | 1 | 2 | 1 | 3 | 1 | 0 | 1 | 1 | 1 | 1 | 0 | 0 | 0 | 1 | 0 | 0 | 0 | 1 | 1 | 0 | 1 | 1 |
| | | 14 | 0 | 2 | 3 | 4 | 0 | 2 | 0 | 0 | 2 | 1 | 2 | 1 | 2 | 1 | 2 | 2 | 1 | 0 | 1 | 2 | 1 | 1 | 0 | 1 | 1 | 0 |
| | P and Sv | 15 | 0 | 2 | 1 | 0 | 1 | 2 | 1 | 1 | 0 | 2 | 2 | 1 | 1 | 0 | 1 | 1 | 1 | 0 | 0 | 0 | 0 | 1 | 1 | 0 | 1 | 0 |
| | | 16 | 0 | 3 | 2 | 3 | 2 | 2 | 1 | 1 | 1 | 2 | 2 | 1 | 1 | 0 | 0 | 0 | 0 | 0 | 0 | 0 | 0 | 0 | 0 | 0 | 0 | 0 |
| | | 17 | 1 | 3 | 3 | 1 | 1 | 1 | 0 | 1 | 0 | 0 | 1 | 1 | 0 | 0 | 0 | 0 | 0 | 0 | 1 | 1 | 0 | 0 | 0 | 0 | 0 | 0 |
| | | 18 | 0 | 1 | 1 | 0 | 1 | 0 | 0 | 1 | 3 | 0 | 1 | 1 | 1 | 1 | 1 | 1 | 1 | 1 | 0 | 1 | 2 | 1 | 0 | 1 | 0 | 1 |
| | | 19 | 0 | 1 | 1 | 3 | 1 | 2 | 0 | 1 | 2 | 1 | 1 | 0 | 1 | 0 | 1 | 1 | 0 | 0 | 0 | 0 | 0 | 0 | 0 | 0 | 0 | 0 |
| | | 20 | 1 | 3 | 2 | 5 | 1 | 1 | 0 | 0 | 0 | 0 | 1 | 1 | 0 | 0 | 0 | 0 | 0 | 0 | 0 | 0 | 0 | 0 | 0 | 0 | 0 | 0 |
| | | 21 | 1 | 4 | 2 | 6 | 1 | 1 | 0 | 1 | 0 | 0 | 0 | 1 | 1 | 0 | 0 | 0 | 0 | 0 | 1 | 2 | 1 | 0 | 1 | 1 | 0 | 0 |
| | | 22 | 3 | 6 | 5 | 6 | 1 | 1 | 0 | 1 | 0 | 0 | 0 | 0 | 1 | 0 | 0 | 0 | 0 | 0 | 0 | 1 | 0 | 0 | 0 | 0 | 0 | 0 |
| | | 23 | 2 | 4 | 2 | 3 | 3 | 1 | 2 | 1 | 1 | 1 | 0 | 0 | 2 | 1 | 1 | 0 | 0 | 0 | 0 | 1 | 1 | 1 | 0 | 1 | 0 | 0 |
| | | 24 | 1 | 2 | 6 | 4 | 2 | 2 | 1 | 2 | 2 | 2 | 2 | 3 | 3 | 1 | 1 | 0 | 0 | 0 | 0 | 1 | 1 | 1 | 1 | 0 | 0 | 1 |
| | | 25 | 1 | 4 | 3 | 7 | 1 | 3 | 2 | 1 | 1 | 2 | 2 | 1 | 3 | 1 | 1 | 1 | 1 | 0 | 0 | 0 | 0 | 0 | 0 | 0 | 0 | 1 |

Fig. VII.4.8 Figure caption the same as for Fig. VII.4.6, for propagation at an angle across the North Sea Graben, with a slowness of 1.0 s/km in the y-direction.

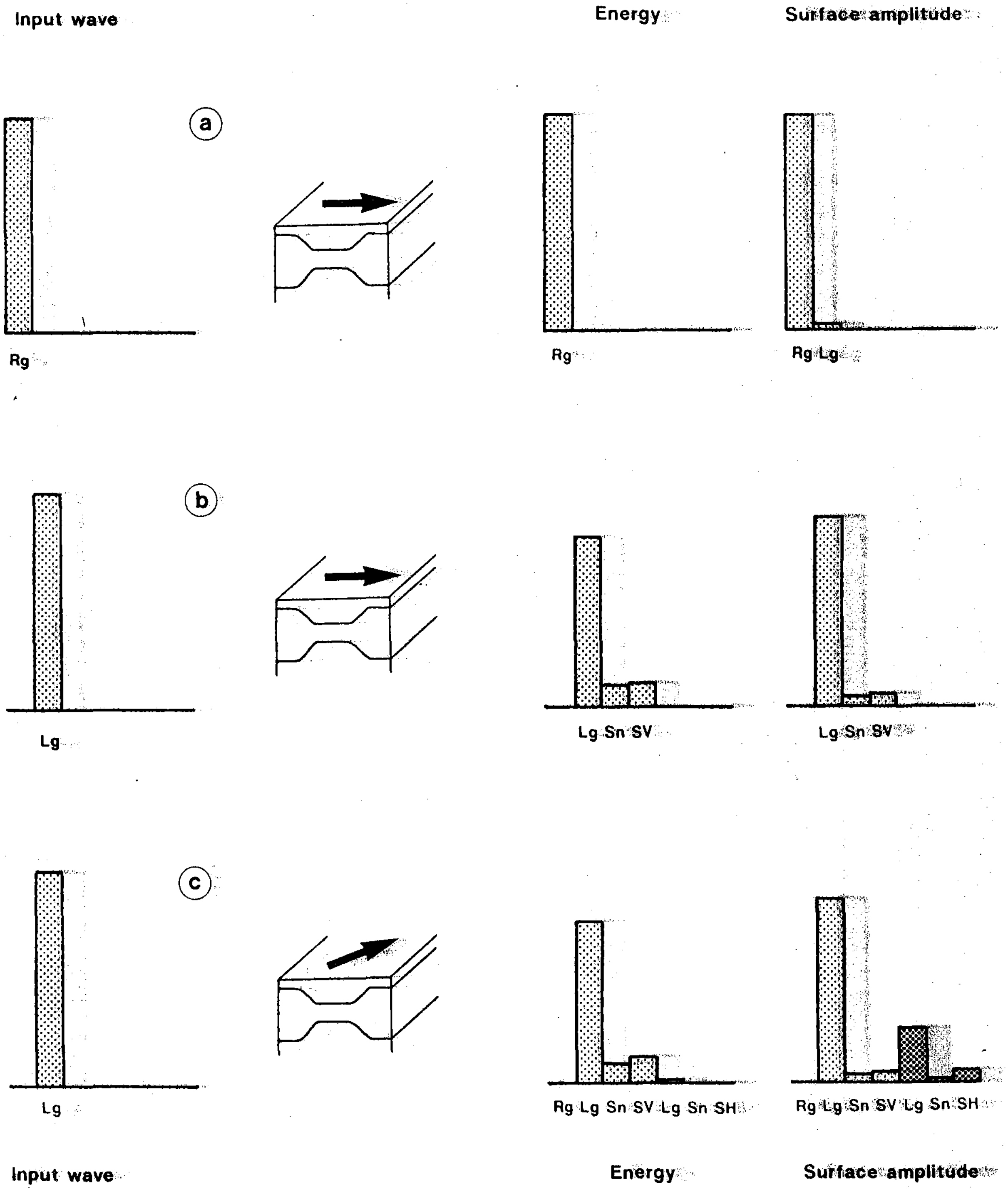

Fig. VII.4.9 Wavetrain transmission across the North Sea Graben at 1 Hz for incoming Rg and Rayleigh-type Lg wavetrains. The repartition of the total energy and the surface amplitude of the wavetrains at the output of the model are plotted normalized to the energy or amplitude of the input wave. Small-dotted pattern indicates Rayleigh-type wavetrain and large-dotted pattern indicates Love-type wavetrain. The arrow indicates the propagation direction in the model.

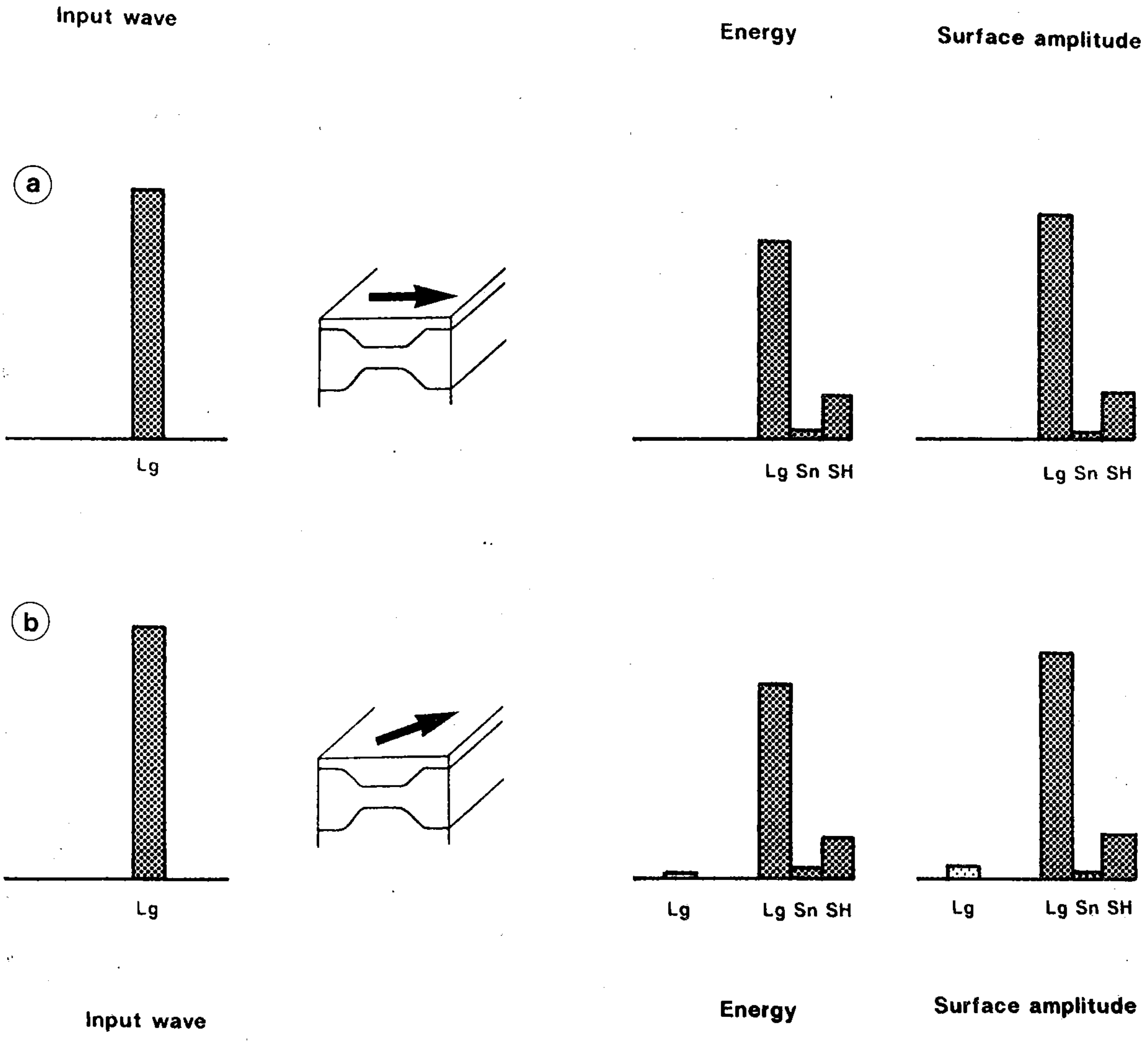

Fig. VII.4.10 The same as for Fig. VII.4.9, for incoming Love-type Lg wavetrains.

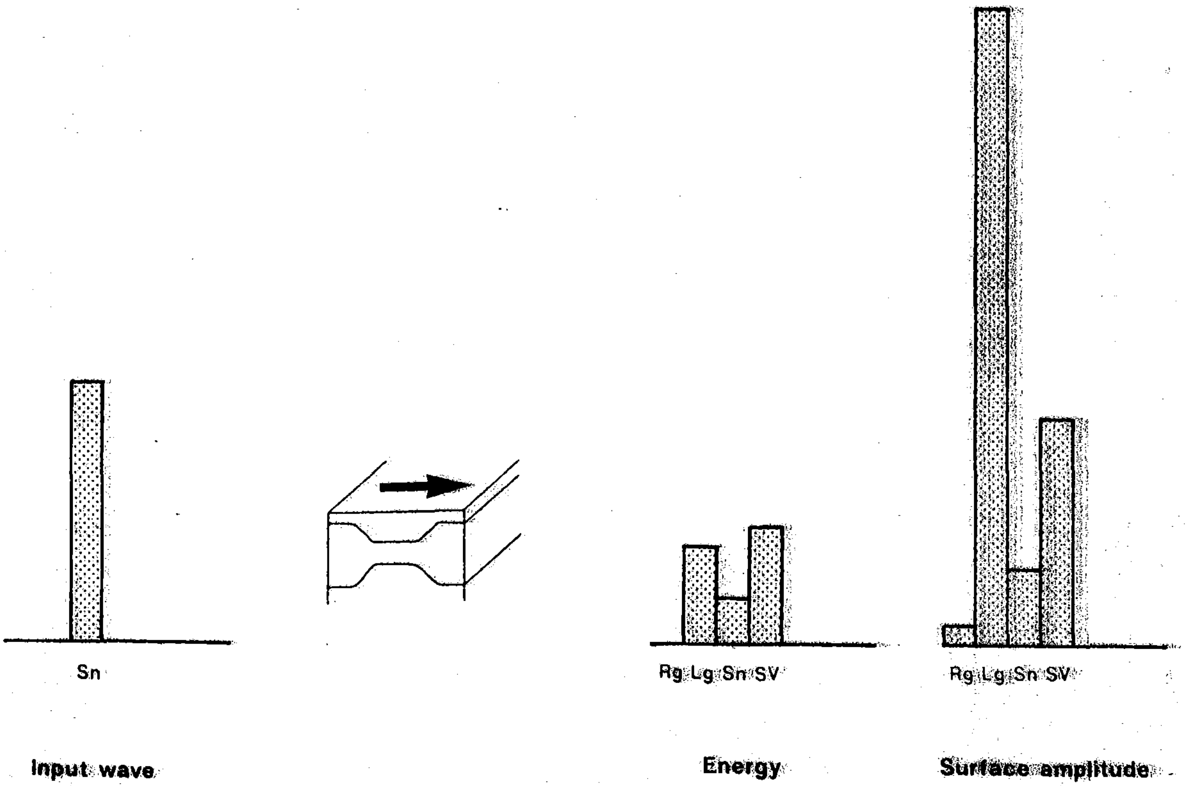

Fig. VII.4.11 The same as for Fig. VII.4.9, for an incoming Sn wave.

## VII.5 Seismicity of northern Norway and adjacent areas as inferred from ARCESS and SEISNOR data

Over the last years the seismic instrumentation in Norway and surrounding areas has been improved through the installation of regional and local networks. The increased number of stations has resulted in developing more detailed seismicity patterns and improved focal mechanisms (e.g., Havskov and Bungum, 1987), which in turn can be correlated with similarly detailed information from geological investigations.

This paper will concentrate on the analysis of the combined data from two such recently installed sets of seismic instruments. One is a regional network termed SEISNOR (Surveillance of Earthquake Activity Offshore Northern Norway, Bungum et al, 1988), and the other is the Arctic Regional Seismic Array (ARCESS), which is a 39-element seismic array very similar to the NORESS array (Norwegian Regional Seismic Array, Mykkeltveit, 1985). The SEISNOR regional network stations and the ARCESS array are shown in Fig. VII.5.1, together with the main geological structures off northern Norway.

As an introduction, Fig. VII.5.2 illustrates the previously known seismicity patterns in northern Fennoscandia and the Norwegian and Barents Seas. These data are taken from a NORSAR data base and cover the period from 1955 through 1987 (Bungum, 1988). To maintain a compromise between location precision and magnitude completeness in this figure, only events recorded on at least eight stations have been included. The figure shows, in addition to the seismicity zones in northern Finland and the eastern coast of Sweden, the following main characteristics:

- The mid-oceanic ridge, with the Knipovich Ridge west of Svalbard and the Mohn's Ridge further south and west.

- An extended seismicity zone between the Mohn's Ridge and northern Norway, limited by the Senja Fracture Zone and covering large parts of eastern Lofoten Basin.

- A seismicity zone along the coast of northern Norway (Rana Fault Complex) as well as one offshore zone (following the Kristiansund-Bodø Fault Complex).

- Some earthquake activity near the intersection between the Vøring Plateau Escarpment and the eastern part of the Jan Mayen Fracture Zone.

## Data analysis

As outlined above, the monitoring of seismic events in northern Norway has improved significantly following the installation of new seismic stations in 1987. In this report we therefore will concentrate on the time period from April 1987 through April 1988, analyzing events recorded by the SEISNOR network and the ARCESS array.

The SEISNOR network is a regional seismic network consisting of six seismographic stations distributed from 62.6°N to 69.0°N within Norway (see Fig. VII.5.1). The sites contain a mixture of single component, three-component and vertical component mini-array stations with the primary purpose of recording offshore events. The unique features of this network are two-fold. First, this is a computer-controlled network of field stations capable of detecting and storing events locally at each field station and transferring desired data in near real time as instructed by a central processing computer. Detections from all the remote field stations can be processed automatically at the central computer or manually extracted for particular events of interest. Secondly, the northernmost station, KTK, and the centrally located station, MOR, are small mini-arrays with horizontal dimensions of about

450 meters. With this distribution of sensors, estimates of the slowness vectors of the incoming wave field for local and regional seismic events can be used for better identification of seismic phases and calculation of event locations. The network has been operational since April 1987 (Bungum et al, 1988).

The Arctic Regional Array, ARCESS, is an almost circular array of sensors with an aperture of 3 km comprising a total of 39 sensors including single component short period, three-component, broadband and long period instruments. This array, which is very powerful both in terms of detection threshold and location capability, began operation near the end of October 1987 (Mykkeltveit et al, 1987).

The analysis of the data obtained from these two sets of seismic instruments consists of various filtering and wave separation algorithms for phase identification and estimation. The real value of incorporating mini-arrays and the ARCESS array into the SEISNOR network centers around the use of frequency-wavenumber (F-K) analyses (e.g., Capon, 1969).

An earthquake location program capable of using the azimuth data for both initial starting locations and in the formal inverse problem (Bratt and Bache, 1988) has been used for the present study, and all the seismic phases possible have been analyzed from SEISNOR and ARCESS as well as any other available stations within Norway. A careful identification and timing of the seismic phases has been combined with the azimuth information already obtained from a broadband F-K analysis (Kværna and Doornbos, 1986) of array data and three-component sites in order to obtain a high quality data set for the earthquake locations.

## Spatial distribution of seismicity

During its first year of operation, the SEISNOR network has recorded 163 locatable seismic events. Additionally, the ARCESS array has detected 36 offshore events between November 1987 and April 1988. The magnitudes ($M_L$) range from about 1.5 to 4.0, with almost complete coverage for events above $M_L$ 2.5. Fig. VII.5.3 shows the locatable seismicity between 60° and 80°N, recorded on at least one of the stations in the networks for a one-year period. If we compare Fig. VII.5.3 with Fig. VII.5.2 showing more than 30 years of seismicity we can see a quite consistent pattern. The earthquakes, even for such a short time period as one year, seem to line up along the main fault and fracture systems and known regions of higher seismicity.

Shortly after the SEISNOR network began operation, several earthquakes appeared near 64°N and 12°E. These events were also felt by people in the area, and with magnitudes in the range 2.2-2.7 they appeared in a region that has been relatively quiet earlier. The events lie on the northern part of the Møre-Trøndelag Fault Zone, where the southern part is known to exhibit a relatively high seismicity.

Along the Nordland coast, the Rana Fault Complex separates the coastal areas from the seismically less active Trøndelag Platform. Events recorded around this fault complex during the last year may indicate a larger seismic activity here than earlier known, extending northwards to the intersection with Kristiansund-Bodø Fault Complex, which is one of the most active areas along the Norwegian coast.

In addition to the seismicity along the coast from Møre to Lofoten, there is a noticeable level of activity also offshore along the Kristiansund-Bodø Fault Complex west of the Trøndelag Platform as well as further north along and on the continental side of the Vøring Plateau Escarpment.

Further north, events have been located along the Senja Fracture Zone and eastwards to the Ringvassøy-Loppa Fault Complex. The Senja Fracture Zone has been known for a long time as a very active area (Bungum, 1988), separating the oceanic crust to the west from the continental crust to the east.

The western Barents Sea, i.e., the region east of the Senja Fracture Zone, contains the Ringvassøy-Loppa Fault Complex. This area was until recently assumed to be more or less aseismic, but several earthquakes have been located here, especially after ARCESS was set in operation in late 1987. Since the magnitude threshold for locatable events east of the Senja Fracture Zone is below $M_L$ 2.0 north to 75°N, the Barents Sea may be divided into two different parts with respect to seismicity. The western Barents Sea includes the Ringvassøy-Loppa Fault Complex, which is a system of deep listric faults accompanied by a moderate seismicity dropping smoothly eastwards away from the Senja Fracture Zone. This region has shown very little seismic activity before, with very few events reported the last 30 years (Fig. VII.5.2). When considering the level of seismicity now recorded, with events in the magnitude range of $M_L$ 1.7 - 3.1, this illustrates very clearly the recent significant improvement in detectability for these areas. The seismicity seems to extend more or less continually north to the more active southern part of Svalbard. It should be noted that the onshore seismicity in Fig. VII.5.3 possibly contains some explosions, in particular close to the MOR station, in northern Sweden and within the Kola peninsula.

In order to illustrate the effects the various types of geologic structures have on the propagation of seismic waves through the crust and upper mantle, a suite of seismograms are shown for comparison in Figs. VII.5.4 and VII.5.5. By comparing seismograms at the ARCESS array from earthquakes occurring at many different locations, particular characteristics can be correlated with the gross features of the known lateral variations in the crustal structure of the area in this study. Figs. VII.5.4 and VII.5.5 show panels with six pairs of seismograms from earthquakes located in different areas in the region studied. It turns out that few of the events show very clear Lg phases, which are often seen for events with continental type propagation paths (Kennett et al, 1985). However, Lg phases are seen on the event from Lofoten (LOF), and perhaps also on the event from southern Ringvassøy-Loppa Fault Complex. These events are located closer to the coast than the other two offshore (SFZ and BARNT), which appear to have no Lg phase. The Lg phase is also missing for events from the Viking Graben area, where the graben structure is instrumental in the blocking of Lg energy (Kennett et al, 1985). Since most of the offshore events in the present case lack Lg phases even when located in essentially continental type crust (the Barents Sea), this might be a result of stronger attenuation in the upper crust.

## Conclusion

The data from recently installed seismographic stations have shown that several regions in the northern part of the Norwegian coastline are exposed to a greater rate of seismicity than reflected in earlier seismicity maps. Even though the seismic networks have only been in operation for one year, they have unveiled new and important information about a large number of earthquakes. These have been found in general to follow the main fault systems, with increasing activity along the coast from Møre to Lofoten, and northwards along the continental margin to the Svalbard Islands. The area around the Vøring Plateau and where the Kristiansund-Bodø Fault Complex intersects with the Rana Fault Complex shows an activity that may be as large as the activity off Møre.

The seismic activity is also relatively high along the escarpment and associated fault zones. Since the data used in this analysis only reflects one year of operation (only six months for ARCESS), it is not known to which extent the apparent clustering of events could be related to temporal variations in seismicity.

The Senja Fracture Zone and Western Barents Sea are exposed to a greater rate of seismicity than earlier known. Especially interesting are the events in the Western Barents Sea which occur in a region with traditionally very low seismicity.

The southern and eastern Barents Sea still appear to be seismically quiet. Even during the last year there have been no events detected east of 30°E or in the basin just north of the northern part of mainland Norway. In these areas the detection threshold for earthquakes should be slightly below magnitude 1.5 due to the continental type crustal structure and assumed mild lateral heterogeneity. This suggests that the area has indeed very low seismic activity; however, a longer time period of monitoring is necessary before drawing any firmer conclusions on this.

In general, it turns out that ARCESS has a very good detectability eastwards and northwards. The detection threshold in these directions is below magnitude $M_L$ 1.5 up to distances of at least 600 km. However, the rather complicated geological structures to the west, with events along and beyond the continental margin, may lead to phase identification problems for the detection algorithm at the ARCESS array.

L.B. Kvamme
R.A. Hansen, Univ. of Bergen

## References

Bratt, S.R. and T.C. Bache (1988): Locating events with a sparse network of regional arrays. Bull. Seism. Soc. Am., 78, 780-798.

Bungum, H. (1988): Earthquake occurrence and seismotectonics in Norway and surrounding areas. In: S. Gregersen and P. Basham (eds.): Causes and Effects of Earthquakes at Passive Margins and Areas with Postglacial Rebound on both Sides of the North Atlantic, NATO Advanced Research Workshop Proceedings (in press).

Bungum, H., R.A. Hansen, J. Havskov and L.B. Kvamme (1988): An Introduction to SEISNOR: The Northern Norway network. SEISNOR Technical Report.

Bungum, H. and P.B. Selnes (eds.) (1988): ELOCS: Earthquake Loading on the Norwegian Continental Shelf, Summary Report. Norwegian Geotechnical Institute (Oslo), NTNF/NORSAR (Kjeller) and Principia Mechanica Ltd. (London).

Capon, J. (1969): High-resolution frequency-wavenumber spectrum analysis. Proc. IEEE, 57, 1408-1418.

Havskov, J. and H. Bungum (1987): Source parameters for earthquakes in the northern North Sea. Nor. Geol. Tidsskr., 67, 51-58.

Kennett, B.L.N., S. Gregersen, S. Mykkeltveit and R. Newmark (1985): Mapping of crustal heterogeneity in the North Sea basin via the propagation of Lg-waves. Geophys. J.R. astr. Soc., 83, 299-306.

Kværna, T. and D.J. Doornbos (1986): An integrated approach to slowness analysis with arrays and three-component stations. NORSAR Semiannual Technical Summary, 1 Oct 1985 - 31 Mar 1986, NORSAR Sci. Rep. No. 2-85/86, Kjeller, Norway.

Mykkeltveit, S. (1985): A new regional array in Norway. Design work and results from analysis of data from a provisional installation. In: Ann U. Kerr (eds.), The VELA Program. A Twenty-five Year Review of Basic Research, Defense Advanced Research Projects Agency.

Mykkeltveit, S., F. Ringdal, J. Fyen and T. Kværna (1987): Initial results from analysis of data recorded at the new regional array in Finnmark, Norway. NORSAR Semiannual Technical Summary, 1 April - 30 September 1987, NORSAR Sci. Rep. No. 1-87/88, Kjeller, Norway.

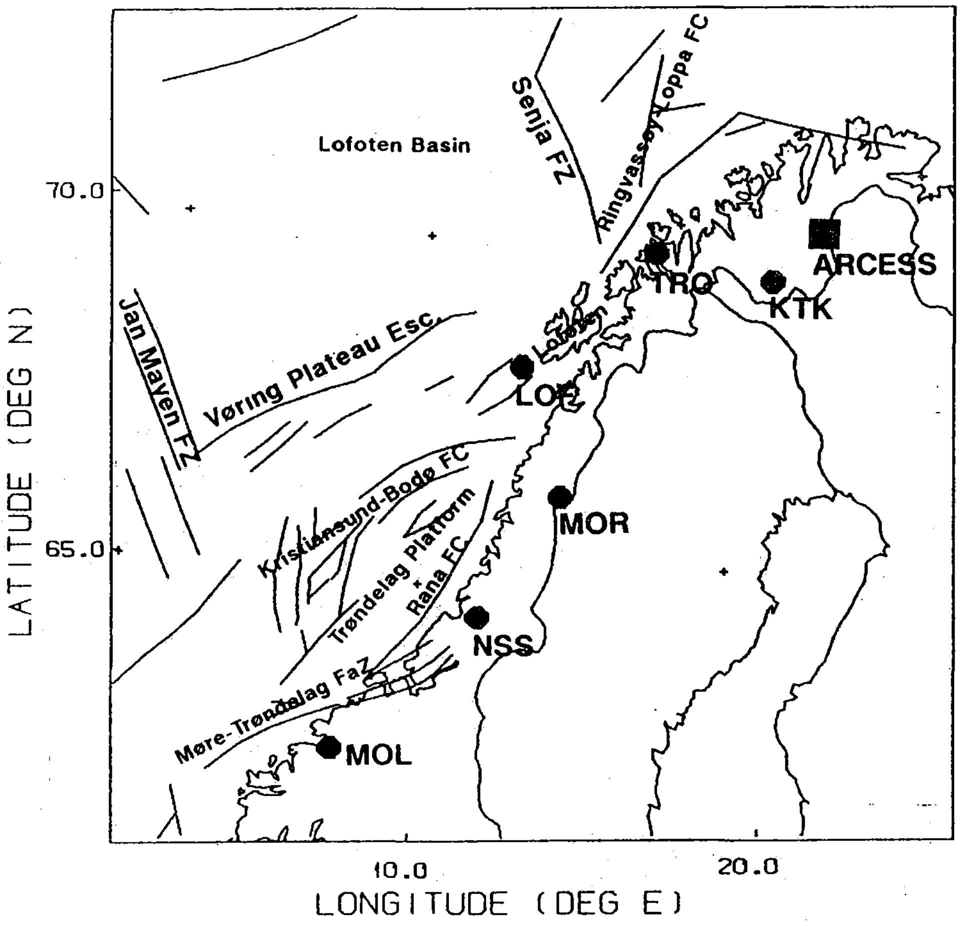

<u>Fig. VII.5.1</u> Location of the stations in the SEISNOR regional network, and the ARCESS regional array. The figure also contains the major structural elements as given in Bungum and Selnes (1988).

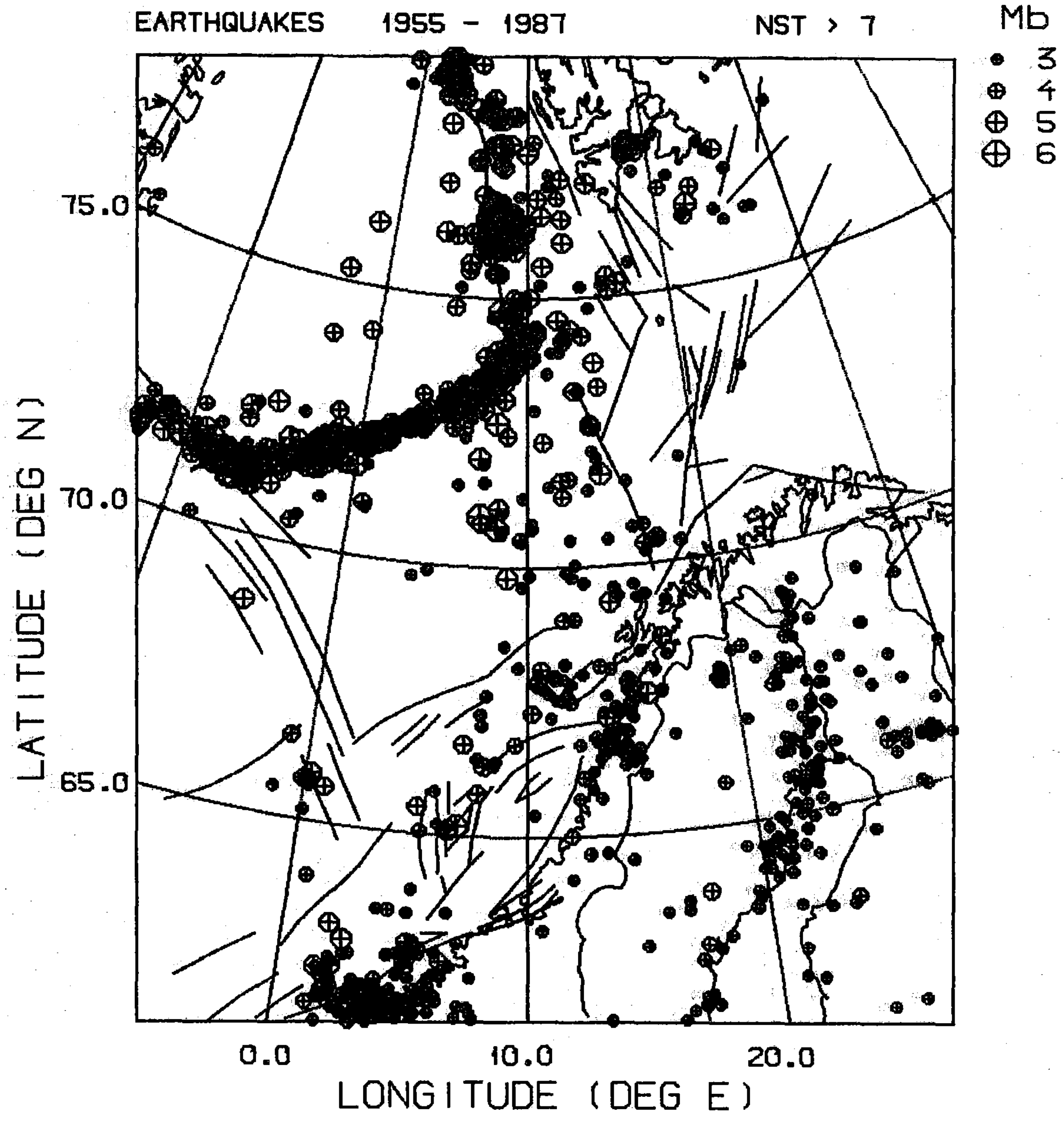

Fig.VII.5.2 Earthquake distribution for the time period 1955 to 1987, reported from at least 8 recording stations (Bungum, 1988). Structural information as for Fig. VII.5.1.

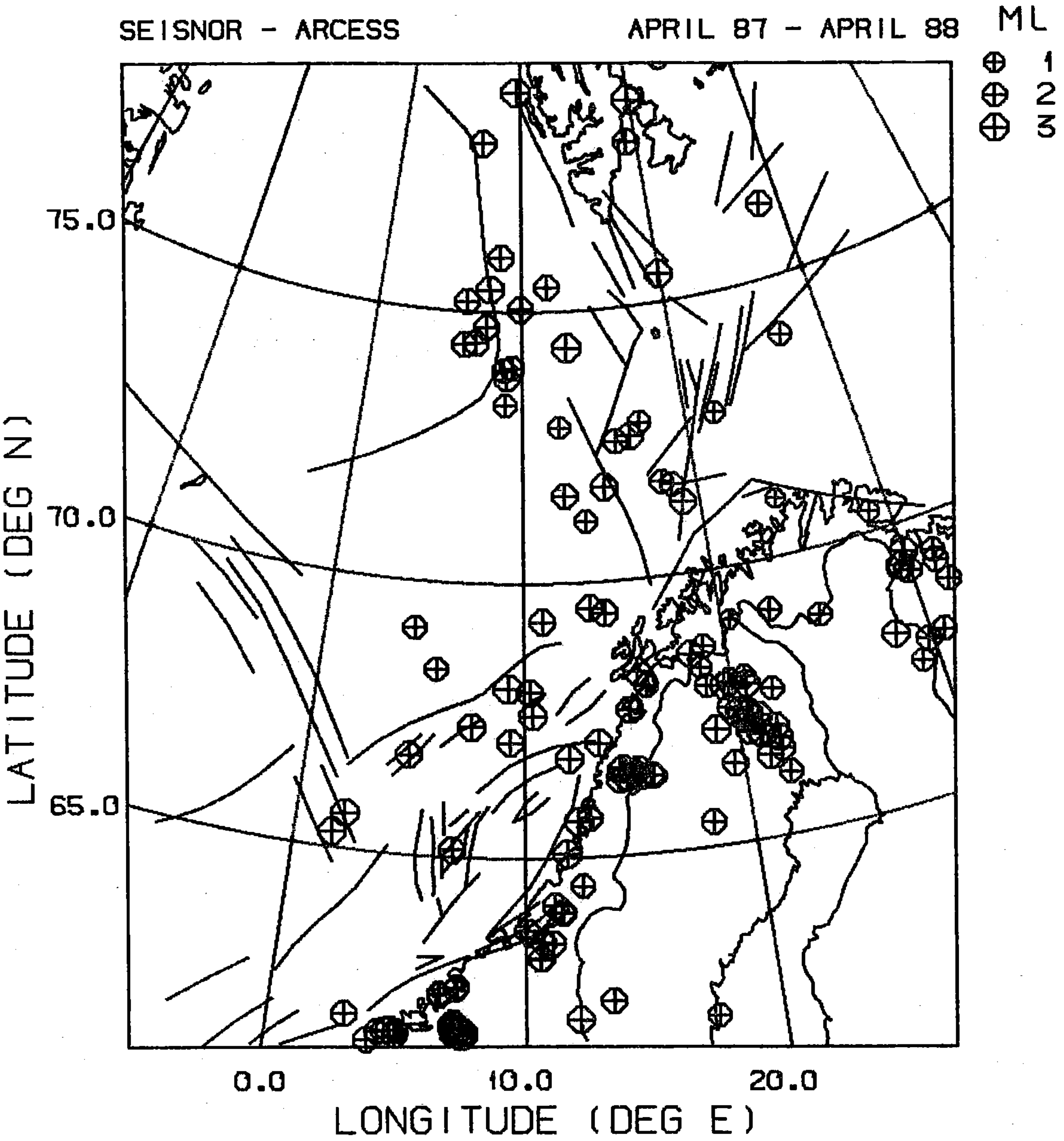

Fig. VII.5.3 Recorded events from April 1987 to April 1988 reported at SEISNOR and ARCESS, where all offshore events are earthquakes. Structural information as for Figs. VII.5.1 and VII.5.2.

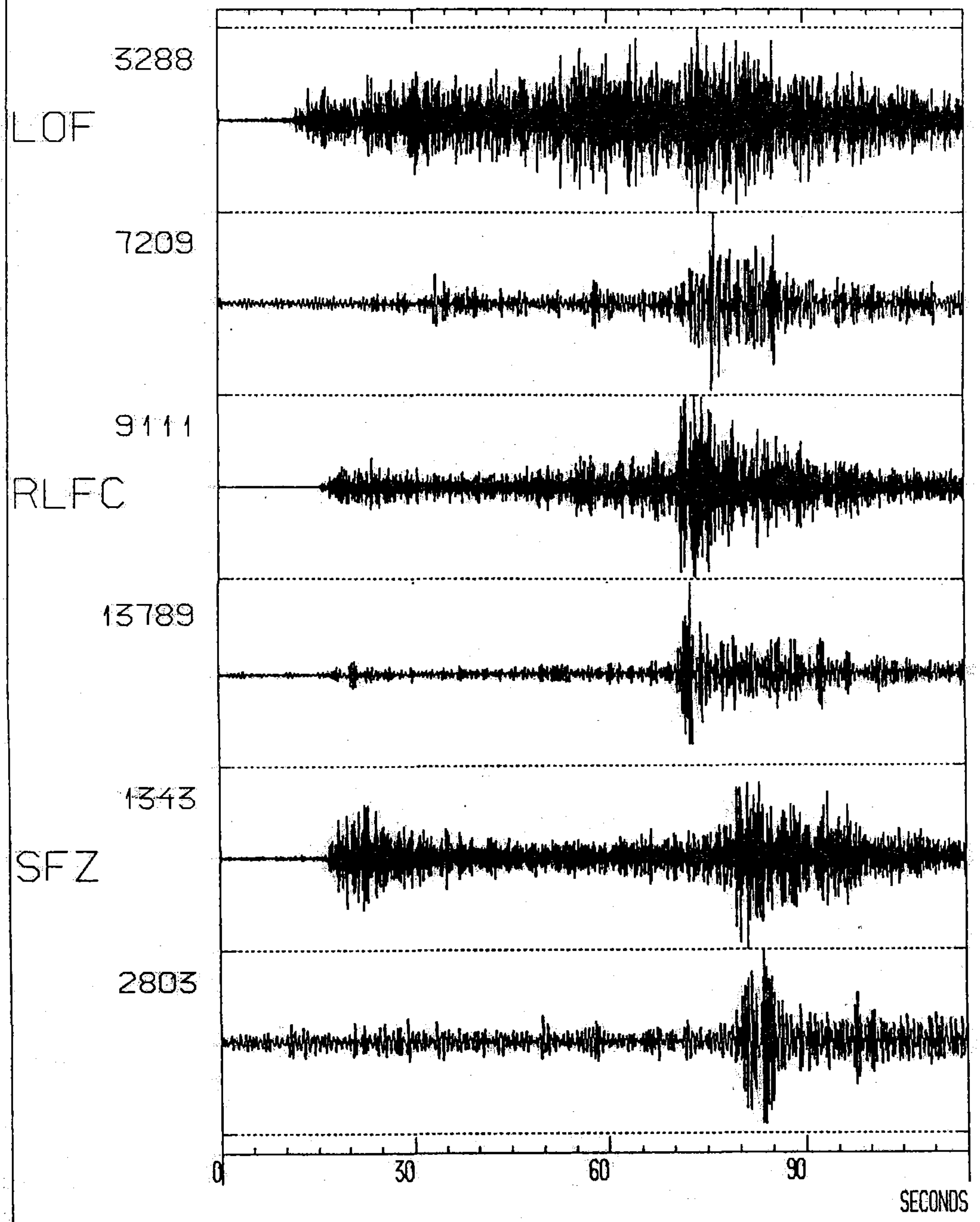

Fig.VII.5.4 Seismograms of three events recorded at ARCESS. The two traces for each event are high-pass filtered (at 6 Hz) and bandpass filtered (1.5 to 3 Hz), respectively. The events are located at LOFOTEN (LOF, 68.1°N, 16.0°E), Ringvassøy-Loppa Fault Complex (RLFC, 72.3°N, 18.7°E), and Senja Fracture Zone (SFZ, 71.6°N, 12.4°E)· Axes are seconds versus amplitude in number of counts, with the maximum number indicated.

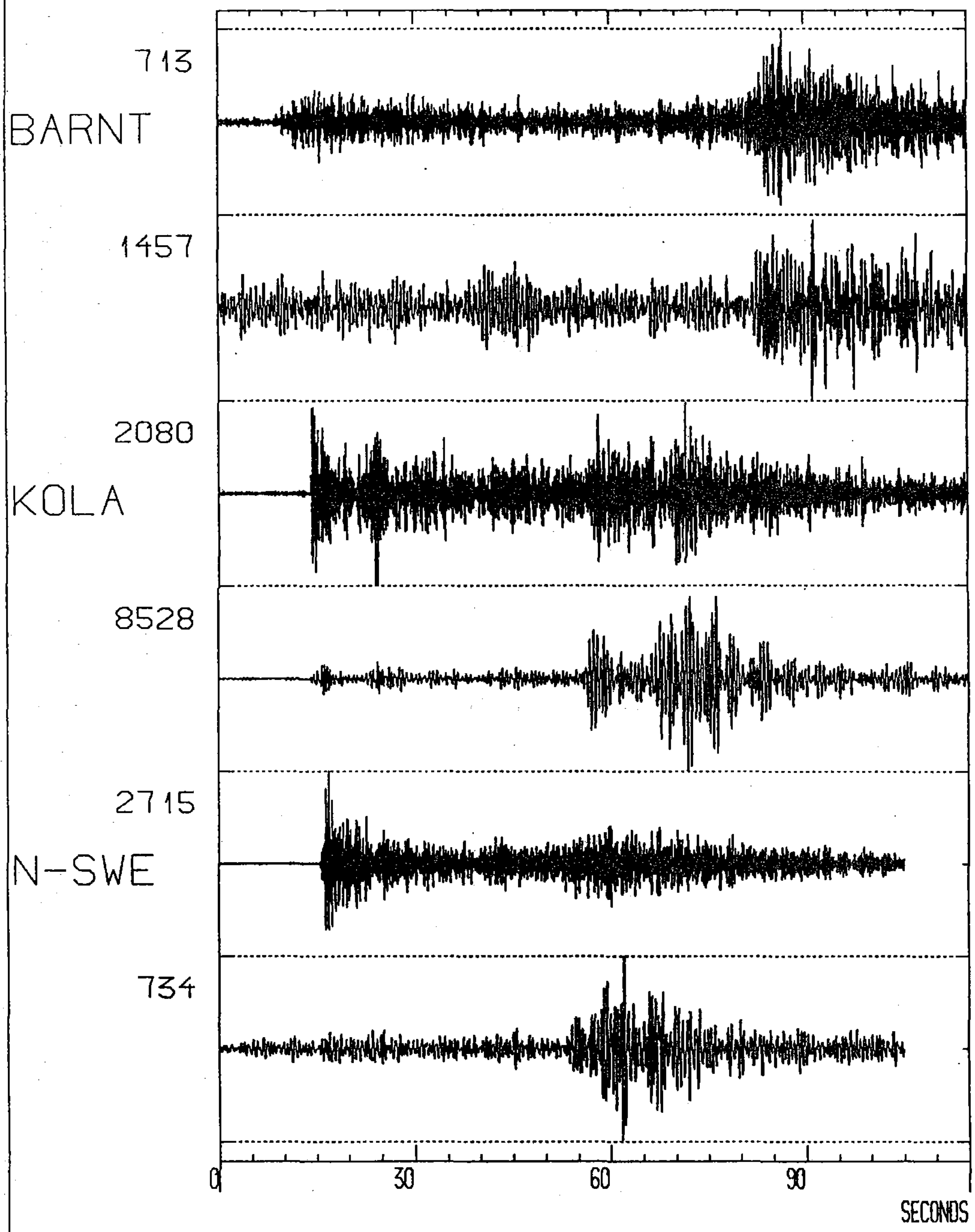

Fig.VII.5.5 Seismograms of three events recorded at ARCESS, where the first in each pair is high-pass filtered (at 6 Hz), while the second is bandpass filtered from 1.5 to 3 Hz. The events are located at Western Barents Sea (BARNT, 73.9°N, 27.1°E), Kola Peninsula (KOLA, 67.6°N, 33.4°E), and northern Sweden (67.3°N, 20.6°E)· Axes are seconds versus amplitude in number of counts, with the maximum number indicated.

## VII.6 New results from processing of data recorded at the new ARCESS regional array

The previous NORSAR Semiannual Technical Summary contained a contribution (Mykkeltveit et al, 1987) that described the NORESS-type array installed in northern Norway during the fall of 1987, and also gave some initial results from analysis of data recorded during its first phase of operation. In the present contribution, we report on some additional findings resulting from analysis recorded at ARCESS, which is the name now adopted for this new array.

### Analysis of data from the ARCESS High Frequency Seismic Element

The first High Frequency Seismic Element (HFSE) was installed at NORESS in 1985 and has been described by Ringdal (1986a). Another HFSE was installed in ARCESS at the same time as the array was deployed, and we have selected seven events as shown in Fig. VII.6.1 for further analysis using these high frequency recordings. The raw data and bandpass filtered data 30-50 Hz are shown in Figs. VII.6.2 and VII.6.3, respectively, for the vertical component of the HFSE.

As we can see from these figures, there is appreciable energy to beyond 500 km distance in the 30-50 Hz band. However, it is noteworthy that no energy in this band is seen above the background noise for event 7 ($M_L$ = 2.6) at the distance of 714 km.

This behavior is to some degree similar to what was found by Ringdal (1986a) for NORESS, but there are also indications from these seven events that the propagation of high-frequency energy is not quite as efficient around ARCESS as around NORESS. We emphasize, however, that further study is needed before such a conclusion can be reliably established.

## Propagation of Rg waves at ARCESS

The 1 Hz surface wave of Rayleigh type, often referred to as Rg, is clearly observed for many events recorded at ARCESS. It is generally known that it takes a shallow source to generate such waves. At NORESS, the Rg phase is never observed for events at distances larger than 70-90 km, irrespective of azimuth. At ARCESS, on the other hand, we have observed clear Rg phases for events located more than 400 km away.

Fig. VII.6.4 shows the Rg phase recorded at the ARCESS high frequency station for an event (no. 4 in Fig. VII.6.1) located at a distance of 349 km. For event no. 3 in Fig. VII.6.1, no Rg waves are observed, even though this is a mining explosion at shorter distance than event no. 4. This shows that the occurrence of Rg is dependent on azimuth. In view of the potential of using Rg in discriminating between shallow and deep sources, this phase will be the subject of further study in our future work.

## ARCESS regional P-wave detection capability

An initial assessment of the detection capabilities of ARCESS has been made using the method described by Ringdal (1986b). Adopting the Helsinki seismic bulletin as a reference, we have associated P-phases detected by the on-line procedure with the reported reference events. The time interval processed is essentially January - March 1988, with some events during 1987 also included. The results for a source region comprising mainly the mining areas of western Russia and Finland surrounding the Bothnian Bay are shown in Fig. VII.6.5. This figure gives a histogram of the number of reference events at each magnitude, with the events detected by ARCESS marked specially. The figure further contains a detection probability curve with associated confidence limits, estimated by the maximum likelihood method of Ringdal (1975).

We note that the 90 per cent P-wave detection capability in the region studied (distance range 800-1200 km) is close to $M_L$ = 2.5. This can be compared to the NORESS threshold of $M_L$ = 2.7 found by Ringdal (1986b) for a similar distance range (700-1400 km). It must be noted here that the reference events were on the average at a slightly greater distance in the case of NORESS, and this may to some extent account for the difference. Nevertheless, we conclude that the new array appears to have a regional detection capability that at least matches that of NORESS.

## Regional location capability

The capability of ARCESS to locate seismic events at regional distances has been evaluated and compared to that of NORESS. In addition, we have investigated the joint location capabilities of the two arrays. The data base for this study has comprised a set of seven regional events in October/November 1987, for which we have accurate independent location estimates computed at the University of Helsinki, on the basis of the Fennoscandian network of data.

For the purpose of estimating event location, we have used the program TTAZLOC developed by Bratt and Bache (1988). This program takes into account arrival times, back azimuth estimates and associated uncertainties, and incorporates these data into a generalized-inverse location estimation scheme. TTAZLOC can be applied both to single-array and multiple-array situations, assuming that a sufficient number of phase detections is available.

Table VII.6.1 lists the events in the data base, together with the main results from the data processing. For each event both the network location and the joint two-array location has been listed, as well as the difference (in km) between the two estimates. For comparison purposes, the differences are also given between network location and locations computed on the basis of each individual array.

We note that the joint two-array location procedure produces excellent results, which on the average differ from the network estimates by only 34 km. In contrast, the error in the single-array results are typically more than 100 km. It must be emphasized that six of these events are of very low magnitude ($M_L$ 2.1 to 2.5), and all are at an appreciable distance from both arrays (see Fig. VII.6.6). It is known from earlier NORESS studies that distant regional events are much more difficult to locate accurately than close-in events.

It is noteworthy that the above results have been obtained using arrival times and azimuths estimated automatically using the on-line RONAPP processing system. There is clearly a potential of improvement in using interactive analysis to extract more precise phase arrival times. Also by taking into account regional wave propagation effects, e.g., in a joint epicentral determination scheme, using nearby reference events, it is likely that increased accuracy can be obtained. On this background, the results are quite encouraging.

## Conclusions

The initial results from analyzing data from ARCESS show that it fully matches the capabilities of NORESS in terms of regional detection, location and phase identification capabilities. Some significant differences in phase characteristics have been observed between the two arrays, in particular regarding high frequency (>30 Hz) signal propagation and propagation characteristics of the Rg phase. This confirms that optimum multi-array processing will need to take into account regionally based corrections tailored specially to each array. The joint analysis of data from NORESS and ARCESS has been shown to give significantly more precise event location estimates for weak seismic events than each individual array, and a network of such arrays would be expected to provide further improvements.

As the ARCESS array is still in an initial phase of operation, the results presented in this study are based on a limited time interval of recordings. Comprehensive assessments of ARCESS capabilities as well as the joint detection, location and identification potential of the NORESS/ARCESS system will require a much more extensive data base, and will be the subject of further study.

S. Mykkeltveit
F. Ringdal

## References

Bratt, S.R. and T.C. Bache (1988): Locating events with a sparse network of regional arrays. Bull. Seism. Soc. Am., 78, 780-798.

Mykkeltveit, S., F. Ringdal, J. Fyen and T. Kværna (1987): Initial results from analysis of data recorded at the new regional array in Finnmark, Norway. Semiannual Technical Summary, 1 Apr - 30 Sep 1987, NORSAR Sci. Rep. No. 1-87/88, Kjeller, Norway.

Ringdal, F. (1975): On the estimation of seismic detection thresholds. Bull. Seism. Soc. Am., 65, 1631-1642.

Ringdal, F. (1986a): Initial results from the NORESS High Frequency Seismic Element (HFSE). Semiannual Technical Summary, 1 Oct 1985 - 31 Mar 1986, NORSAR Sci. Rep. No. 2-85/86, Kjeller, Norway.

Ringdal, F. (1986b): Regional event detection using the NORESS array. Semiannual Technical Summary, 1 Oct 1985 - 31 Mar 1986, NORSAR Sci. Rep. No. 2-85/86, Kjeller, Norway.

| Event No. | Origin date, time | | Mag. $M_L$ | Network Location (1) | | NORESS/ARCESS Joint Location (2) | | Location "error" (2) - (1) | Single array location "error" (km) | |
|---|---|---|---|---|---|---|---|---|---|---|
| | | | | Lat. | Lon. | Lat. | Lon. | (km) | NORESS | ARCESS |
| 1 | 10/31/87 | 10.09.08 | 4.2 | 61.11 | 4.51 | 60.84 | 5.35 | 54 | 33 | 191 |
| 2 | 11/02/87 | 13.28.00 | 2.5 | 61.40 | 31.60 | 61.74 | 31.18 | 43 | 277 | 154 |
| 3 | 11/03/87 | 22.35.12 | 2.3 | 68.37 | 15.21 | 68.02 | 16.56 | 67 | 269 | 125 |
| 4 | 11/06/87 | 08.25.21 | 2.1 | 66.51 | 14.87 | 66.45 | 14.93 | 8 | 15 | 27 |
| 5 | 11/10/87 | 11.06.58 | 2.2 | 59.63 | 22.36 | 59.60 | 22.13 | 13 | 93 | 148 |
| 6 | 11/10/87 | 12.29.01 | 2.3 | 61.50 | 30.40 | 61.58 | 29.80 | 33 | 21 | 84 |
| 7 | 11/13/87 | 12.15.20 | 2.3 | 59.30 | 27.60 | 59.35 | 27.84 | 15 | 86 | 92 |
| | | | | | | | Averages | 34 | 113 | 117 |

Table VII.6.1 Comparison of epicentral location estimates from NORESS/ARCESS and the Fennoscandian network (reference to Helsinki bulletin) for a set of seven events. The location accuracy of each individual array is also given. Events 1, 3 and 4 are earthquakes; events 2, 6 and 7 are mining explosions and event 5 is a presumed underwater explosion.

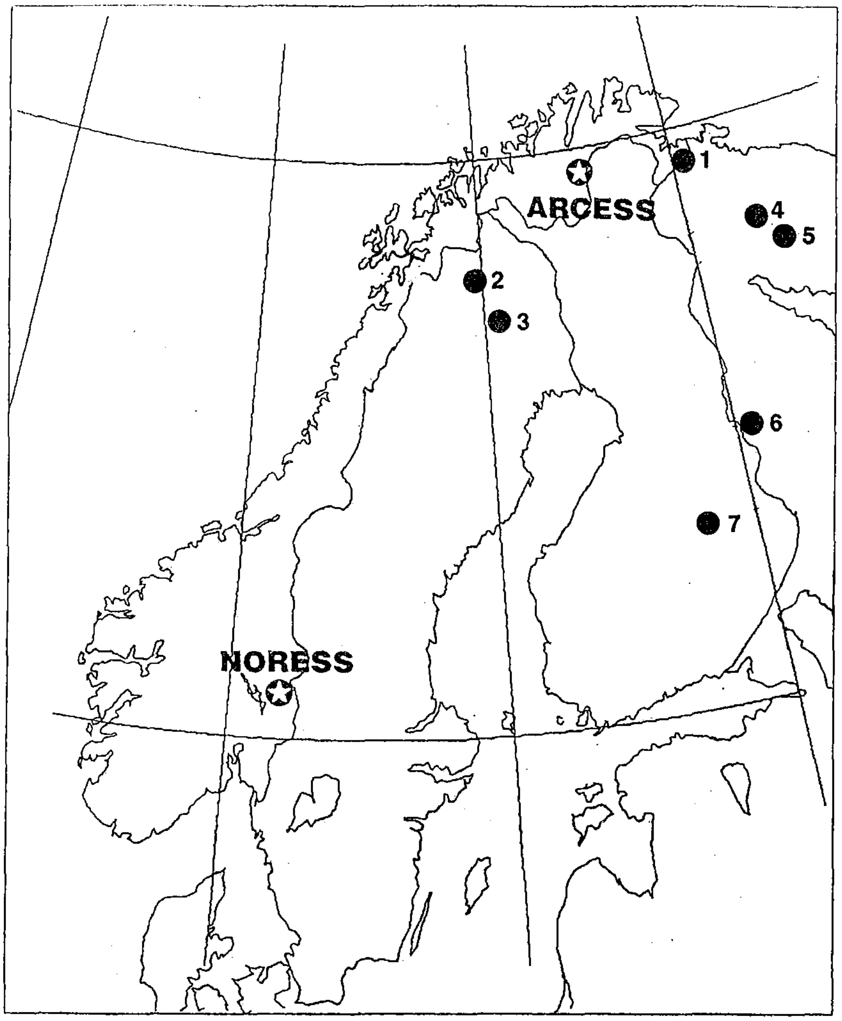

Fig. VII.6.1 The seven events for which ARCESS high frequency data are plotted. The locations of the NORESS and ARCESS arrays are also shown.

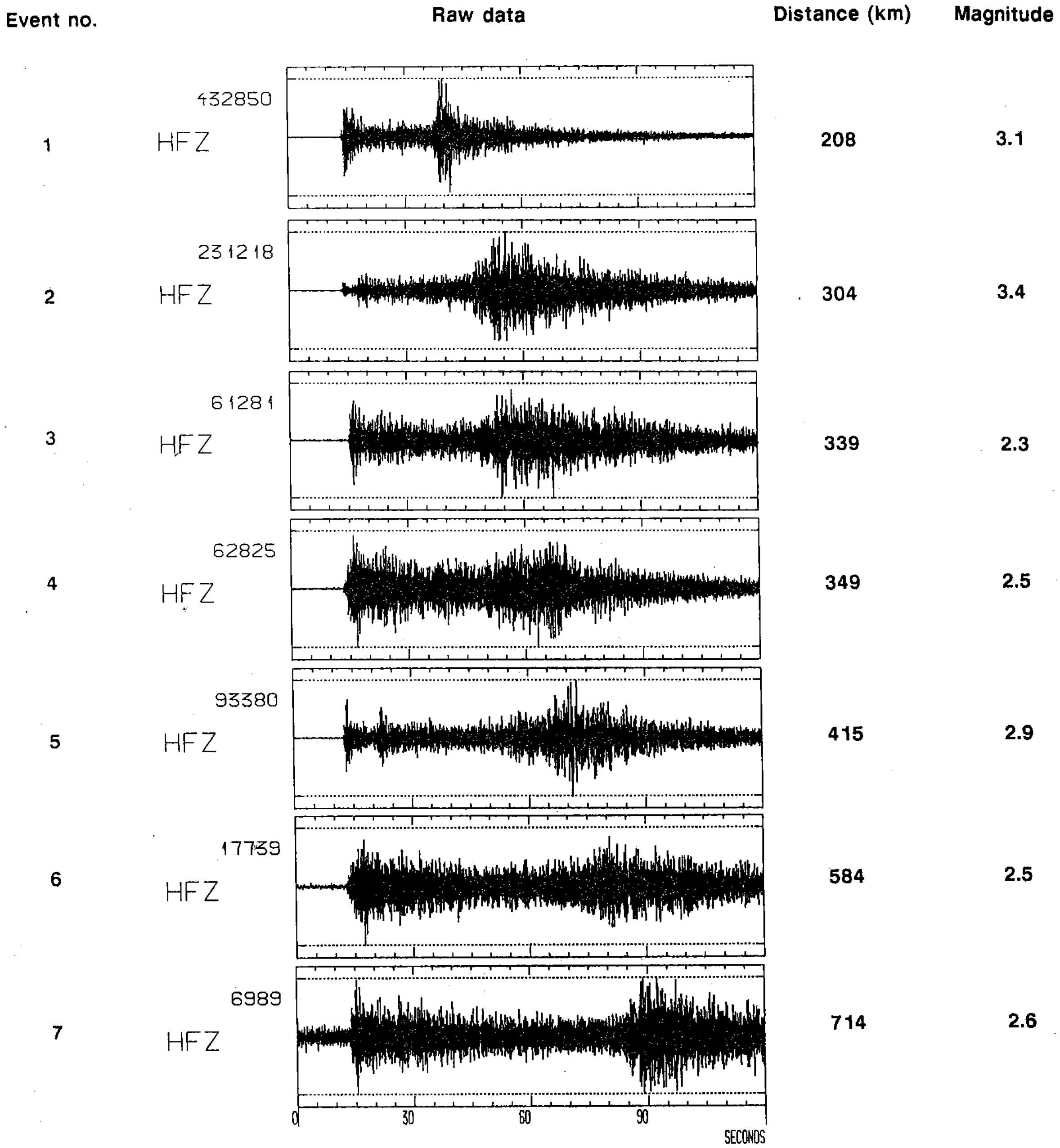

Fig. VII.6.2 Raw data for the HFSE vertical component for the seven events of Fig. VII.6.1.

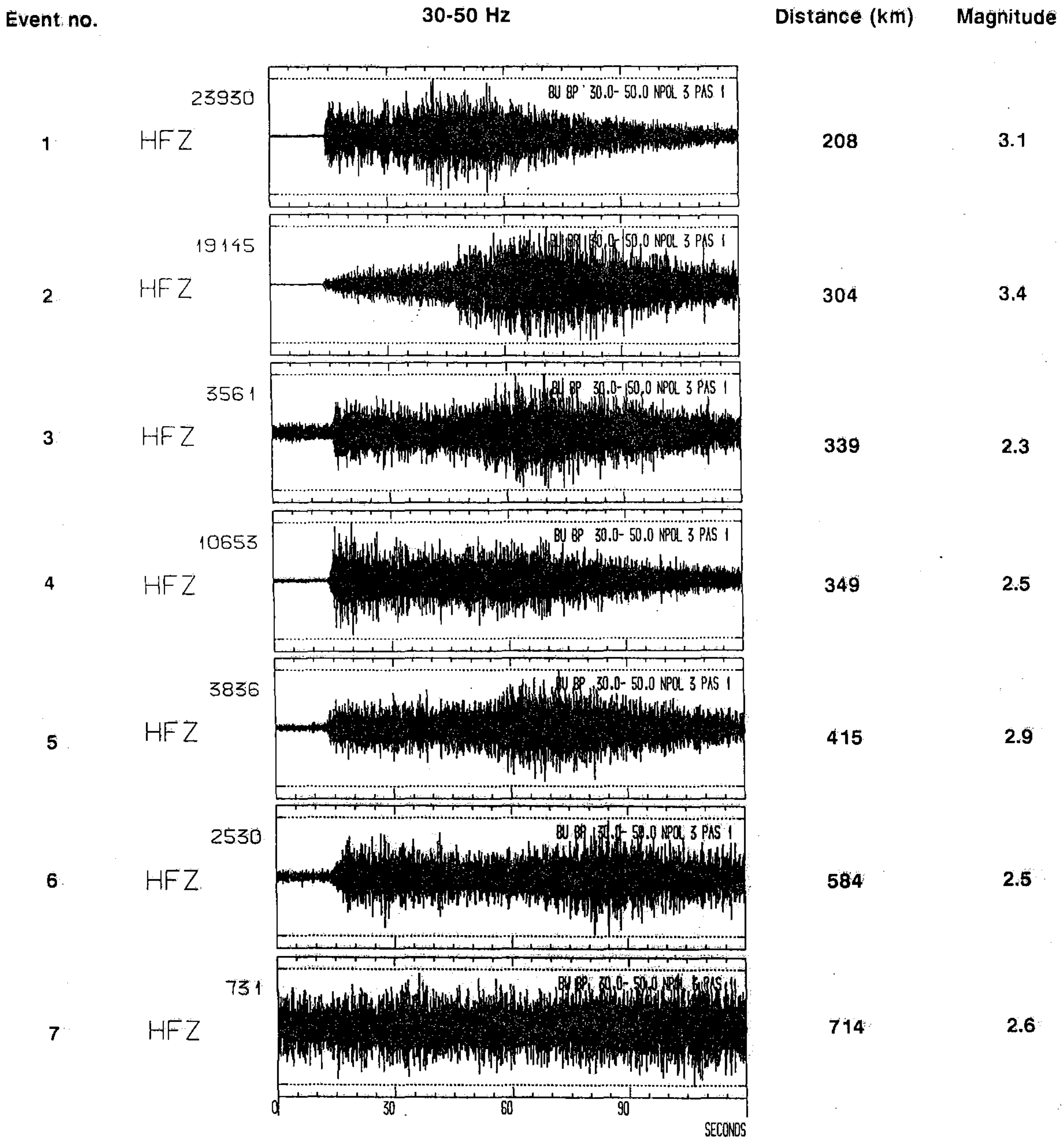

Fig. VII.6.3 Bandpass filtered data 30-50 Hz for the HFSE vertical component for the seven events of Fig. VII.6.1.

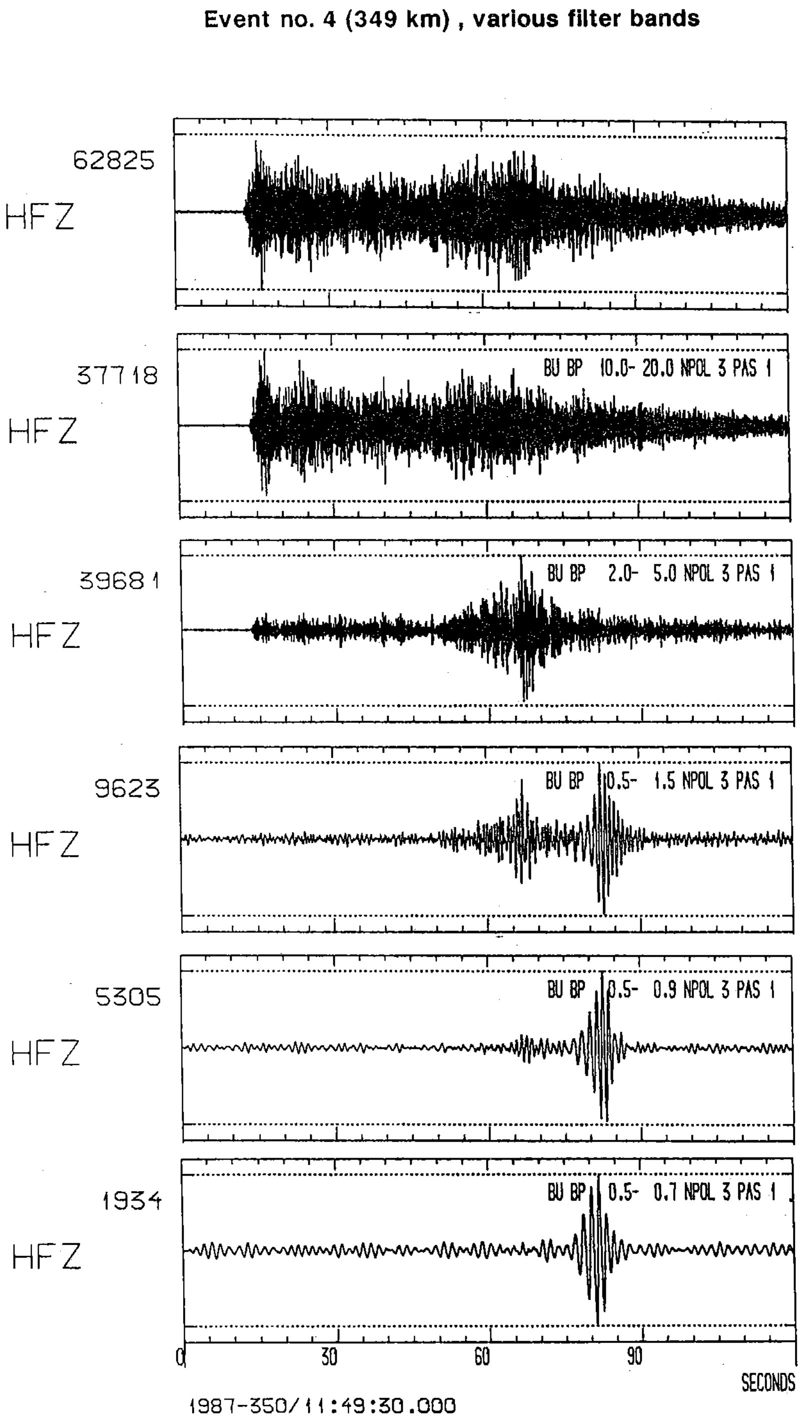

Fig. VII.6.4 The Rg phase for event no. 4 in Fig. VII.6.1 is clearly seen in the three bottom traces.

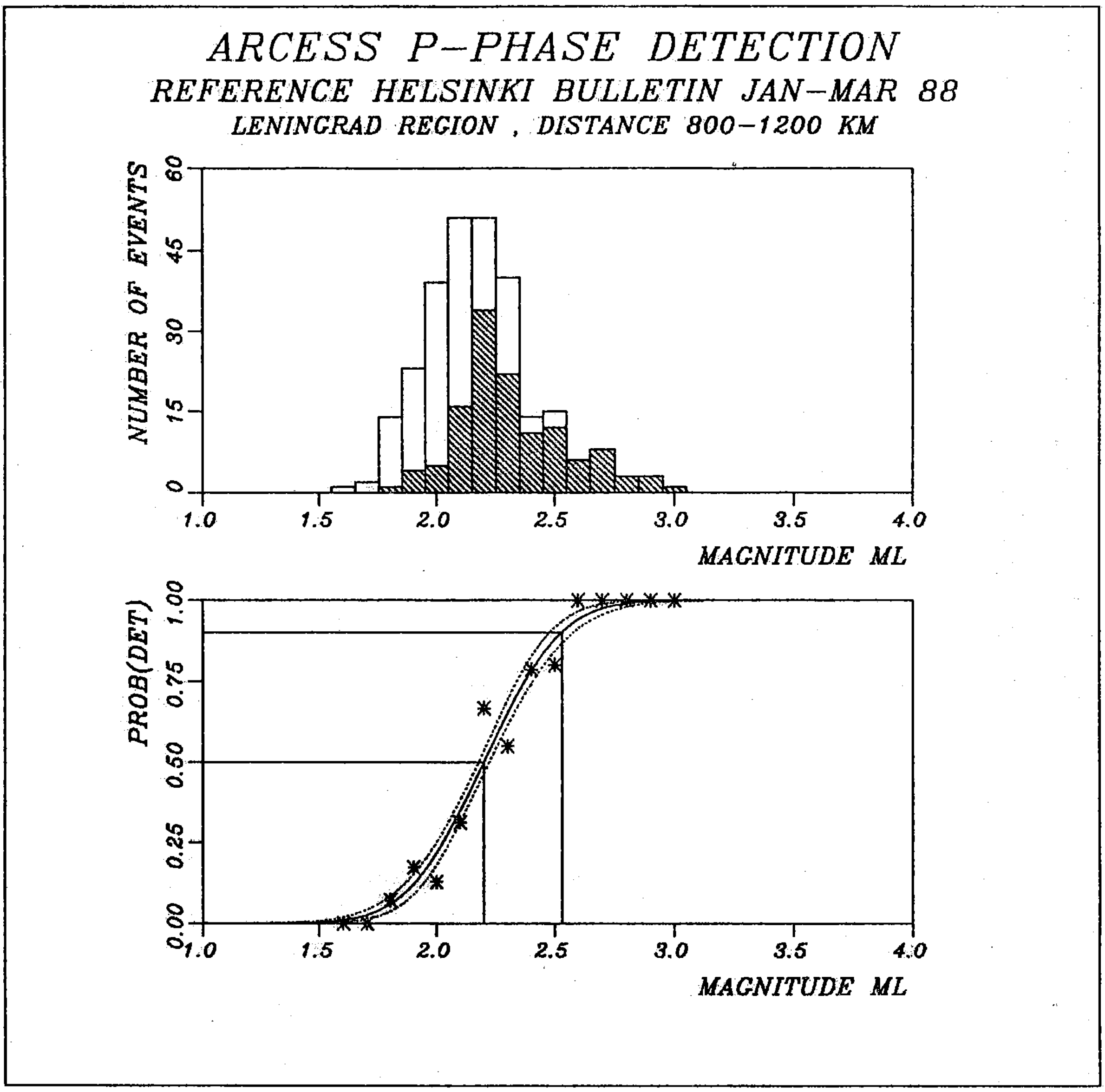

Fig. VII.6.5 P-phase detection statistics for ARCESS for regional events in the distance range 800-1200 km, using the Helsinki bulletin as a reference. The upper part of the figure shows the distribution of events by magnitude with detected events corresponding to the hatched columns. The bottom part of the figure shows the estimated detection probability curve as a function of magnitude, with the observed detection percentages marked as asterisks. The stippled curves mark the 90 per cent confidence limits.

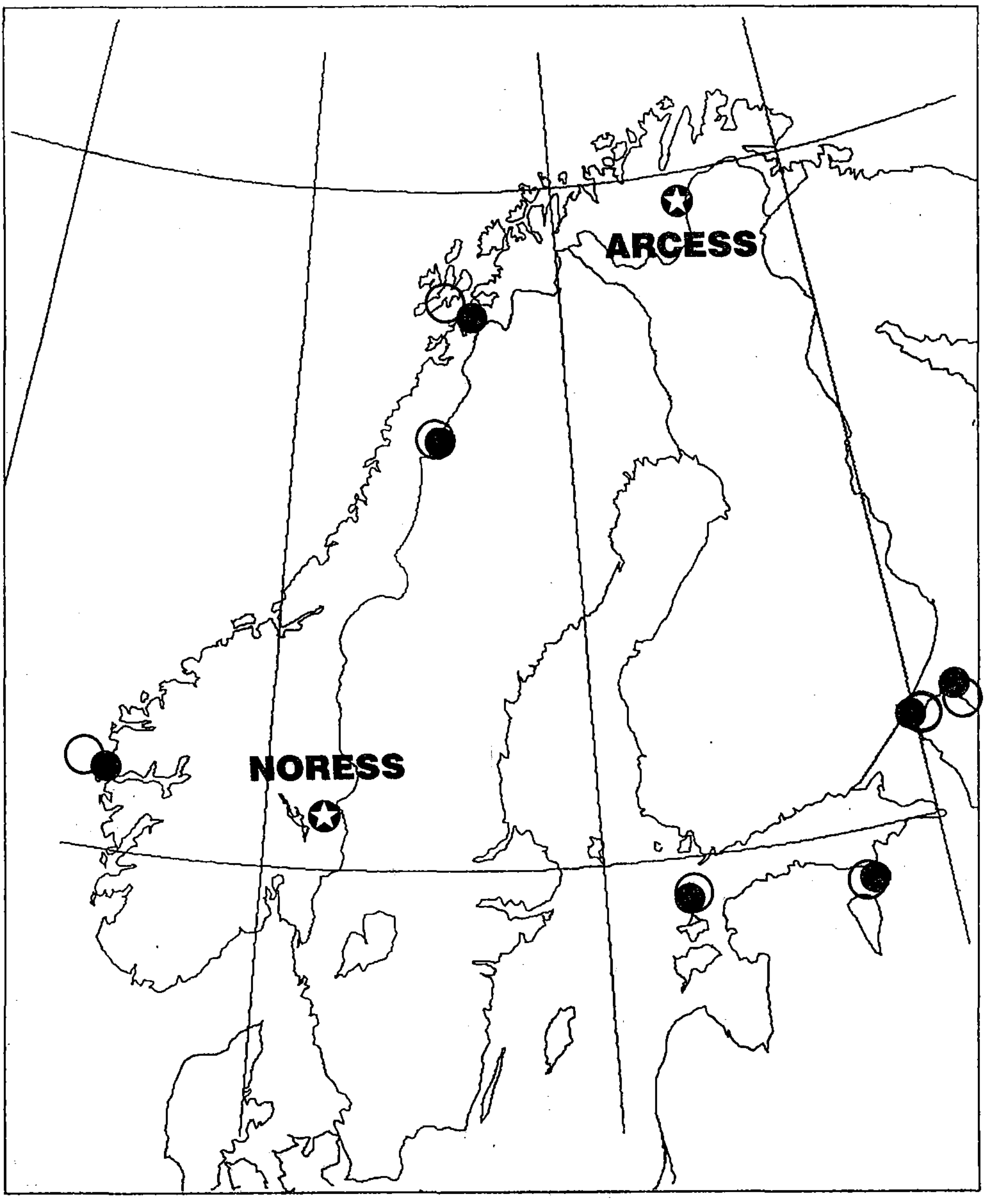

Fig. VII.6.6 Joint two-array location results for the events listed in Table VII.6.1. The open circles are centered at the epicenter locations computed at the University of Helsinki on the basis of Fennoscandian network data, wheras the filled circles are centered at the locations computed from the TTAZLOC program using data from the two arrays (marked on the figure). Note the excellent correspondence of the respective location estimates.

## VII.7 Analysis of Gräfenberg Lg recordings of Semipalatinsk explosions

In the previous NORSAR Semiannual Technical Summary, it was demonstrated that Lg measurements from NORSAR recordings can provide very stable magnitude estimates for large underground nuclear explosions at the Semipalatinsk test site (Ringdal and Hokland, 1987).

In this paper, initial results are presented from a study of Gräfenberg Lg recordings, using the same estimation method as for NORSAR. At this stage, the main purpose has been to determine the degree of consistency that can be obtained between Lg measurements from two arrays, with a further aim being to extend the study to a network of stations and obtain additional improved stability through network averaging.

The Gräfenberg array (GRF) is located in southern Germany as shown on Fig. VII.7.1, where the propagation paths from Semipalatinsk to NORSAR and GRF are also indicated. The unique feature of the Gräfenberg array is that all data are recorded broadband, with an instrument response that is flat to velocity from about 20 second period to 5 Hz (Harjes and Seidl, 1978). Altogether, the array comprises 13 instrument sites, of which three are 3-component systems (Fig. VII.7.2).

The data base used for this initial study comprised GRF recordings of 58 Semipalatinsk explosions between 1976 and 1987. Of the 58 events, 39 were sufficiently large to produce Lg wave amplitudes significantly exceeding the background noise level in the frequency band 0.6-3.0 Hz, and these are listed in Table VII.7.1. Specifically, we required that the RMS Lg should be at least 1.5 times the RMS of noise preceding P in this selection process. We also deleted from further analysis three events which had interfering phases in the Lg time window.

Data analysis was carried out using the same procedure as described by Ringdal and Hokland (1987). Briefly, all channels were filtered using a

Butterworth 3rd order recursive bandpass filter (0.6 - 3.0 Hz), and RMS values were then computed from a 60-second noise window (starting 80 seconds before P onset) and for a 120-second Lg window (starting 14 minutes after P onset). A noise compensation procedure was then carried out (as in the paper cited above), and a constant correction was applied to obtain the GRF Lg magnitudes. This constant was determined by requiring that the average GRF Lg magnitudes should equal the average NORSAR Lg magnitudes for the common event set.

The resulting magnitudes are listed in Table VII.7.1. These data are based only on the instruments A1, A2, A3 and A4 (vertical components), since our data base for the earliest events did not comprise recordings from all 13 channels. (We considered it important to use the same instruments for the entire data base, in order to avoid possible bias effects due to local receiver anomalies.)

Fig. VII.7.3 gives a comparison of Lg magnitudes determined from Gräfenberg and NORSAR data. The consistency between these estimates is excellent, with the standard deviation of the differences being only 0.051 magnitude units. If we consider only well-recorded events at GRF, i.e., requiring at least 3 stations and signal-to-noise ratio (RMS Lg to RMS noise) of at least 1.75, the standard deviation is reduced even further, to 0.043 magnitude units (Fig. VII.7.4).

It appears from the two figures that the GRF Lg magnitudes tend to be slightly higher than NORSAR Lg magnitudes for the largest events. It must be noted here that the estimates are less accurate for the smaller events, due to greater noise interference, but it is also possible that the differences in instrument responses at GRF and NORSAR could be a contributing factor. In this initial study, we have not attempted to compensate for this response difference, although this is certainly a natural next step.

Fig. VII.7.5 shows P-Lg (GRF) magnitude residuals on the basis of geographical epicenter location within the Shagan River area. The location estimates and maximum likelihood ISC-based magnitudes used for generating this figure have been obtained from Blacknest (Marshall et al, 1985; Marshall, personal communication). We note the systematic difference between the northeast and southwest portion of the test site; in fact this pattern is almost identical to that found using NORSAR Lg data (Ringdal and Hokland, 1987). The fact that this anomaly is confirmed using an entirely different array for Lg measurements is by itself significant, as it demonstrates that this observation is not a function of the particular propagation path from Semipalatinsk to NORSAR.

## Conclusions

From this initial study, we can conclude that the Lg RMS estimation methods provide very stable, mutually consistent results when applied to two widely separated arrays (NORSAR and GRF). This is of clear significance regarding the potential use of such Lg measurements for yield estimation. Further research will be directed toward expanding the data base and number of instruments in the Gräfenberg study, including addressing the instrument response issue, and in addition conduct similar studies using other available station data as well as study Lg recordings from other test sites.

F. Ringdal
J. Fyen

## References

Harjes, H.-P. and D. Seidl (1978): Digital recording and analysis of broadband seismic data at the Gräfenberg (GRF) array. J. Geophys. Res., 44, 511-523.

Marshall, P.D., T.C. Bache and R.C. Lilwall (1985): Body wave magnitudes and locations of Soviet underground explosions at the Semipalatinsk Test Site. AWRE Report No. 0 16/84, AWRE, MOD(PE), Aldermaston, Berksh., UK.

Ringdal, F. and B.Kr. Hokland (1987): Magnitudes of large Semipalatinsk explosions using P coda and Lg measurements at NORSAR. Semiannual Technical Summary, 1 Apr - 30 Sep 1987, NORSAR Sci. Rep. No. 1-87/88, Kjeller, Norway.

| ORIGIN DATE | ORIGIN TIME | GRF LG RMS | NCH |
|---|---|---|---|
| 04/07/76-186: | 02.56.57.60 | 5.781 | 04/04 |
| 28/08/76-241: | 02.56.57.50 | 5.673 | 03/04 |
| 23/11/76-328: | 05.02.57.28 | 5.811 | 03/03 |
| 07/12/76-342: | 04.56.57.38 | 5.721 | 03/03 |
| 29/05/77-149: | 02.56.57.80 | 5.592 | 03/03 |
| 11/06/78-162: | 02.56.57.70 | 5.748 | 02/06 |
| 29/08/78-241: | 02.37.06.50 | 6.005 | 03/07 |
| 04/11/78-308: | 05.05.57.50 | 5.640 | 03/06 |
| 29/11/78-333: | 04.32.58.00 | 5.894 | 01/06 |
| 23/06/79-174: | 02.56.57.60 | 6.101 | 03/06 |
| 07/07/79-188: | 03.46.57.40 | 5.926 | 04/10 |
| 04/08/79-216: | 03.56.57.60 | 6.093 | 04/12 |
| 18/08/79-230: | 02.51.57.30 | 6.144 | 04/10 |
| 28/10/79-301: | 03.16.56.90 | 6.062* | 00/10 |
| 02/12/79-336: | 04.36.57.50 | 5.955 | 04/12 |
| 23/12/79-357: | 04.56.57.60 | 6.058 | 04/09 |
| 29/06/80-181: | 02.32.57.70 | 5.699 | 03/13 |
| 12/10/80-286: | 03.34.14.10 | 5.954 | 04/13 |
| 14/12/80-349: | 03.47.06.60 | 5.946 | 02/13 |
| 27/12/80-362: | 04.09.08.20 | 5.866 | 03/13 |
| 22/04/81-112: | 01.17.11.40 | 5.967 | 03/13 |
| 13/09/81-256: | 02.17.18.25 | 6.081 | 04/09 |
| 18/10/81-291: | 03.57.02.64 | 5.945 | 04/09 |
| 27/12/81-361: | 03.43.14.10 | 6.114 | 03/11 |
| 05/12/82-339: | 03.37.12.60 | 5.995 | 04/13 |
| 26/12/82-360: | 03.35.14.10 | 5.603 | 04/13 |
| 07/03/84-067: | 02.39.06.40 | 5.556 | 04/13 |
| 29/03/84-089: | 05.19.08.20 | 5.948 | 04/13 |
| 26/05/84-147: | 03.13.12.40 | 6.109 | 04/13 |
| 02/12/84-337: | 03.19.06.30 | 5.842 | 04/13 |
| 03/04/87-093: | 01.17.08.00 | 6.129 | 04/13 |
| 17/04/87-107: | 01.03.04.00 | 5.912 | 04/13 |
| 06/05/87-126: | 04.02.05.50 | 5.883 | 04/13 |
| 20/06/87-171: | 00.53.04.00 | 5.947 | 03/13 |
| 17/07/87-198: | 01.17.07.00 | 5.686 | 04/13 |
| 02/08/87-214: | 00.58.08.00 | 5.835 | 04/13 |
| 15/11/87-319: | 03.31.08.00 | 6.006 | 04/13 |
| 13/12/87-347: | 03.21.08.00 | 6.066 | 04/13 |
| 27/12/87-361: | 03.05.08.00 | 6.044 | 04/13 |

<u>Table VII.7.1</u> List of events used in this study, with estimated Lg magnitudes from Gräfenberg recordings as described in the text. The number of A-ring GRF channels used for these measurements are also given, together with the total number of GRF channels available in the data base. For the event marked with an asterisk, the estimate is based on GRF B-ring data.

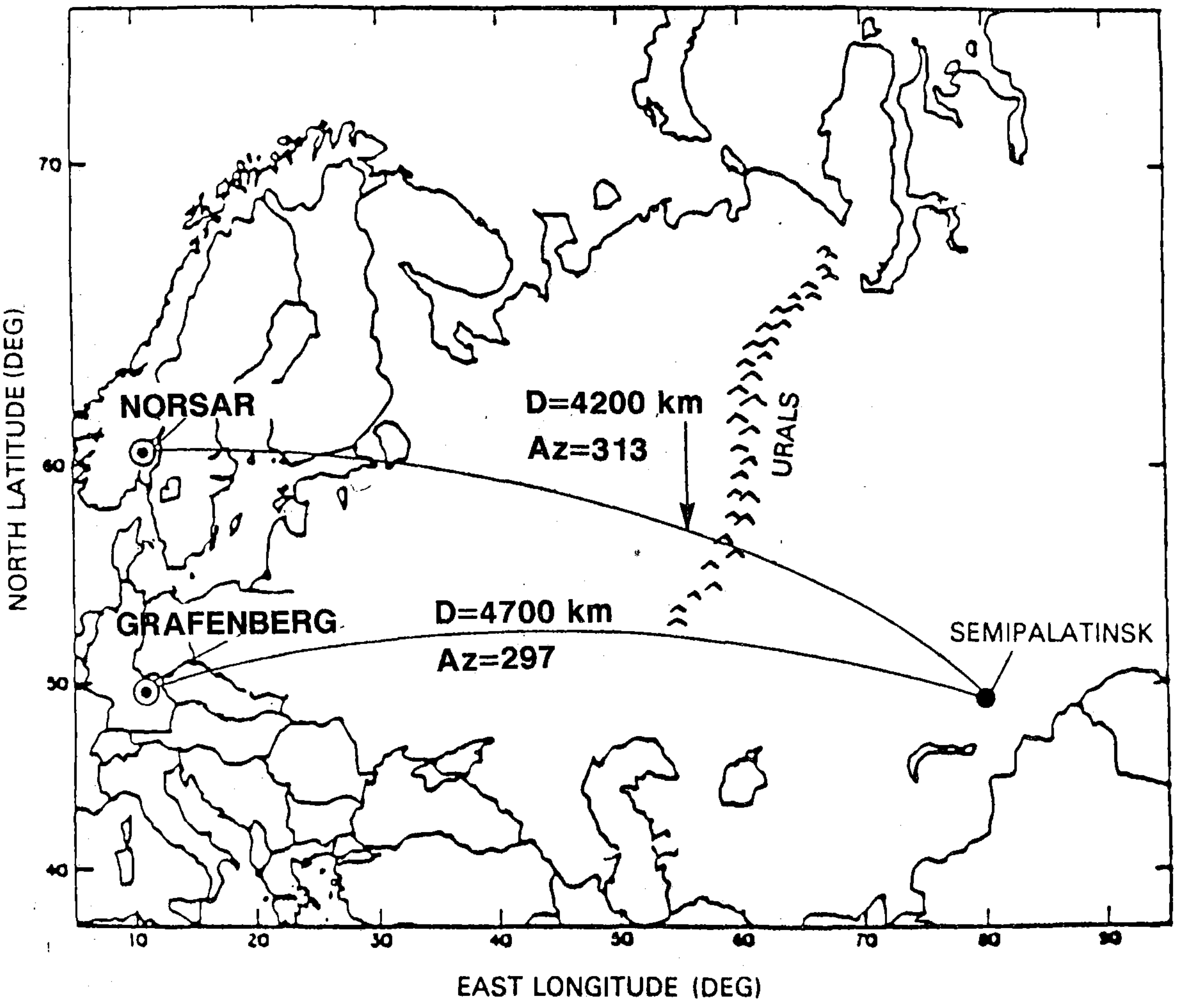

Fig. VII.7.1 Location of the NORSAR and Gräfenberg arrays in relation to the Semipalatinsk test site.

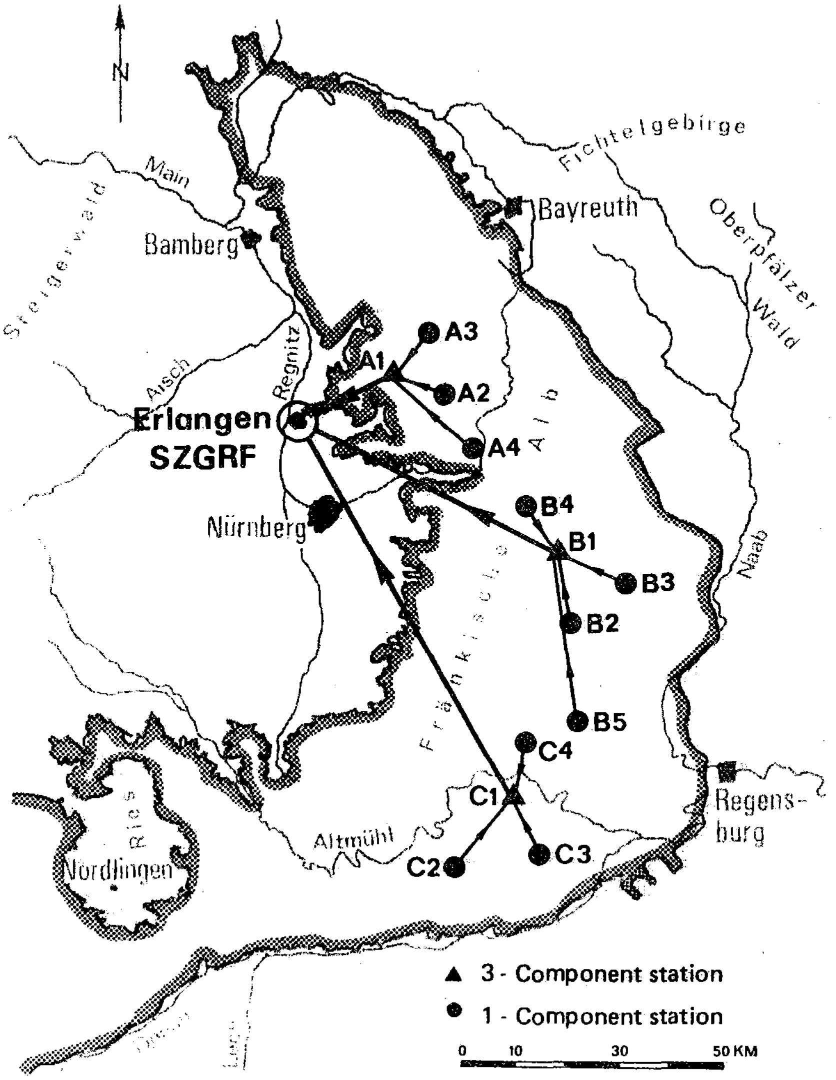

Fig. VII.7.2 Geometry of the Gräfenberg array.

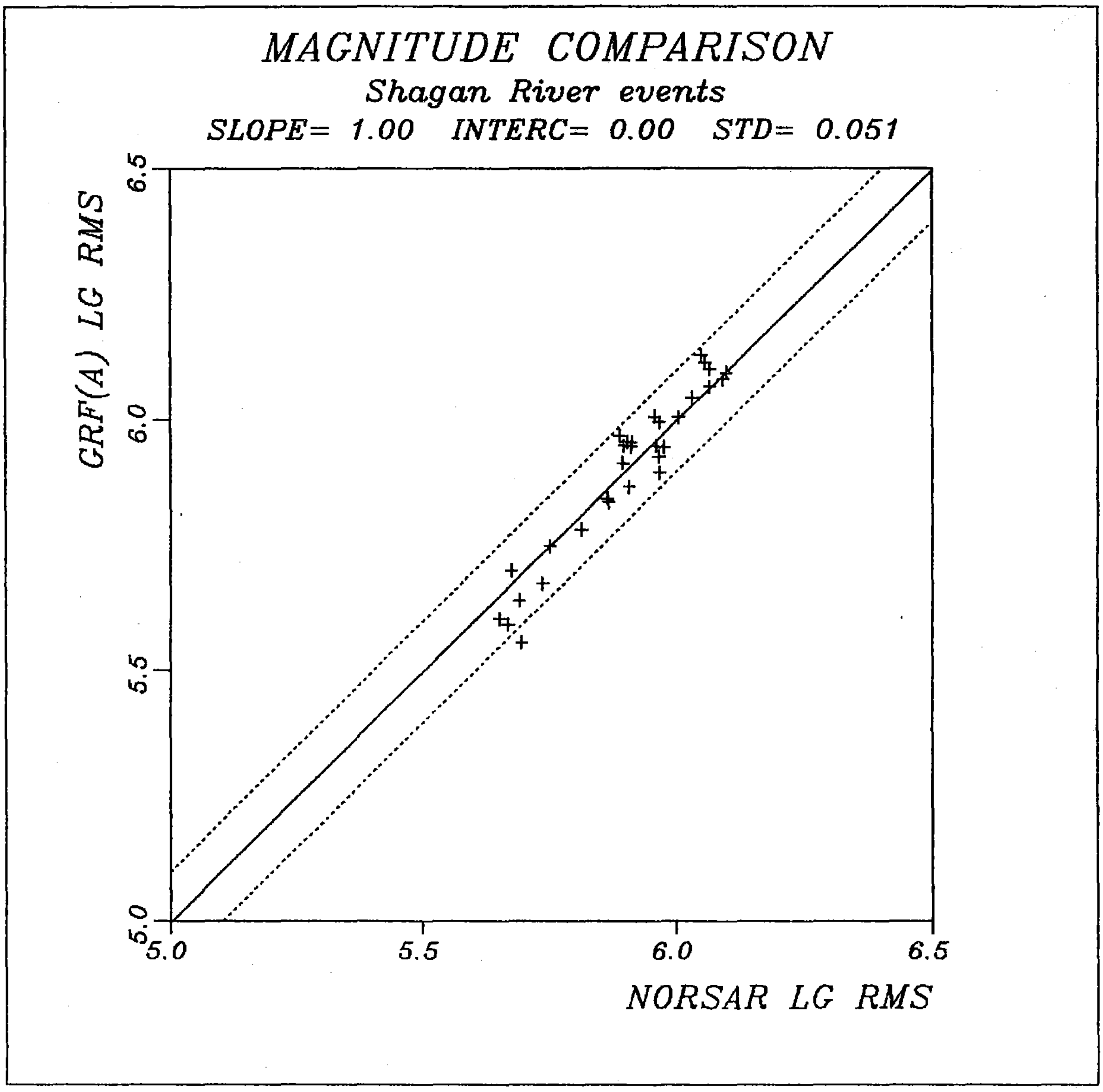

Fig. VII.7.3 Plot of Gräfenberg versus NORSAR Lg magnitudes for Semipalatinsk explosions. The slope has been restricted to 1.00, and the dotted lines correspond to plus/minus two standard deviations.

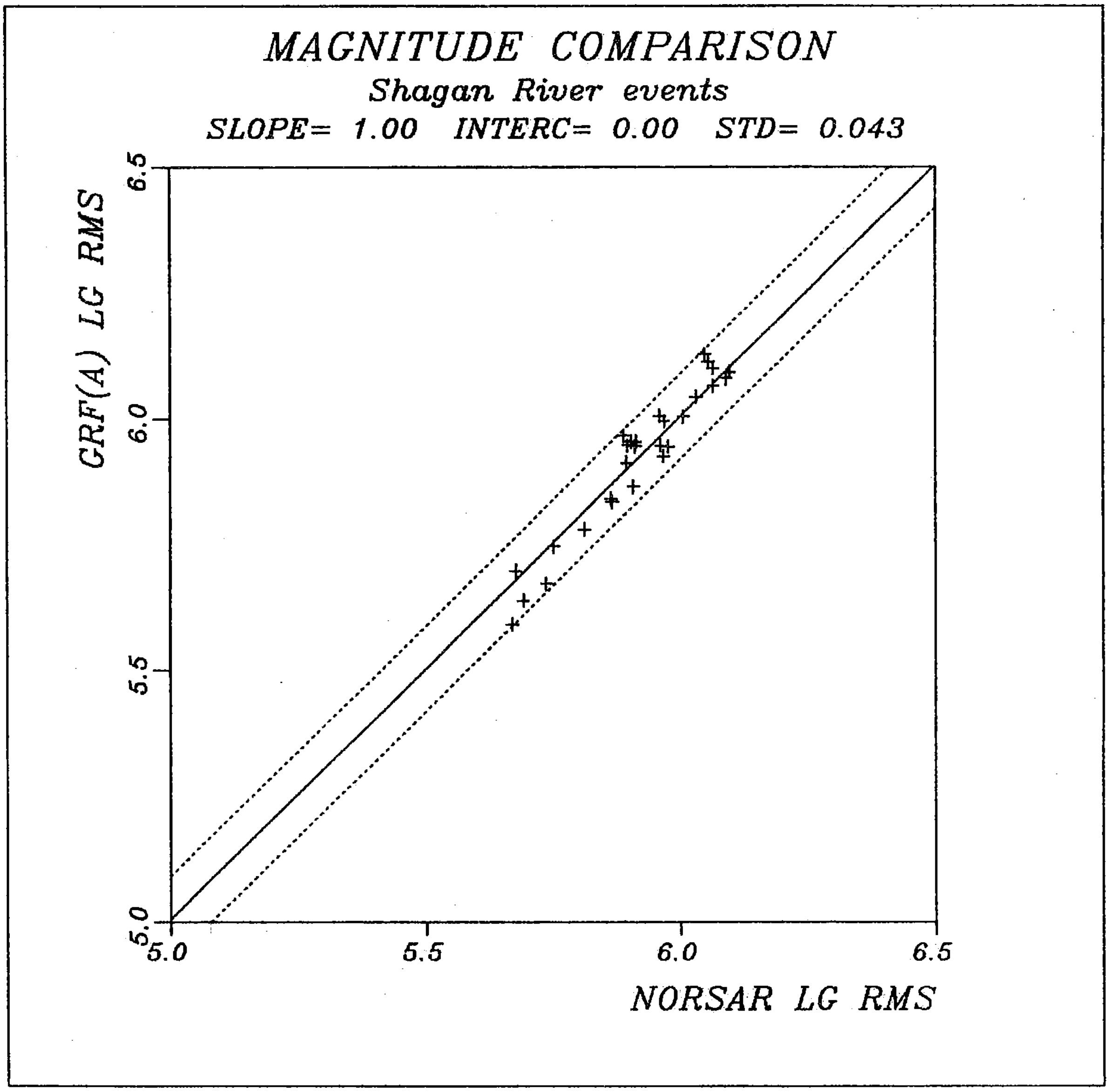

Fig. VII.7.4 Same as Fig. VII.7.3, but including only events with GRF Lg measurements based on at least three channels, and having signal-to-noise ratio exceeding 1.75 (see text for details). Note that the scatter is considerably reduced compared to Fig. VII.7.3.

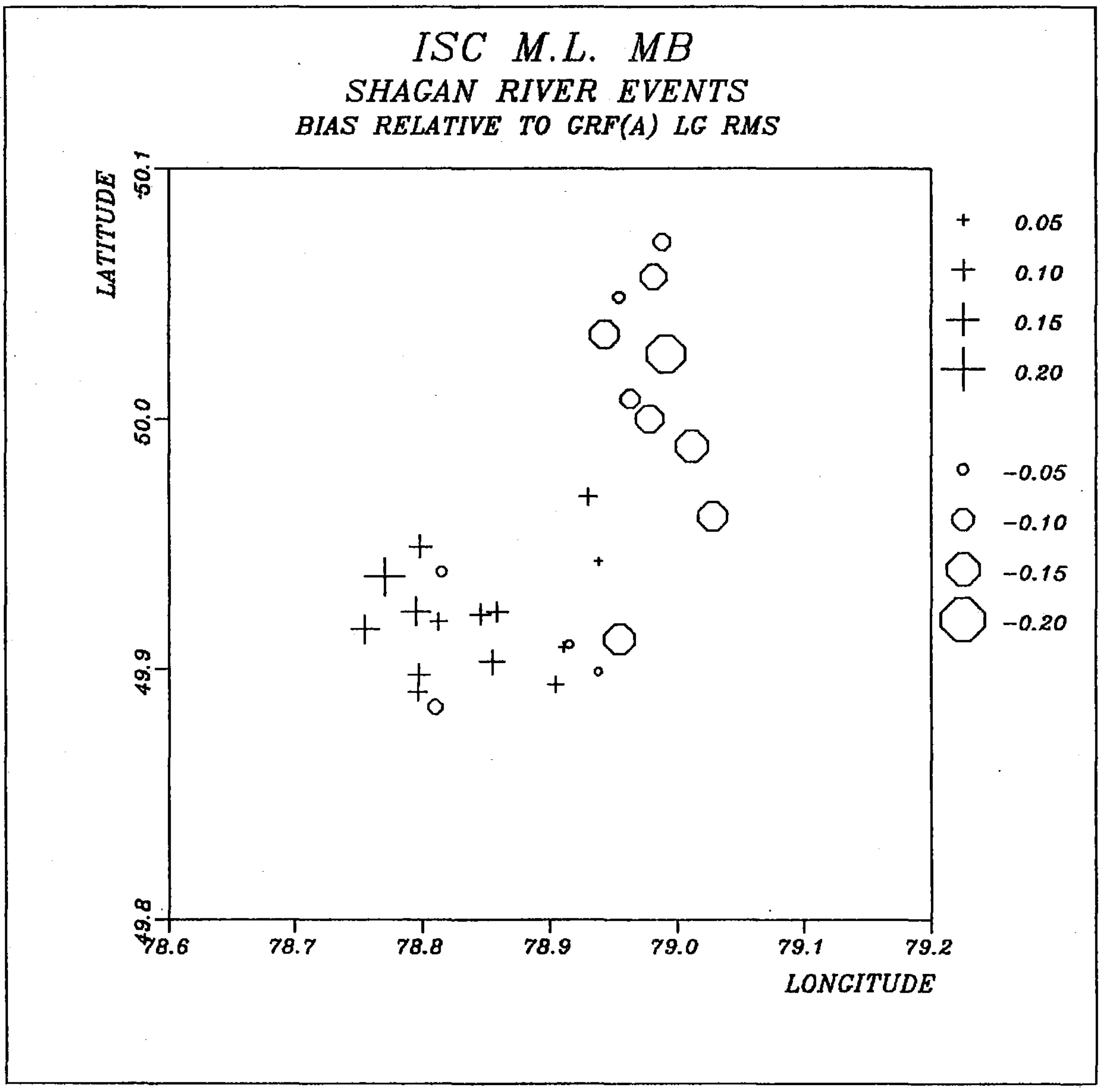

Fig. VII.7.5 Plot of magnitude residuals (ISC max. likelihood $m_b$ minus Gräfenberg Lg RMS magnitudes) as a function of event location for events in the data base. Plusses and circles correspond to residuals greater or less than the average, respectively, with symbol size proportional to the deviation. Location estimates are those of Marshall et al (1985) where available, otherwise NEIS estimates have been used. Note the systematic variation within the Shagan River area.